# Thermal Selection of Seneca Valley Virus Gives Rise to a Novel Thermostable Mutant

**Cormac McCarthy**

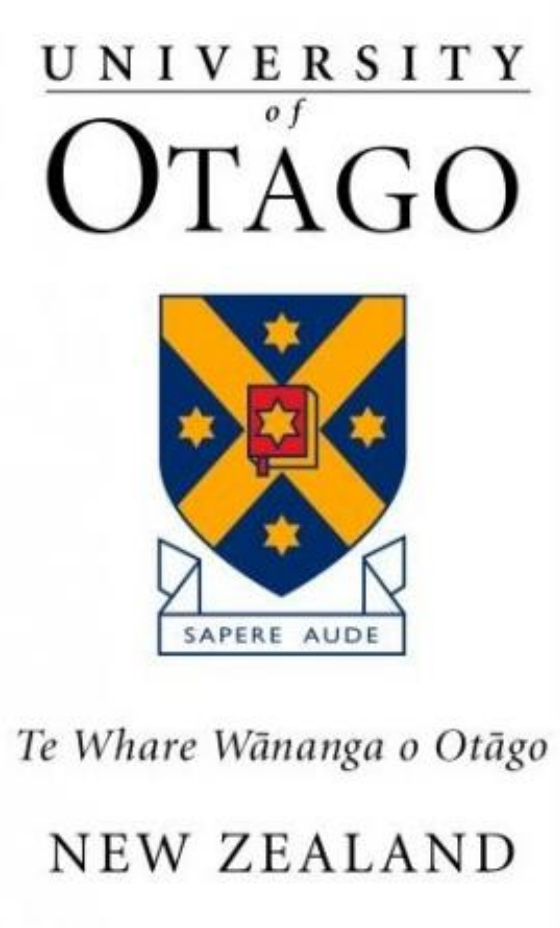


A Report Submitted in Fulfilment of the Degree of

**Master of Science**

At the University of Otago, Dunedin,

New Zealand

## Abstract

This project aimed to improve the stability of the novel oncolytic virus, Seneca Valley virus (SVV). This was with the overarching goal of determining the residues and mutations thereof within the viral capsid that are responsible for capsid stability, to inform the future production of SVV Virus-Like Particles (VLPs) for use as a drug delivery vector.

The thermal stability of wild-type SVV-001 was first investigated to determine a baseline to which thermostable mutants could be compared, and to inform a regimen of heating and passage to derive thermostable mutants. During optimisation of these initial experiments, heating of a sample containing approximately $10^7$ PFU/mL SVV-001 to 58.5 °C for 30 minutes produced a single viral plaque. Virus collected from this plaque was shown to be resistant to heating at 56 °C, an improvement on the wild-type, which was shown to lose approximately 99% viral titre to heating at 53.5 °C for 30 minutes. This thermostable phenotype was also confirmed using Particle Stability Thermal Release Assays (PaSTRy). Attempts to select for increasingly thermostable virus were unsuccessful.

Mutant virus was purified and the capsid-coding region of the genome sequenced. This revealed four mutations in the thermostable mutants. One of these mutations, A1776G, was predicted to have an effect on the maturation of capsid proteins, which was supported by initial results of SDS-PAGE gel analysis. The other three mutations were either synonymous mutations well-conserved in Senecavirus isolates, or outside of the capsid coding region of the genome, and so were of limited applicability to the production of VLPs.

Thermostable virus was then optimised for cryo-electron microscopy to determine its structure, with a low-resolution structure derived as a proof-of-principle.

Future studies are warranted to determine if the A1776G confers a thermostable phenotype to the wild-type virus, and in turn to the SVV VLP. The basis for this phenotype should also be investigated, as well as a means to introduce the desired drugs into the genomeless capsid.

## Acknowledgements

Firstly, I would like to thank Dr. Laura Burga for her patience and expertise for the duration of this project. Her support and tutelage have been invaluable.

I would also like to thank Dr. Mihnea Bostina for extending me the opportunity to be part of the Bostina Lab and facilitating this research.

I would like to express my sincere appreciation for Nadishka Jayawardena and for his advice and mentorship over the course of the project.

My gratitude goes to Richard Easingwood, Allan Mitchell, Gillian Grayston and Sharon Lequeux from Otago Micro and Nano Imaging (OMNI) for their technical support and training.

Thanks also to the rest of the Bostina Lab, Sailakshmi, Guillaume, Kai and Shakeel, for creating a warm and supportive lab environment.

I owe tremendous gratitude to the Department of Microbiology and Immunology, with whom I earned my Bachelor of Science and Bachelor of Science with Honours, and who generously provided me with the Department of Microbiology and Immunology Masters scholarship.

My thanks go to my parents Gerard and Brenda, without whom none of this would have been possible. Their ongoing love and support, as well as that from my siblings Finbarr, Diarmaid and Niamh, is something I have always been able to rely on.

# List of Abbreviations

| | |
|---|---|
| 3’ | 3 Prime |
| 5’ | 5 Prime |
| ACT | Adoptive Cell Transfer |
| ANTXR1 | Anthrax Toxin Receptor 1 |
| BBB | Blood-Brain Barrier |
| BEV | Bovine Enterovirus (e.g. BEV1, BEV2) |
| °C | Degrees Celcius |
| CAR | Chimeric Antigen Receptor |
| CAR | Coxsackievirus and Adenovirus Receptor |
| CD | Cluster of Differentiation (e.g. 28, 3ζ, 155) |
| cDNA | Complementary Deoxy Ribonucleic Acid |
| CDR | Complementarity Determining Region |
| CPR | Otago’s Centre for Protein Research |
| CRE | Cis-acting Replicative Element |
| CSC | Cancer Stem Cell |
| CTF | Contrast Transfer Function |
| CTL | Cytotoxic T-Lymphocytes |
| CVA | Coxsackievirus A (e.g. CVA21, CVA13, CVA15, CVA18) |
| CVB | Coxsackievirus B (e.g. CVB3, CVB6) |
| DAF | Decay Accelerating Factor |
| DAMP | Damage-Associated Molecular Pattern |
| DC | Dendritic Cell |
| dNTP | Deoxy Nucleotide Triphosphate |
| DRBP76 | Double-stranded RNA Binding Protein 76 |
| dsRNA | Double-stranded Ribonucleic Acid |
| ECHO | Enteric Cytopathic Human Orphan |
| EMCV | Encephalomyocarditis Virus |
| eIF | Eukaryotic Initiation Factor |
| ESST | Environment-Specific Substitution Table |
| EV | Echovirus (e.g. EV7) |
| FBS | Foetal Bovine Serum |
| FMDV | Foot-and-Mouth Disease Virus |

| | |
|---|---|
| $H_2O$ | Water |
| HRV2 | Human Rhinovirus 2 |
| HSP | Heat-Shock Protein (e.g. HSP 60, HSP 70, HSP90) |
| IBD | Inflammatory Bowel Disease |
| ICAM-1 | Intercellular Adhesion Molecule-1 |
| ICTV | International Committee for the Taxonomy of Viruses |
| IFN | Interferon (e.g. INF-β) |
| IL | Interleukin (e.g. IL-12) |
| IRES | Internal Ribosome Entry Site |
| kDa | Kilodalton |
| LAPV | Live Attenuated Poliovirus |
| LEV | Live Enterovirus Vaccine |
| mA | Milli-Amperes |
| MART-1 | Melanoma-associated Antigen Recognised by T-cells-1 |
| MALDI-TOF | Matrix-Assisted Laser Desorption Ionisation-Time of Flight |
| MEV | Mengovirus |
| MHC-II | Major Histocompatibility Complex-II |
| mL | Millilitre |
| MOI | Multiplicity of Infection |
| MWCO | Molecular Weight Cut-Off |
| NCI CTCAE | National Cancer Institute Common Terminology Criteria for Adverse Events |
| Necl5 | Nectin-Like molecule 5 |
| OMNI | Otago Micro and Nano Imaging |
| OR | Odds Ratio |
| OV | Oncolytic Virus |
| OVA | Ovalbumin |
| PBS | Phosphate Buffered Saline |
| PCR | Polymerase Chain Reaction |
| PET | Positron Emission Tomography |
| PFU | Plaque-Forming Units |
| pmol | picomolar |
| PV | Poliovirus |
| PVR | Poliovirus Receptor |

| | |
|---|---|
| RdRp | RNA-dependent RNA Polymerase |
| RNA | Ribonucleic acid |
| SCLC | Small Cell Lung Cancer |
| SDS-PAGE | Sodium Dodecyl Sulfide Polyacrylamide Gel Electrophoresis |
| SVV | Seneca Valley Virus |
| TCR | T-cell Receptor |
| TEM8 | Tumour Endothelial Marker 8 |
| TIL | Tumour Invading Lymphocytes |
| TMEV | Theilers Murine Encephalomyelitis Virus |
| TNF-α | Tumour Necrosis Factor-alpha |
| T-VEC | Talimogene Laherparepvec |
| UCSF | University of California San Francisco |
| µL | Microlitre |
| US | United States (of America) |
| US FDA | United States Food and Drug Administration |
| UTR | Untranslated Region |
| V | Volts |
| VCN | Vibrio Cholera Neurominidase |
| VLP | Virus-Like Particle |
| $vMC_{24}$ | Poly-C truncated Mengovirus |
| VPg | Viral Protein genome-linked |
| WHO | World Health Organisation |

# List of Figures

# Table of Contents

# 1 Introduction

## 1.1 Cancer

### 1.1.1 Incidence, epidemiology & contributing factors

Globally, cancer remains one the greatest causes of mortality in humans. In 2018, there was an estimated 18 million new cases of cancer worldwide, as well as 9.5 million deaths (International Agency for Research on Cancer, 2019). Among the most prevalent cancers worldwide are lung, breast, prostate and colorectal cancers, which together are thought to make up approximately 6.5 million of these new cases and 3.3 million of the overall deaths (Bray et. al., 2018).

The incidence of individual cancers and their mortality in a given population is informed by the complex intersection of biological and cultural factors. Lung cancer represents a fairly straightforward example, in that it is most often related to the recreational smoking of tobacco. Recent statistics indicate that as the rates of smoking decline, for instance in males in higher income countries, so too the incidence of lung cancer decreases (Torre et. al., 2015). As 10-15% of lung cancer sufferers in the US have ever smoked, smoking is not the sole modality through which people place themselves at risk of lung cancer (Samet et. al., 2009). Air pollution, through occupation or environment, increases risk to populations with low rates of smoking, with Chinese women as an example (Torre et. al., 2015). Other risk factors also include second-hand smoke exposure, aspects of diet, and infections (Samet et. al., 2009).

In most countries throughout the world, breast cancer is among the chief causes of death for women (Ghoncheh, Pournamdar & Salehiniya, 2016). Whereas the risk factors that underpin lung cancer are largely dictated by lifestyle, those which underpin breast cancer in women appear to be mostly biological, including advanced age, age at first pregnancy, early onset

menarche and later than average menopause (McPherson, Steel & Dixon, 2000). Note that this is not an exclusive rule, as alcohol, oral contraceptive and therapeutic hormone use have each been identified as risk factors (Barnard, Boeke & Tamimi, 2015).

Prostate cancer in men can be thought of as being the equivalent of breast cancer in women. It is an interesting cancer, as 80% of men who live to age 80 are thought to develop the condition, but clinically the lifetime risk is 8% (Bostwick et. al., 2004). For this reason, the observation has been made that "most men die *with* prostate cancer, rather than *from* it" (Bostwick et. al., 2004 p. 2372). Genetics seems to play a significant role in the development of prostate cancer. One Quebec-based study showed that the odds ratio (OR) of developing prostate cancer if one to four of a man's first-degree relatives also has prostate cancer is 9 (Ghandirian et. al., 1991). Another study from Jamaica showed that the OR for developing prostate cancer is 2.1 if a single first degree relative also has, or had, prostate cancer (Glover et. al., 1998).

Colorectal cancer is the third most common cancer in both men and women worldwide, differentially effecting Westernised societies such as North America, New Zealand, Australia and Europe (Haggar et. al., 2009). This may be explained in part by vices such as alcohol and tobacco use, which are both shown to be associated with early onset colorectal cancer (Zisman et. al., 2006). Inflammatory bowel disease (IBD) and genetic inheritance can also play a role in colorectal cancer (Haggar et. al., 2009).

### 1.1.2 Contemporary cancer treatments

Common treatments for cancer include mono- or combination therapy regimens of surgery, chemotherapy and/or radiation therapy. None of these interventions are without risk, and often carry side effects which can be severe. In surgery, masses of cancer cells are physically

removed from the surrounding tissue, which by definition causes damage to this tissue. Taking the example of rectal cancer, results from multiple studies indicate that of those who receive surgery, 7% will develop a wound infection, 11% will suffer from anastomotic leakage (transfer of matter across the intestinal lumen into the body), and 12% will develop pelvic sepsis (Paun et. al., 2010).

Chemotherapy encompasses a large range of therapies of different modalities. Chemotherapy drugs are most often introduced intravenously, exerting effects systemically, but preferentially against malignancies. This systemic toxicity manifests in negative side effects, for instance cisplatin, oxaliplatin, vincristine, methotrexate and cytarabine, among others, are known to cause central and/or peripheral nervous system complications (Verstappen et. al., 2003). Advances in understanding of cancers have brought about targeted chemotherapies, which include monoclonal antibodies and small molecule inhibitors. While generally considered less toxic, these too have side effects. These include the gastrointestinal perforation and haemorrhage that can be caused by bevacizumab, and the cardiac toxicity associated with lapatinib (Gerber, 2008).

Radiation therapy utilises high-energy ionising radiation to cause DNA damage, and thereby cellular destruction, of healthy and tumour cells in the treatment field. The complications that can arise from therapeutic irradiation are well demonstrated in an oral context, where radiation therapy can cause mucositis (inflammation of oral mucosa), xerostomia (lack of saliva, altered properties of saliva), and osteoradionecrosis (tissue and bone degeneration) (Sciubba & Goldenberg, 2006).

In recognition of the toxicity, and sometimes lack of efficacy, of traditional cancer therapies, new strategies are being developed constantly. These include adoptive T-cell transfer (ACT) and the use of oncolytic viruses (OVs). ACT can be subdivided into three categories: tumour invading lymphocytes (TILs) transgenic T-cell receptor T-cells (TCR T-cells) and chimeric antigen receptor T-cells (CAR T-cells) (June et. al., 2018). TIL therapy is a personalised treatment strategy wherein invading tumour lymphocytes are extracted from excised patient tumours and co-incubated with tumour cells in the presence of IL-2. TILs which are shown to destroy tumour cells *in vitro* are then expanded and re-introduced to the patient to exert therapeutic effect (Rosenberg & Restifo, 2015). Transgenic TCR T-cell therapy makes use of T-cells transduced to express T-cell receptors specific to cancer antigen (Ping, Liu & Zhang, 2018). An example of the cancer antigen targeted in TCR T-cell therapy is melanoma associated antigen recognised by T-cells-1 (MART-1). MART-1-recognising transgenic TCR T-cell therapy was able to produce objective responses in up to 30% of patients trialled in one study, but not without targeting of melanocytes in the skin, eyes and ears of patients (Johnson et. al., 2009). CARs are fusion proteins which contain an extracellular domain based on complementarity-determining region (CDR)-containing heavy and light chains of antibodies, and hinge domain, a transmembrane domain, and an intracellular signalling domain. CAR T-cells have gone through multiple "generations" in their development based on the intracellular domains that can be incorporated. First generation CARs had the intracellular domain of CD3ζ, second had CD3ζ and either CD28 or 4-1BB, and third generation CARs have all three (June et. al., 2018). Second generation CAR T-cells have shown great efficacy against B-cell malignancies such as Chronic Lymphoid Leukaemia, at the cost of B-cell hyperplasia (Porter et. al., 2011). Figure 1 below surmises therapeutic strategies for the treatment of malignancies that are well established, such as surgery, chemotherapy and radiation therapy, as well as upcoming therapies like ACT and OVs.

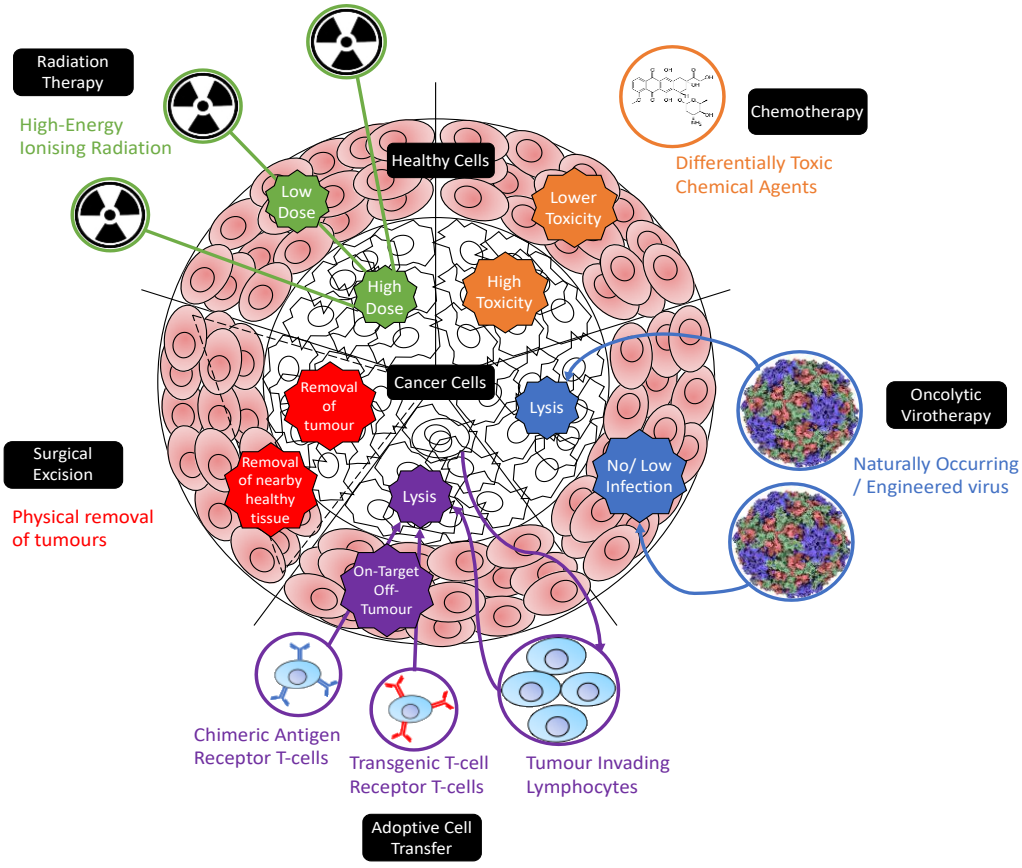


**Figure 1: Contemporary treatments for cancers.** A summary of the anti-tumour and off-target effects of surgery, chemotherapy, radiation therapy, adoptive cell transfer therapy and oncolytic virotherapy.

OVs will be discussed in greater detail in the coming text, but as the focus will be on those OVs from the picornavirus family, it would be beneficial to first define *Picornaviridae*.

## 1.2 Picornaviruses

### 1.2.1 Picornaviral biology

From the Latin "pico" meaning small, *Picornaviridae* are a family of small, non-enveloped, positive sense, single-stranded RNA viruses. The picornavirus family is well researched, with notable members such as poliovirus, foot and mouth disease virus and hepatitis A virus. The

genomes of picornaviral species have a characteristic “L-4-3-4” format, where the single polyprotein is cleaved by virally encoded proteases into the Leader protein, which is not always present, and three polypeptide regions P1 (four structural proteins), P2 (three non-structural proteins) and P3 (four non-structural proteins), hence “L-4-3-4” (Bedard & Semler, 2004). At the 5’ extreme of picornaviral genomes is the 5’ untranslated region (UTR). The 5’ UTR associates with the viral genome associated protein (VPg) and contains important secondary structural features, such as the internal ribosome entry site (IRES). Ordinarily, an essential step in human cellular RNA translation is the 7-methyl guanosine cap interacting with the eukaryotic initiation factor (eIF) protein, this function in the cap-independent translation of picornaviral genomes however, is served by the IRES (Svitkin et al., 2001). Immediately following the IRES, the Leader protein is a protease that sits at the 5’ end of the translated picornaviral polyprotein. It should be noted that the Leader protein is not present in all species encompassed by the *Picornaviridae* family. The Leader protein is followed by the four capsid proteins, in what is denoted as the P1 region of the picornaviral polyprotein. From 5’ to 3’, the capsid proteins are VP4, VP2, VP3 and VP1 respectively. While VP1 and VP3 are cleaved from P1 proteolytically, VP4 and VP2 are usually processed from the precursor VP0 following genome packaging inside the viral capsid.

The P2 region of the translated polyprotein consists of 2A, 2B and 2C. The picornaviral 2A protein is somewhat enigmatic, as it can be absent, present, or in some cases, be coded for twice in the genome. 2A proteins can be organised into five groups based on function and conserved residues, these are: chymotrypsin-like protease, parechovirus-like, hepatitis-A-like, apthovirus-like and cardiovirus 2A proteins (Yang et. al., 2017). The roles of 2B and 2BC are in the formation of pores in membranes of intracellular organelles, disturbing cation balances and impairing glycoprotein trafficking (Neiva et. al., 2003). 2C by itself has a range of activities

that can be specific to various viral taxa. In Seneca Valley virus (SVV) for example, 2C is shown to induce apoptosis (Liu et. al., 2019), whereas in Encephalomyocarditis Virus (EMCV), it has been shown to antagonise that IFN-β (Li et. al., 2019). Most commonly, picornaviral 2C proteins are thought to associated with membranes and bind viral genomic RNA (Banerjee & Dasgupta, 2001).

P3 consists of 3A, 3B, 3C and 3D. A sole function for 3A is not known, but it has been shown to interact with 3B, and the hydrophobic carboxy terminus of 3A is presumed to act as an anchor for 3AB in cellular membranes (Cameron, Suk Oh & Moustafa, 2010). 3B, which is also known as the viral genome associated protein (VPg) is a small protein which interacts with the 5' terminus of the genome and plays an essential role in genome replication. 3B does this by providing a primer for RNA synthesis when uridylated by cis-acting replicative elements (CREs). The CREs are looped secondary structural elements which can occur at several places in the RNA genome, including 5' and 3' UTRs, and 2C regions. The protease encoded by 3C performs most cleavages of the picornaviral polyprotein as well as inhibiting host transcription. Last among the picornaviral proteins is 3D, the RNA-dependent RNA polymerase (RdRP) (Porter et.al., 1993). The 3CD protein has protease and CRE-binding activity, but does not have polymerase activity. Finally, the 3' UTR of picornaviruses includes features such as the poly-A tail, and occasionally a CRE (Cameron, Suk Oh & Moustafa, 2010).

Figure 2 below describes the genome organisation and phylogenetic relationship between a number of picornaviral species.

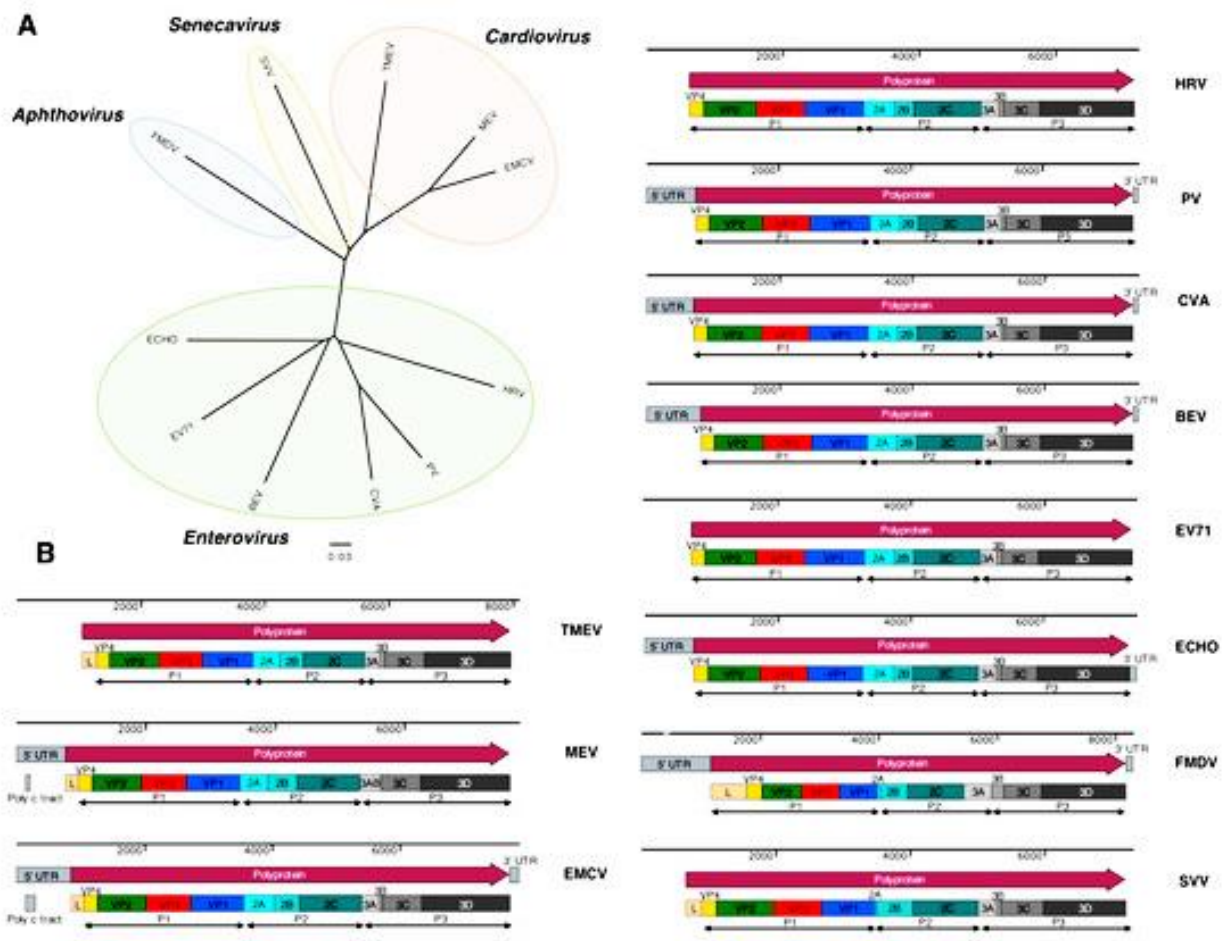


**Figure 2: Genomic relatedness of a select group of picornaviruses. A)** Radial phylogenetic tree showing the relatedness of several picornaviral species grouped into the Aptho-, Seneca-, Cardio- and Enterovirus genera respectively. **B)** RNA sequences of picornaviral isolates were aligned using clustal omega (Sievers et. al., 2011). Abbreviations: **TMEV** Theiler's murine encephalomyelitis virus **MEV** Mengovirus **EMCV** Encephalomyocarditis virus **HRV** Human Rhinovirus **PV** Poliovirus **CVA** Coxsackievirus A **BEV** bovine enterovirus **EV71** enterovirus 71 **ECHO** echovirus **FMDV** foot and mouth disease virus **SVV** Seneca Valley virus.

### 1.2.2 Quasispecies: An RNA viral phenomenon

The concept of quasispecies is crucial to understanding the evolutionary success of many RNA viruses, including picornaviruses. Rather than existing as clonal populations derived from a consensus nucleotide sequence, RNA viruses exist as mutant spectra, or mutant clouds as they can be termed (Domingo, Sheldon and Perales, 2012). Quasispecies therefore refers to the fact that individual virions within the same species can be sufficiently distinct so as to appear to be

from separate species (Domingo, Sheldon and Perales, 2012). This is due in no small part to the activity of virally encoded RdRPs. The activity of RdRPs is inherently error-prone, with most thought to introduce an error rate of between $10^{-4}$ to $10^{-6}$ mutations per base-pair per round of replication (Stern et. al., 2014). The consequences of this error-rate for a hypothetical 10,000 base-pair RNA virus is that for every genome duplication event, an average of one to 0.01 mutations occur. The mutant spectra that are produced from this process are not reflective of a truly random process wherein bases at all positions are equally likely to be mutated, rather they are constrained by the functional consequence of each specific mutation by negative selection of unfit genomes (Domingo, Sheldon and Perales, 2012). Figure 3 below surmises the concept of RNA-viral quasispecies.

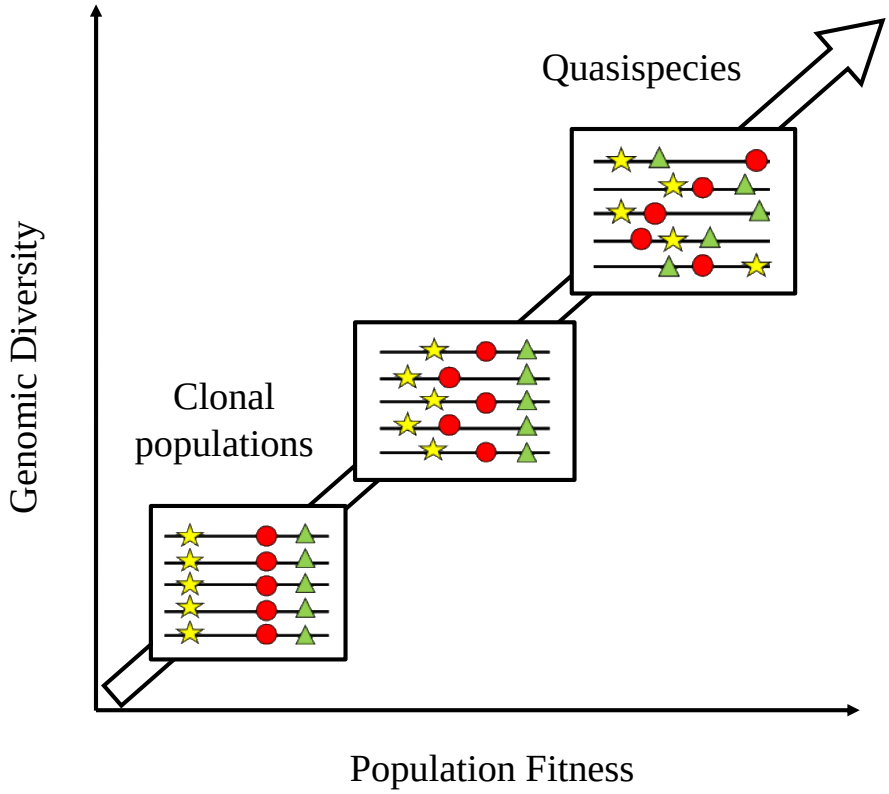


**Figure 3: Principle of adaptive advantage of the quasispecies phenomenon.** The genomic diversity of RNA viral quasispecies provides the maximal fitness to the viral population.

Taking the example of picornaviruses to expand on the idea of mutational constraints, the joint role of RNA secondary structures and the translated capsid proteins in forming functional virions means that the implications for mutations are two-fold. Firstly, there are several RNA secondary structures that need to be preserved for production of viral progeny, including IRESs, CREs, and as shown in the case foot and mouth disease virus (FMDV), packaging signals regularly interspersed throughout the genome (Logan et. al., 2018). Genomic RNA bound within picornaviral capsids has also been shown to be highly ordered, interacting with the interior aspects of capsid proteins (Shakeel et. al., 2016). Secondly, mutations are constrained by how they preserve the function of the translated viral proteins.

## 1.3 Oncolytic Picornaviruses

### 1.3.1 The field of oncolytic virotherapy

The inception of oncolytic virotherapy was a product of the early 20$^{th}$ century, inspired by reports of patients with cancers such as leukaemia and Hodgkin's disease surviving concomitant viral infections and showing evidence of clinical remission (Hoster, Zanes & Von Hamm, 1949, Pelner, Folwer & Nauts, 1958). These observations lead to a number of trials from the mid-to-late 20th century such as West Nile virus Egypt 101 against various cancers (Southam & Moore, 1952), Adenovirus versus cervical carcinomas (Georgiades et. al., 1959) and Mumps virus against various terminal cancers (Asada, T., 1974). Each of these trials showed varying degrees of protective effect. For instance, the trial concerning Adenovirus showed that 26 of 40 inoculations resulted in tumour necrosis (Georgiades et. al., 1959), and the Mumps virus trial resulted in complete regression of tumours in of 37 out of 90 trial subjects, as well as 42 instances of growth suppression (Asada, T., 1974). In 2015, an important milestone in the endeavour to make oncolytic virotherapy a viable therapy was reached. This

was the approval of the first oncolytic virus, modified herpes *simplex* virus-1 a.k.a. Talimogene Laherparepvec (T-VEC), by the US FDA for the treatment of malignant melanomas (Greig, S. L., 2016). Important to note is that T-VEC was not the first oncolytic virus to be approved worldwide, as Echovirus 7 (Rigvir) and modified adenovirus (Oncorine) have been approved in Latvia since 2004 (Alberts et. al., 2018) and China since 2005 respectively, (Xia et. al., 2004, Garber, K., 2006).

### 1.3.2 Naturally occurring oncolytic picornaviruses

There are species within the picornavirus family which, for a variety of reasons, have an innate selective toxicity against human cancers over healthy tissue. Figure 4 provides examples of picornaviruses shown in literature to have oncolytic activity, with little or minimal pathogenesis in humans.

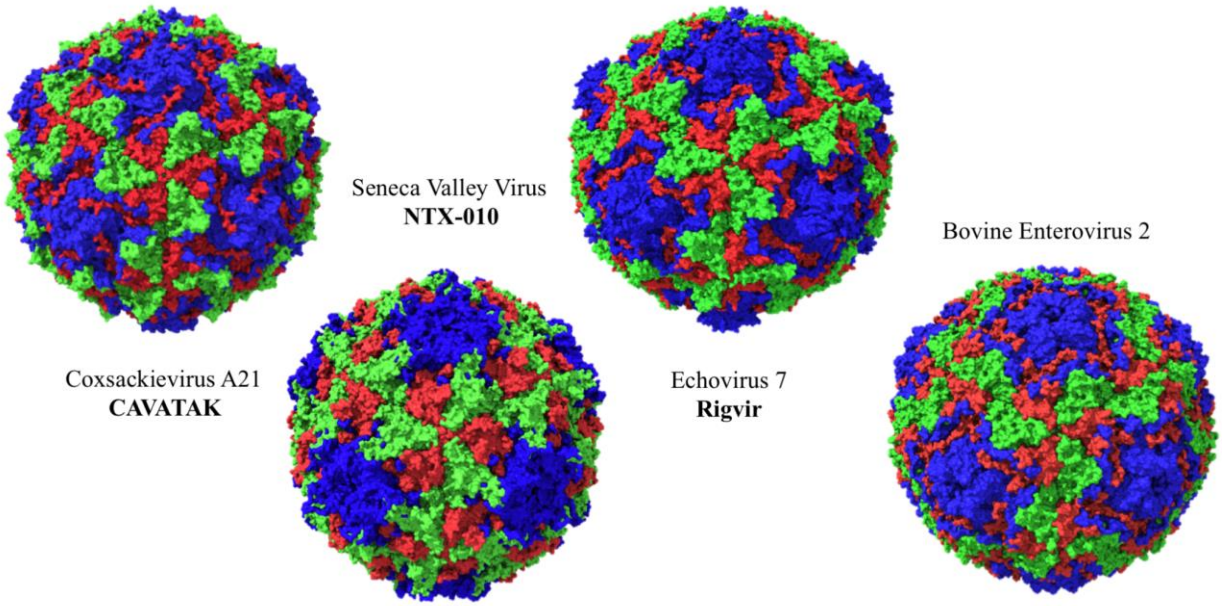


**Figure 4: Naturally occurring oncolytic picornaviruses.** A selection of picornaviral species whose oncolytic activity will be discussed, including coxsackievirus A21 (PDB accession number: 1Z7S) Seneca Valley virus (PDB accession number: 3CJI) echovirus 7 (PDB accession number: 2X5I) and bovine enterovirus 2 (PDB accession number: 1BEV).

#### 1.3.2.1 Coxsackievirus

The discovery of coxsackievirus is accredited to Dalldorf and Sickles. In attempting to isolate Poliovirus from affected patients using unweaned "suckling" mice, the two observed an atypical paralysis of these mice due to skeletal muscle destruction, rather than the central nervous system damage as would be expected in Poliovirus infection (Dalldorf & Sickles, 1948). The filtrable agent isolated from these mice could be inactivated in human sera and was shown to be distinct from other known viruses by host range (Dalldorf & Sickles, 1948). Since then the coxsackievirus species has broadened to include 29 serotypes, 23 in coxsackievirus A, which infect the skeletal muscle of mice, and 6 in coxsackievirus B, which infect a broader range of tissues (Bradley et. al., 2014). In humans, coxsackieviruses are considered "common-cold viruses", causing mild upper respiratory tract infections (Buckland, Bynoe & Tyrell, 1965). Most coxsackieviruses use Intercellular Adhesion Molecule 1 (ICAM-1) as a primary receptor to facilitate viral infection of susceptible cells, with Decay Accelerating Factor (DAF) as a secondary receptor (Bradley et. al., 2014). Exceptions do exist however, such as coxsackievirus B3, which utilises coxsackievirus and adenovirus receptor (CAR) (Shafren et. al., 2004).

The lion's share of research into coxsackievirus as an oncolytic agent has gone into coxsackievirus A 21 (CVA21), registered as CAVATAK® by Viralytics Inc. (Bradley et. al., 2014). CVA21 was investigated *in vitro* and *in vivo* in a range of cancers, including melanoma (Shafren et. al., 2004, Au et. al., 2005, Shafren et. al., 2014, Yuan et. al., 2015), multiple myeloma (Au et. al., 2007), breast cancer (Skelding et. al., 2009) and bladder cancer (Annels et. al., 2018). Highlights from these studies include that across these various cancers, ICAM-1 and DAF expression were strong predictors of susceptibility to CVA21 infection, and that in animal models, CVA21 reliably suppressed (Au et. al., 2005, Skelding et. al., 2009, Shafren et.

al., 2014, Yuan et. al., 2015) or cleared (Shafren et. al., 2004, Annels et.al., 2018) introduced tumours. CVA21 was also shown to act in concert with other drugs such as immune checkpoint inhibitors (Shafren et. al., 2014, Yuan et. al., 2015) or viral-receptor upregulators (Annals et. al., 2018) to produce synergistic effects in eliminating *in vivo* tumours.

Results from the previously mentioned experiments inspired Phase I - II clinical trials with CAVATAK® in melanoma (Shafren, Smithers & Formby, 2011, Andtbacka et. al., 2015, Andtbacka et. al., 2015), late-stage cancers (Pandha et. al., 2015, Pandha et. al., 2016, Pandha et. al., 2017) and bladder cancer (Pandha et. al., 2016). The findings of these clinical trials have been overwhelmingly positive, with CAVATAK® having been shown to be safe (Pandha et. al., 2017), as well as in some cases producing objective or complete responses (Shafren, Smithers & Formby, 2011, Pandha et. al., 2015, Pandha et. al., 2016). Clinical trials with CAVATAK® are still underway, with multiple clinical trials currently recruiting patients.

Returning to the idea that CVA21 is a common cold virus, the transient and relatively mild infection brought about by this virus means that pre-existing immunity is common in humans (Au et. al., 2011). Pre-existing immunity of patients against CVA21 could mean that the virus is cleared before exerting therapeutic effects in a clinical setting. In anticipation of this phenomenon, a number of other less common coxsackievirus serotypes and strains have been investigated for a similar selective oncolytic activity to that of CVA21. For example, coxsackievirus A 13, A 15 and A 18 (CVA13, CVA15, CVA18) have each been tested as putative substitutions for CVA21, with CVA18 having the strongest selective activity against *in vivo* melanoma models, where all treated animals completely cleared tumours (Au et. al., 2011). Importantly, no donated serum samples from melanoma patients or commercial IgG samples were shown to have neutralising antibodies against CVA13, CVA15 or CVA18,

whereas 20% of melanoma patients and both commercial IgG samples contained neutralising antibodies to CVA21 (Au et. al., 2011).

Another trial pitted 28 enteroviral strains against 12 human cancer cell lines and a healthy bone marrow stroma control (Miyamoto et. al., 2012). From this trial CVB2 Ohio-1, CVB3 Nancy and CVB4 JBV emerged as promising candidates for oncolytic viruses, especially CVB3 Nancy, which could clear a number of lung cancer tumours *in vivo*, though at the cost mild hepatic dysfunction and myocarditis (Miyamoto et. al., 2012). CVB3 Nancy, as well as other strains of CVB3 including 31-3-93, H3 and PD, were later tested for their activity against colorectal cancers (Hazini et. al., 2018). In this study it was CVB3 PD that stood out, having not only the greatest oncolytic activity, but also having the least toxicity to the murine hosts (Hazini et. al., 2018). CVB3 strain 2035 was also shown to have dose-dependent toxicity against endometrial cancers in animal models as well as *ex vivo* patient derived samples (Lin et. al., 2018). Lastly, three coxsackievirus B 6 live enterovirus vaccine (LEV) strains, LEV8, LEV14 and LEV15 were evaluated for toxicity against a panel of cancers of diverse origin (Svyatchenko et. al., 2017). LEV15 distinguished itself amongst the other strains by virtue of its selectivity for cancer cell lines. Importantly, LEV15 was shown to be able to bio-adapt to cell lines such as RD rhabdomyosarcoma cells and MCF-7 breast cancer cells, after repeat passage through these cells (Svyatchenko et. al., 2017). This observation, as well as that of the previously mentioned study wherein CVB3 PD was shown to have developed some adaptation to healthy cells, provides an interesting dual consideration (Hazini et. al., 2018). While it is encouraging that the host cell range of coxsackieviruses can be widened, thereby increasing the pool of patients that can potentially benefit from coxsackievirus virotherapy, this has to be measured against the converse eventuality that the virus becomes increasingly pathogenic.

#### 1.3.2.2 Echovirus

Enteric cytopathic human orphan (Echo)-viruses belong to the enterovirus B species. Like coxsackieviruses, clinical focus has largely centred around one particular strain of Echovirus, Echovirus 7 (EV7), registered as Rigvir® (Alberts et. al., 2018). Rigvir® is named for Riga, Latvia, where the viromic monitoring of patients receiving the Salk inactivated Poliovirus vaccine lead to the discovery of EV7 (Donina et. al., 2015). In Latvia, it is thought that as many as 75% of cases of melanoma are treated with Rigvir®, its widespread use possibly influencing its approval in Georgia, Armenia and Uzbekistan (Alberts et. al., 2018). However, in countries with the most stringent requirements for experimentally proven drug safety and efficacy, such as many countries of the European Union, United States of America, and Japan, Rigvir® has yet to be approved (Babiker et. al., 2017). This is likely due to the unavailability of the results of clinical trials which are alluded in the literature to have occurred between 1965 and 1991 (Alberts et. al., 2018).

Most of the experimental data that are available is in the form of case studies and retrospective studies, with some *in vitro* work. Beginning with *in vitro* experiments, EV7 has shown cytotoxicity against melanoma, pancreatic adenocarcinoma, muscle rhabdomyosarcoma, mesenchymal stem cells, gastric carcinoma, lung carcinoma and human normal dermal fibroblasts (Tilgase et. al., 2018). To date, five case studies have been published in peer-reviewed journals. These detail the improved outcomes of patients of a range of cancers and stages thereof after treatment with Rigvir®. One paper followed a stage IV melanoma patient, stage IIIA small-cell lung cancer patient and stage IV histiocytic sarcoma patient on a long-term Rigvir® regimen (Alberts et. al., 2016). Each of the patients were given different drugs alongside Rigvir®, and so the role of Rigvir® in improving their condition is unclear, but in any case, all three had improved conditions and were stable at the time of publication, with no

parameters exceeding NCI CTCAE grade 1 (Alberts et. al., 2016). The other case studies followed patients for whom the prognosis was especially poor. Rigvir® along with FOLFOX-4 and bevacizumab was used to treat a patient with a stage IV poorly-differentiated rectal adenocarcinoma, which carries a five-year predicted survival rate of 5% (Tilgase et. al., 2018). This drug cocktail caused sufficient suppression of metastases to allow further surgical resection of affected tissues, and further treatment post-surgery lead to complete response (Tilgase et. al., 2018). Finally, a case study in the treatment of a basal cell carcinoma (median expected survival 5 months) with Rigvir® as a monotherapy resulted in the patient being alive for 3.9 years up to the time up publication (Proboka et. al., 2018).

The last bodies of work on Rigvir® are retrospective studies. The results of one indicated a statistically significant increase in 3-year survival time of melanoma patients receiving Rigvir® when compared to patients from a historical cohort who had opted for surgery alone or surgery in combination with other immunomodulators (Donina et. al., 2015). This study also suggested that direct, intratumoural injection of Rigvir® was more efficacious than intramuscular infusion, an effect which may be in part explained by another finding that administering Rigvir® locally increases the total proportion of active (CD38+) and cytotoxic (CD8+) T-cells present (Bruvere et. al., 2002). Another retrospective trial enrolled stage IB through to stage IIC melanoma patients, with 52 patients enrolled for Rigvir therapy and 27 in a control group. The Rigvir® group in this case had a lower mortality rate, but the time spent disease-free was unchanged between the two (Donina et. al., 2015).

#### 1.3.2.3 Bovine Enteroviruses

The International Committee for the Taxonomy of Viruses (ICTV) regularly releases reports on the official nomenclature of viruses. It does so in an attempt to create a cohesive system

through which the disparate and varied virology research around the world can be produced and evaluated by virologists universally. As a consequence of this, viruses often have their names changed and are retroactively moved between species etc. While currently bovine enterovirus 1 (BEV1) & bovine enterovirus 2 (BEV2) are now categorised as enterovirus E & enterovirus F respectively (Adams et. al., 2013), much of the research into their oncolytic activity occurred before this distinction made, and so it becomes convenient to discuss them together.

Bovine enteroviruses do not cause disease in humans, but as their name suggests they are endemic pathogens of cows (Smythe et. al., 2002). The cytotoxicity of BEV1 against human cancer cell lines was first tested in 1971, when 65% of cancer cell lines tested met the threshold for significant viral killing by BEV1, compared to 4% of healthy cell lines (Taylor et. al., 1971). Of those cancer cell lines that were susceptible to BEV1 mediated killing, the degree of susceptibility varied widely, between 18% cell death in Ehrlich ascites and 98% cell death in L-cells (Taylor et. al., 1971). The variability of BEV1 cytotoxicity against these cell lines was thought to be receptor based, as cellular treatment with *Vibrio cholerae* neuraminidase (VCN) showed a dose and time dependent inverse correlation between VCN exposure and viral titre following BEV 261 infection in a panel of susceptible cancer cells (Stoner et. al., 1973).

Referring briefly back to coxsackievirus, CVB3 (Svyatchenko et. al., 2017) and CVB6 (Hazini et. al., 2018) were shown to be able to adapt to various cell lines through repeated passage, however, the same could not be achieved with BEV1 (Taylor et. al., 1971). The same study also showed that BEV1 could clear sarcoma-1 xenografts and suppress leukemia 4946 tumours in mice (Taylor et. al., 1971).

Somewhat atypically, in addition to the studies in mice, BEV1 has been tested in rabbits and dogs with cancer, which both tolerated BEV1 well (Hodes et. al., 1973). Of note: BEV1 treated mice were shown to suppress ascites sarcoma 180 tumours, and a BEV1 treated dog had a transient positive response to its seminoma (Hodes et. al., 1973). In the most recent study of oncolytic bovine enterovirus *in vivo*, rabbits with induced adult T-cell-like leukemia showed increased survival when given BEV MZ-468, with treatment animals surviving up to four months until the end of the trial, whereas control animals died by day 11 (Shingu et. al., 1991).

#### 1.3.2.4 Encephalomyocarditis Virus

Encephalomyocarditis virus (EMCV) was discovered in 1945 as a result of a captive male gibbon suddenly and inexplicably dying of pulmonary oedema and myocarditis (Helwig & Schmidt, 1945). Mice treated with the filtered fluid from this oedema developed paralysis and myocarditis (Carocci & Kassimi, 2012).

Columbia-SK virus, the name by which EMCV was known in 1965, was shown experimentally to exert therapeutic effects on fructose sarcomas in mice and rats, especially in rats (Kuwata et. al., 1965). While research into EMCV continued, research into its oncolytic properties underwent a 50-year hiatus before EMCV was shown to have significant selective toxicity against retinoblastomas (Adachi et. al., 2006) and clear-cell renal cell carcinomas (Roos et. al., 2010) *in vivo*.

### 1.3.3 Engineered oncolytic picornaviruses

While some picornaviruses have an innate selective toxicity for human cancers, there also exist picornaviruses specifically engineered for the purpose of oncolytic virotherapy. There are a number of reasons why these viruses may be altered, including attenuation of pathogenesis and

to increase immune evasion. Figure 5 contains examples of engineered picornaviral species, as well as the changes implemented for oncolytic virotherapy, which will be discussed in greater detail.

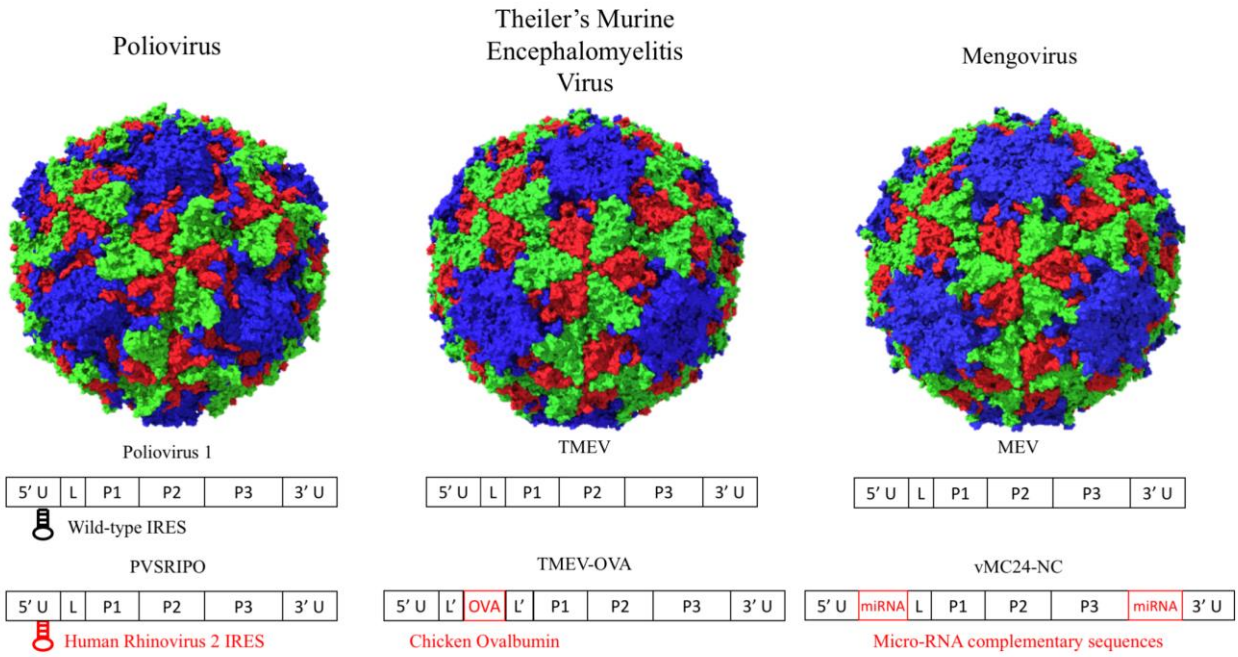


**Figure 5: Engineered oncolytic picornaviruses.** Poliovirus (PDB accession number: 1HXS) has been altered in a number of ways for oncolytic virotherapy, among them is the replacement of the wild-type IRES of the sabin strain of poliovirus 1 with that of human rhinovirus 2 to construct PVSRIPO. Theiler's murine encephalomyelitis virus (PDB accession number: 1TME) can be engineered to express tumour antigen in the leader protein, with chicken ovalbumin commonly used as a proof-of-principle. Oncolytic mengovirus (PDB accession number: 2MEV) attenuated by the introduction of sequences complementary to micro-RNAs upregulated in healthy tissue.

#### 1.3.3.1 Poliovirus

Poliovirus (PV) is best known as the causative agent of poliomyelitis, a disease which causes extensive paralysis in 1-2% of those people infected (Mehndiratta, Mehndiratta & Pande, 2014). The basis for PV causing poliomyelitis in humans is the gastric and neuronal cell expression of CD155, also known as Necl5 (nectin-like molecule 5) or PVR (Poliovirus receptor) (Strauss et. al., 2015). As wild-type poliovirus carries the inherent risk of poliomyelitis, the

investigation into poliovirus as a cancer therapeutic has been with the express goal of ameliorating neurotoxicity while retaining oncolytic activity. Among the engineered polioviruses investigated for their use in oncolytic virotherapy are live attenuated poliovirus (LAPV), poliovirus replicons, $A_{133}$Gmono-cre PV and perhaps most importantly PVSRIPO.

LAPV, which is the attenuated Sabin strain of poliovirus 1 (PV1), was shown to have infectivity in bone and soft tissue cancer cell lines *in vitro*, as well as being able to significantly decrease sarcoma xenograft tumours *in vivo* (Atsumi et. al., 2012).

Another method to attenuate PV neurotoxicity is by using replication incompetent poliovirus 1 (PV1) replicons. Encapsidated replicons with the P1 segment of the PV1 genome deleted have been produced by co-infection of helper cells with a complementing P1-encoding Vaccinia virus vector (Ansardi et. al., 2001). Once inside the targeted cell, the PV1 replicon RNA genome is capable of replicating and causing cell lysis. However, the replicons cannot form full encapsidated virions to spread to other cells, as the lack of the P1 region prevents capsid formation. PV1 replicons have shown broad spectrum cytotoxicity against central nervous system and non-central nervous system tumours, and *ex vivo* primary patient tumours (Ansardi et. al., 2001). PV1 replicons significantly prolong survival of murine glioblastoma models by infecting primary tumours as well as distal metastases (Ansardi et. al., 2001).

$A_{133}$Gmono-cre PV is a PV mutant engineered specifically for oncolytic virotherapy (Toyoda et. al., 2007). The development of $A_{133}$Gmono-CRE PV began with the observation that base substitutions in the 5' UTR can attenuate wild-type PV. The issue with this however, was that these substitutions were never stable (Toyoda et. al., 2007). To decrease the chance of revertant mutants, researchers designed mono-CRE PV, which was wild type PV1 with the CRE moved

from the 2C protein to the 5' UTR (Toyoda et. al., 2007). This both interrupted the 5' UTR and prevented escape mutants due to essential function of the CRE. Mono-CRE PV strains developed a range of adaptations to infecting neuroblastoma cells *in vivo* and *in vitro*, though a single mutant, $A_{133}G$, arose in both instances (Toyoda et. al., 2007). Going forward then, $A_{133}G$mono-cre PV was shown experimentally to have potent activity against neuroblastomas *in vivo* (Toyoda et. al., 2007). Both the $CD8^+$ T-cells from $A_{133}G$mono-CRE treated mice and the non-infectious lysate from $A_{133}G$mono-CRE treated neuroblastoma cell cultures were later shown to effectively vaccinate mice from neuro-2a neuroblastoma cell challenge (Toyoda et. al., 2011).

The greatest current prospect for the use of PV as a cancer therapy is PVSRIPO. PVSRIPO (sometimes referred to as "PV1(RIPOS)" in early literature) is the Sabin strain of PV1 (PVS) with IRES substituted with that of Human Rhinovirus 2 (HRV2) (Gromeier, Alexander & Wimmer, 1996, Jahan, Wimmer & Mueller, 2011). This attenuates PVSRIPO in neuronal cells (Jahan, Wimmer & Mueller, 2011, Cello et. al., 2008). There are a few reasons for this attenuation. For one, the HRV2 IRES is thought to have properties unsuited for the recruitment and activity of translation complexes specific to neurons (Brown & Gromeier, 2015). Another is the sequestration of double stranded RNA binding protein 76 (DRBP76) to the nuclear compartment of neoplastic cells, as opposed to its role in binding secondary structural elements of the HRV2 IRES in the cytoplasm of healthy cells (Brown & Gromeier, 2015). Cancer cells, generally speaking, have deregulated mitogenic signalling, and as such favour the $m^7G$ cap-independent translation of viral genomes (Brown & Gromeier, 2015).

PVSRIPO has demonstrated potent oncolytic activity in a breadth of cancers, including gliomas (Merrill et. al., 2004), breast cancers (Ochiai et. al., 2004, Holl et. al., 2016), glioblastoma

multiforme (Ochiai et. al., 2006), melanomas (Walton et. al., 2018), astrocytomas (Yang et. al., 2009, Dobrikova et. al., 2008) and prostate cancers (Holl et. al., 2016).

The oncolytic activity of PVSRIPO is in part due to its immunostimulatory properties. PVSRIPO causes sub-lethal infection in human macrophages, inducing expression of major histocompatibility complex class II (MHC II) and costimulatory molecules, leading to IFN-β, IL-12 and TNF-α production (Brown et. al., 2015). This immune stimulating effect could also be induced in human dendritic cells (DCs) after incubation with the virus-free lysate of PVSRIPO destroyed cells, stimulating tumour-antigen specific T-cells (Brown et. al., 2017). Similar to macrophages, activation of DCs occurs partially through sublethal infection producing low viral progeny, and is magnified in the presence of tumour lysate, as measured by CD40, CD80, IFN-β and TNF-α expression (Brown et. al., 2015). PVSRIPO oncolysis releases cancer antigens, including MART-1 (melanoma-associated antigen recognised by T-cells-1), DAMPs (damage-associated molecular patterns, e.g., HSP 60/70/90, HMGB1 protein) and double-stranded RNA (dsRNA) (Brown et. al., 2017). In mice, mRIPO, which is PVSRIPO adapted to mouse astrocytoma cells, was used to treat OVA-expressing melanomas. Infection of these melanomas with mRIPO produced cytotoxic T-lymphocytes (CTLs) primed against OVA, as well as native melanoma antigen tyrosinase related protein 2. This delayed tumour growth, increased survival times and induced invasion of neutrophils, DCs and T-cells in to tumours (Brown et. al., 2017).

As with any PV-based vaccine, PVSRIPO has been tested for pathogenesis in macaques, as per World Health Organisation (WHO) standards. *Ex vivo* cultures of macaque and human kidney cells displayed no appreciable infection after exposure to PVS or PVSRIPO (Dobrikova et. al., 2012). In live macaques, PVSRIPO was patently safe, with all animals surviving to trial's end. The tested macaques also did not shed virus in bodily fluids and only one had any measurable

viral titre in the spinal cord and pons / medulla (Dobrikova et. al., 2012). PVSRIPO has been entered in to clinical trials. One Phase I clinical pitted PVSRIPO against a 13-strong cohort of patients with recurrent glioblastoma. Consistent with the trial in macaques, this trial demonstrated the safety of PVSRIPO, with no patients developing adverse NCI CTCAE (National Cancer Institute Common Terminology Criteria for Adverse Events) events grade 3 or above from PVSRIPO, though one experienced a grade 4 event from a catheter removal (Trotti et. al., 2003, Desjardins et. al., 2014). Another Phase I clinical trial of 61 glioblastoma patients focused on dose finding, indicating an optimal treatment dose of $5x10^7$ $TCID_{50}$ (Desjardins et. al., 2018). This trial also showed PVSRIPO had a protective effect on patient survival when compared to historical controls, with a 36-month survival rates of 21% and 4% respectively (Desjardins et. al., 2018).

#### 1.3.3.2 Theiler's Murine Encephalomyelitis Virus

The prospective use of Theiler's murine encephalomyelitis virus (TMEV) for cancer therapy deviates from that of most other oncolytic viruses. This is because rather than direct infection and lysis of tumour cells, TMEV is more often engineered to express tumour antigen, thereby directing the host immune system to clear tumours as an extension of clearing TMEV.

Most commonly in the literature, chicken ovalbumin (OVA) is introduced to the Leader protein of TMEV (TMEV-OVA) to generate a cytotoxic immune response against tumours also exogenously expressing OVA. While the addition of OVA comes at a cost to the virulence of TMEV (Pavelko et. al., 2011, Pavelko et. al., 2013), this alteration has indeed been shown in multiple studies to generate adaptive immunity to OVA (Bell et. al., 2014), leading to suppression of tumours and increased survival times in murine models (Renner et. al., 2015).

TMEV is known to harbour a highly immunogenic region in the VP2 capsid protein ($VP2_{121-130}$) and so any adaptive immune response generated against TMEV-OVA is in part against OVA, and in part against TMEV, including $VP2_{121-130}$ (Bell et. al., 2014). As $VP2_{121-130}$ specific immunity does not further the cause of tumour suppression, attempts have been made to emphasise OVA-specific immune responses over $VP2_{121-130}$ specific immune responses. Deletion of the $VP2_{121-130}$ region in TMEV-OVA was shown to increase the relative amount of Cytotoxic T-Lymphoctyes (CTL's) targeted against OVA *in vivo* (Bell et. al., 2014). Vector silencing on the other hand, the exposure of the host to TMEV viral proteins before TMEV-OVA infection, seemed not to have any effect on the immune response directed toward OVA, tumour progression, or overall survival of mice with melanoma or glioma (Malo et. al., 2017).

OVA is widely used as a model antigen for its high immunogenicity (Martner et. al., 2013), but authentic tumour antigen is often not as immunogenic. That being said, engineered TMEV vaccination does still work with weakly immunogenic tumour antigen, as shown by experiments with TMEV expressing p66 in a murine breast cancer model (Pavelko et. al., 2013).

Not all of the research on TMEV in an oncolytic context has been as a cancer vaccine. While the DA strain of TMEV was ineffective in controlling breast cancers and melanomas *in vivo*, a chimeric fusion with the more neurovirulent strain GDVII was effective, significantly delaying B16 melanoma tumour outgrowth and increased survival when compared to DA strain and vehicle controls (Bell & Pavelko, 2016). This fusion took the 3' end of the 5' UTR to the 3' end of the 2C protein of the DA strain and replaced it with that of the GDVII strain, the resultant chimeric virus named GD7-KS1 (Bell & Pavelko, 2016).

#### 1.3.3.3 Mengovirus

Mengovirus (MEV) was originally isolated from a Rhesus monkey which developed sudden paralysis. MEV is a novel virus in that it has a diverse range of mammalian hosts, including voles, squirrels, elephants, swine, wild boar, racoons, antelope, lions, birds and several species of non-human primate (Carocci & Kassimi, 2012).

Due to the tenacity with which MEV infects a broad range of mammalian cell lines, research into its oncolytic activity has been undertaken with an attenuated version of MEV, $vMC_{24}$, which is a poly-C truncated mutant (Dethlefs et. al., 1997). However, even this mutant caused paralysis in test mice, and so researchers utilised a novel strategy in engineering $vMC_{24}$ to include complementary sequences to micro-RNA's (miRNAs) preferentially expressed in healthy tissues infected by $vMC_{24}$ (Ruiz et. al., 2016). A number of $vMC_{24}$ variants were produced, with combinations of sequences complementary to miR125b (expressed in brain tissue), miR124 (expressed in neurons), miR133 and miR208a (enriched in cardiomyoctyes). Among these, a construct called $vMC_{24}$-NC stood out as producing low viral titres in the brain, spine and heart of infected test mice (Ruiz et. al., 2016). Not only did $vMC_{24}$-NC not cause negative side-effects, but it could also clear multiple myeloma tumours previously shown to be refractory to $vMC_{24}$ infection in 40% of mice (Ruiz et. al., 2016). $vMC_{24}$-NC contained two copies of complementary miR124 sequences in the 5' UTR, and one of each of miR133b and miR208a in the 3' UTR (Ruiz et. al., 2016).

## 1.4 Seneca Valley Virus

### 1.4.1 Introduction and discovery

Seneca Valley virus (SVV) is a member of the *picornaviridae* family as well as the first and namesake species of the senecavirus genus (Hales et. al., 2008.; Cartens, E. B., 2009; Adams et. al., 2015). A schematic representation of the SVV genome as well as the internal and external structures of the protomers, pentamers and capsids based on SVV crystal structure is shown in Figure 6 (Venkataraman et. al., 2008).

The first strain of SVV to be discovered, SVV-001, was initially observed as a cell culture contaminant during development of a paired, replication-deficient adenovirus – helper cell gene therapy vector production system (Fallaux et. al., 1998). When this gene therapy vector production system, PER.C6 cells and E1 deleted adenovirus, was used again in 2002, cell cultures that succumbed to premature cytopathic effect (CPE) were investigated. Purification by ultracentrifugation followed by Sodium Dodecyl-Sulfate Polyacrylamide Gel Electrophoresis (SDS-PAGE) revealed three protein bands of 36, 31 and 27 kDa length. These most likely corresponded to SVV VP2, VP3 and VP1 respectively (Strauss et. al., 2018). N-terminal sequencing of two of the protein bands revealed a close sequence relatedness to cardioviruses. Viral infection of PER.C6 cells was also confirmed with electron microscopy of cells inoculated with purified virus. SVV gets its name from Seneca Valley, Maryland, USA where Gene Therapy Inc., who performed this work, is located.

SVA can be stratified into 3 clades based on temporal isolation. Clade I consists of the originally isolated strain SVV-001, Clade II is a grouping of historical SVV strains taken from samples isolated in the US from the 80's and 90's that were re-tested following discovery of SVV, and Clade III refers to the strains isolated since SVV's discovery (Segales et. al., 2017).

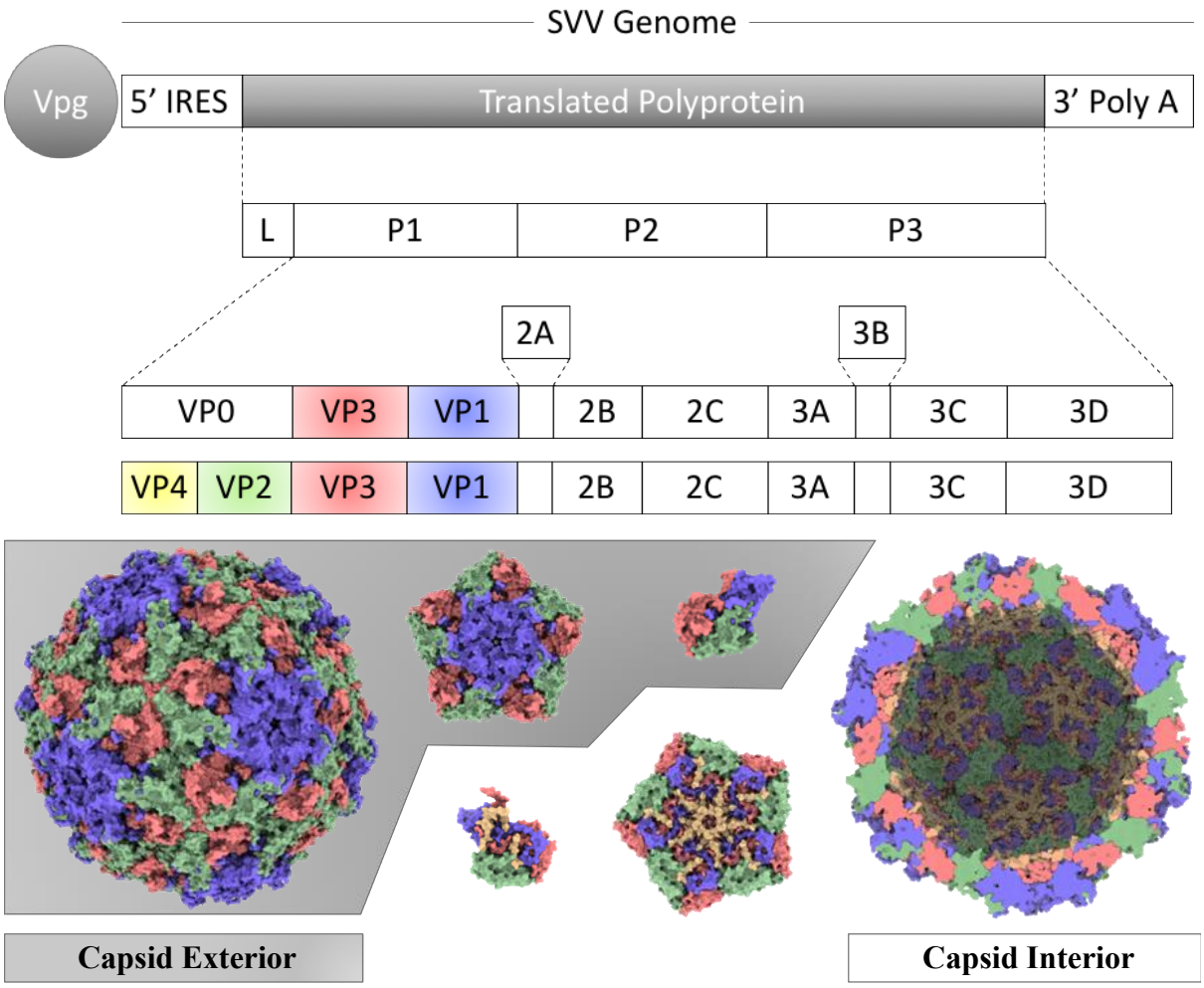


**Figure 6: Organisation of the SVV genome**. Starting with the positive-sense, single stranded RNA genome in its full form, complete with genome associated protein (Vpg), descending through the translated polyprotein, its further division by viral proteases and finally maturation of structural proteins as a result of genome packaging (Hales et. al., 2008). Also shown are the crystal structures of the interior and exterior of the protomer, pentamer and viral capsid (Venkataraman et. al., 2008). Capsid structures generated with UCSF Chimera (Petterson et. al., 2004).

### 1.4.2 A novel oncolytic picornavirus

SVV is counted among the ranks of picornaviruses that display a natural selective tropism for human cancer cells (Morton et. al., 2010).

*In vitro* studies of SVV indicated potent, selective activity against a range of cancer cell lines with a unifying feature of having neuroendocrine features. Figure 7 surmises two *in vitro* studies of SVV-001 (NTX-010) against panels of cancer and non-cancer cell lines.

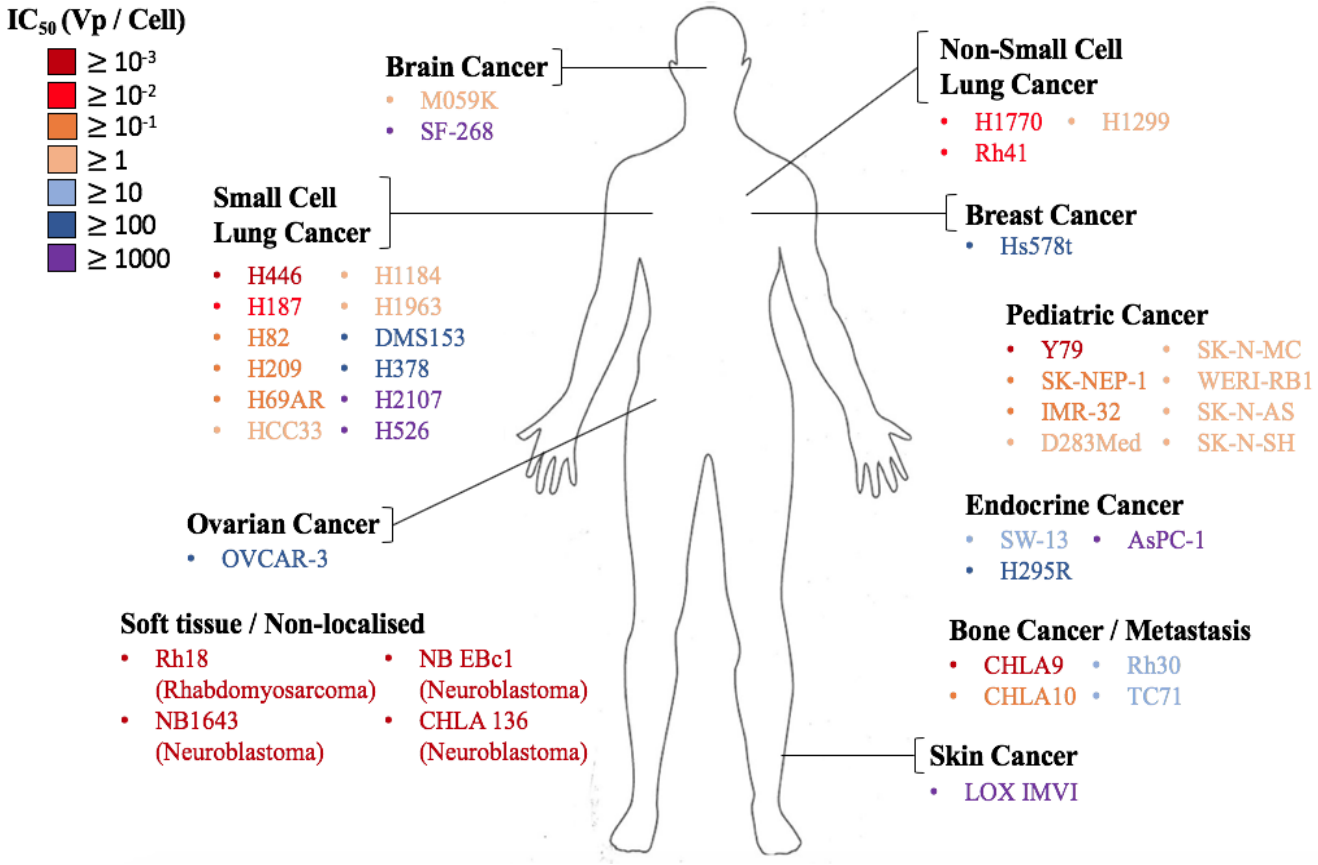


**Figure 7: In-vitro cytotoxicity of SVV-001 for cancer cell lines of human origin.** Human cancer cell lines were organised by the site of original isolation and stratified by $IC_{50}$ (proportion of SVV-001 versus target cell line required to cause death in 50% of those cells) according to pooled results from two studies (Reddy et. al., 2007.; Morton et. al., 2010). Those cell lines studied which showed no permissivity to SVV infection were omitted.

These studies showed the very first signs of the potential for SVV to be used as a cancer therapeutic. One of the *in vitro* studies also showed that SVV-001 is not inactivated by human blood components, does not cause haemagglutination of human erythrocytes and that neutralising antibodies to SVV-001 have a very low prevalence among a random selection of

blood samples (Reddy et. al., 2007). The same study also showed that SVV-001 is well tolerated in murine models (Reddy et. al., 2007).

Researchers then began to evaluate SVV efficacy in an *in vivo* setting. Attached to one of the aforementioned *in vitro* studies was a trial in which H446 (Small Cell Lung Cancer) and Y79 (Retinoblastoma) cells were injected in to the flank of athymic mice. In both cases SVV-001 was sufficient to completely destroy these tumours, and at the lower concentrations a reduction in tumour mass was shown in H446 (Reddy et. al., 2007). Another trial centred around the treatment of retinoblastomas in mouse xenograft models, as the previous trial showed success with the Y79 cell line, but did not address the ability for SVV to diffuse across the blood-brain barrier (BBB). Traversing the BBB would be necessary if SVV-001 were ever to be used in a clinical setting for the treatment of retinoblastoma. SVV-001 was shown in this study to greatly reduce intraocular tumour burden and thus was able to cross the BBB (Wadhwa et. al., 2007). Though some residual tumours were observed to remain post-treatment, this was thought to be due to lack of tumour vasculature, which would not be the case in a human retinoblastoma (Wadhwa et. al., 2007).

The ability for SVV-001 to cross the BBB brings into question other important cancers which are complicated by the necessity of drug permeability across the BBB. One such cancer is medulloblastoma, the most common form of paediatric brain cancer (Rood, MacDonald & Packer, 2004; Huse & Holland, 2010). An *in vivo* study of 10 primary medulloblastoma xenograft mice, 5/10 had significant tumour growth repression, while the other 5 did not (Yu et. al., 2010). Another important finding from this study was that a subpopulation of medulloblastoma Cancer Stem Cells (CSC's), identified as being $CD133^{+}$, are effectively

killed by SVV-001 (Yu et. al., 2010). This is important as CSC's are thought to have increased resistance to radiation therapy (Hambardzumyan et. al., 2008).

Based on encouraging results with medulloblastoma treatment, a similar trial involving 6 glioma xenografts was undertaken. *In vitro* experiments showed among these clinical isolates, 4 were permissive to SVV-001, while 2 were resistant, and this was consistent for both cell monolayers and neurospheres (Liu et. al., 2013). This trial also showed that intravenous SVV-001 injection of $5x10^{12}$ viral particles per kg mouse body weight (vp/kg) had a significant effect in prolonging survival times in mice with medium (1-4 mm) and small (<1 mm) xenograft tumours from permissive cell lines, and interestingly also one of the resistant cell lines (Liu et. al., 2013).

H446 Small-Cell Lung Cancer (SCLC) cells were shown to be particularly susceptible to SVV-001 infection. To interrogate the activity of SVV against SCLC more broadly, tumour cells from three classic and three variant sub-type patient tumours were grown *in vitro* and transplanted into mice (Poirier et. al., 2013). *In vitro* and *in vivo* testing showed that the classic sub-type SCLC was completely resistant to SVV oncolysis, whereas the variant sub-type cells were highly susceptible (Poirier et. al., 2013). This lead to the hypothesis that susceptibility to SVV might be positively correlated to NEUROD1 expression, and negatively correlated with ASCL1 expression (Poirier et. al., 2013).

SVV has entered a number of clinical trials. First, a phase I clinical trial of 30 patients with SCLC was undertaken (Rudin et. al., 2011). Patients treated with NTX-010 between $10^7$ to $10^{11}$ vp/kg showed no dose limiting toxicities, with flu-like symptoms mainly manifesting in the lower dose cohorts. Neutralising antibodies were detected as early as two weeks into treatment. In terms of

outcomes, one patient showed disease stabilisation while another five had minor responses, which were not sufficient to meet response evaluation criteria in solid tumours (RECIST) criteria (Eisenhauer et. al., 2009). The patient with stable disease was alive three years post trial, up until the time of publication, with positron-emission tomography (PET) scans revealing a 50% decrease in tumours (Rudin et. al., 2011). Shortly after, a second Phase I clinical trial was launched in cohort of children with neuroblastoma, rhabdomyosarcoma or other rare tumours with neuroendocrine features (Burke et. al., 2014). In part A of the trial, 13 patients were injected with $10^9$, $10^{10}$ or $10^{11}$ vp/kg NTX-010, and in part B, patients were given oral (days 1 to 14) and intravenous (days 1 and 8) cyclophosphamide, in combination with two doses of $10^{11}$ vp/kg NTX-010. The study showed that NTX-010 was well tolerated with a single dose limiting toxicity event recorded. While no objective response was observed, six patients did show disease stabilisation. A rapid neutralising antibody response to NTX-010 was also shown in this trial (Burke et. al., 2014).

Finally, a single Phase II clinical trial was undertaken in SCLC patients who had been stable or responding after a regimen of four cycles platinum-based chemotherapy (Molina et. al., 2013). Patients were randomised into Arm A or Arm B and treated with a single dose of $1x10^{11}$ vp/kg NTX-010 or the saline control respectively. Within Arm A there were three observed grade 4 events, with none in Arm B. Between Arms A and B there was no difference in progression-free survival and overall survival was only marginally different in Arm A (83%) vs. Arm B (85%). This clinical trial was also put on hold while the death of one patient was confirmed not to have been caused by NTX-010 treatment (Molina et. al., 2013).

The results of the two Phase I clinical trials and the single Phase II clinical trial seemed to be at odds with each other, and with the promising results of the *in vitro* and *in vivo* trials. It

seemed then, that there was a lack of knowledge with respect to the defining characteristic that determined the distinct cellular susceptibility to SVV-001. In 2017 however, this defining characteristic was discovered. This was that the cellular receptor for SVV-001 is Anthrax Toxin Receptor 1 (ANTXR1), known also as Tumour Endothelial Marker 8 (TEM8) (Miles et. al., 2017). This provides a key criterion by which future clinical trials can select patients who might benefit from NTX-010 therapy. ANTXR1 is a useful receptor in cancer therapy as it is upregulated in 60% of human cancers, and only weakly expressed in healthy cells (Miles et. al., 2017). That being said, ANTXR1 expression is necessary but not sufficient for successful infection and lysis of cancer cells (Miles et. al., 2017). Interestingly, the genome-less procapsid of SVV can also bind ANTXR1 (Strauss et. al., 2018).

### 1.4.3 An emerging porcine pathogen

As previously alluded to, SVV-001 was first isolated as a contaminant of cell culture. SVV-001 was thought to be introduced through porcine trypsin, which is used to detach cells from culture vessels. This is because SVV has been shown to cause mild, self-limiting disease in pigs, with the exception of neonatal piglets, for whom SVV infection can be lethal (Segales et. al., 2017). The mild disease experienced by older pigs is characterised by the formation of vesicles around the mouths and coronary bands, which when the aetiological agent is not known, is termed porcine/swine idiopathic vesicular disease (PIVD/SIVD) (Singh et. al., 2012).

Currently, Clade III SVV is causing disease in pigs from Canada (Pasma, Davidson & Shaw, 2008), the United States (Zhang et. al., 2015), Colombia (Sun et. al., 2017), Brazil (Leme et. al., 2015), Thailand (Saeng-Chuto et. al., 2018) and China (Zhao et. al., 2017). While the disease that SVV causes in these countries is not of concern in and of itself, it is clinically

indistinguishable from foot and mouth disease, thereby forcing immediate and costly quarantine and investigation of afflicted animals.

## 1.5 Project

This project comes in the context that cancer is highly prevalent, causing millions of deaths every year. This is despite the advances that have been made with respect to diagnosis of cancer and its treatment with surgery, chemotherapy and radiation therapy. In addition, each of these medical interventions comes with their own side effects which can significantly reduce the quality of life of treated persons. To address the bipartite problem of cancer mortality and the inefficacy and toxicity of contemporary treatments, new treatments are needed that are conversely effective and non-toxic.

The necessity for new safe and effective treatments has born a number of promising therapies such as immunotherapy and the use of oncolytic viruses. Within the broad range of viral taxa that are employed for oncolytic virotherapy are a family of small, positive-sense RNA viruses, called picornaviruses. A number of naturally occurring and engineered picornaviruses have been investigated for their potential use as cancer therapeutics, but the subject of this particular project is Seneca Valley virus (SVV), a naturally occurring virus endemic in pigs. SVV has a selective tropism for cells expressing Anthrax Toxin Receptor 1 (ANTXR1), otherwise known as Tumour Endothelial Marker 8 (TEM8), which is upregulated in many cancers.

ANTXR1 is necessary, but not sufficient, for the successful infection, intracellular replication and subsequent lysis of host cells by SVV. This means that there are cancers to which SVV can attach and infect, but not destroy. To increase the range of cancers that are potentially treatable by SVV, it has been proposed that the empty capsids of SVV, which can still bind

ANTXR1, be utilised as drug delivery vectors to deliver cytotoxic drugs / prodrugs. Among the primary issues with this idea is the intrinsic instability of the SVV empty capsids. To facilitate SVV's use as a drug delivery vector then, there needs to be a way to stabilise these empty capsids.

The aim of this project is to identify the residues and mutations thereof that confer increased stability to the capsid of SVV-001, and the mechanisms by which this occurs.

We hypothesise that the inherently error-prone process of SVV viral replication, which brings about the quasispecies phenomenon, will inevitably produce SVV virions with increased stability. We plan to use exposure to heat to select for these hypothetical thermostable virions out of the heterogeneous population, and on purification and sequencing, determine how they compare to the wild-type. We will then explore this difference.

# 2 Methods and Materials

## 2.1 Cells and virus

### 2.1.1 Cell culture reagents and materials

R10 media: Roswell Park Memorial Institute 1640 medium (GibcoTM, Fischer scientific catalogue number: 11-875-127) plus 20mM HEPES and 3.7 g $L^{-1}$ $NaHCO_3$.

FBS: Foetal Bovine Serum. Moregate FCS, Lot#29827102

### 2.1.2 Sub-culturing reagents

TrypLE (ThermoFisher Scientific catalogue number: 12563-029)

PBS: Phosphate Buffered Saline

15 mL falcon tubes (Greiner Bio-One CELLSTAR catalogue number: 188271)

T25 25 $cm^2$ cell culture vessel (Greiner Bio-One CELLSTAR reference number: 690160)

T75 75 $cm^2$ cell culture vessel (Greiner Bio-One CELLSTAR reference number: 658170)

10 mL tissue culture pipette (Greiner Bio-One CELLSTAR reference number: 607180)

25 mL tissue culture pipette (Greiner Bio-One CELLSTAR reference number: 760180)

### 2.1.3 Sub-culturing protocol

When cells had grown to confluence, commonly every 3-4 days, the media was decanted from the T75 culture vessel. The cells were then washed with PBS twice. 0.5 mL of TrypLE was then added to the cells and they allowed to incubate for a few minutes at 37 °C + 5% $CO_2$. 2 mL of cell line appropriate growth media was added and pipetted up and down to ensure detachment of cells from the T75 tissue culture vessel. The cells and media were then transferred to a sterile 15 mL falcon tube using a 10 mL pipette. The 15 mL falcon tube was centrifuged for 5 minutes at 1,200 rpm. Without disturbing the cellular pellet, the media was decanted. The pellet was then brought up to a single cell suspension in 9 mL by pipetting up in down with a 10 mL tissue culture pipette. A confluent tissue culture vessel would be split 1:3 by 6mL of the cell suspension for being used for other experiments / or discarded. The

remaining 3 mL was then re-seeded in a T75 with 10mL fresh media and the cell line, media, date and passage number were recorded on the vessel.

### 2.1.4 Cell counting

A clean cover slip was placed on a haemocytometer. From a 15 mL falcon tube containing a single cell suspension of cells and media, a small volume (10 µL for one reading, 20 µL for two readings on the same haemocytometer) was taken from the falcon tube and loaded onto the haemocytometer. The haemocytometer was then examined under a light microscope, the cells in the grid counted and the cell numbers enumerated with the following formula.

$$Total\ cell\ numbers = Cells\ counted\ x \frac{1}{dilution\ factor}\ x\ 10{,}000\ x\ Volume\ in\ falcon\ tube$$

### 2.1.5 Viral strains

Initial stocks of SVV-001 kindly provided by collaborators Linde A. Miles and John T. Poirier from the Molecular Pharmacology Program and Department of Medicine, Memorial Sloan Kettering Cancer Center, New York, New York, USA. SVV-001 was further amplified and isolated in the Bostina Lab.

## 2.2 Plaque formation assay

### 2.2.1 Plaque assay: reagents and materials

R10 media (GibcoTM, Fischer scientific catalogue number: 11-875-127)

FBS: Foetal Bovine Serum. Moregate FCS, Lot#29827102

Tissue culture agarose (Lonza catalogue number: 50100)

12-well plates (Greiner Bio-One CELLSTAR reference number: 665180)

### 2.2.2 Plaque formation assay: protocol

Individual wells of 12 well plates were seeded with H446 cells in 1 mL R10 + 10% FBS and allowed to attach overnight. The next day the medium was removed, replaced with 100 µL, 10-fold serial viral dilutions in R10 media + 2% FBS or media only controls. They were allowed to incubate for an hour with regular stirring. The media was then removed from the wells and

replaced with 1 mL 2X R10 + 2% FBS + 1% agarose. This was allowed to set overnight while incubating at 37 °C + 5% $CO_2$. After 24 hours, plaques were counted and viral titres were derived from the following equation.

$$Viral\ titre = Plaques\ counted\ x \frac{1}{dilution\ factor}\ x\ \frac{1\ mL}{volume\ plated\ (mL)}$$

## 2.3 Thermal stability probe

### 2.3.1 Thermal stability probe reagents

R10 media (GibcoTM, Fischer scientific catalogue number: 11-875-127)

Bio-Rad T100™ Thermal Cycler (Bio-Rad, Hercules, California, USA)

0.2 mL PCR tubes (Lab supply catalogue number: AXY321-01-102)

### 2.3.2 Thermal stability probe protocol

Initial method

50 µL of 1:50 dilutions of a $5x10^{10}$ PFU/mL SVV-001 stock in 0.2 mL PCR tubes were sonicated and heated to desired temperatures in thermocycler for 30 minutes and cooled back down to 12 °C. The viral titres of the heated samples, as well as unheated controls were enumerated using plaque formation assays (See: 2.2 Plaque formation assay).

Revised method

From a 1:1000 dilution of a $5x10^{10}$ PFU/mL SVV-001 stock, paired 50 µL samples were taken, one would be heated to the desired temperature in a thermocycler for 30 minutes, and the other kept at room temperature for the same time. Both were then enumerated with plaque formation assays (See: 2.2 Plaque formation assay).

## 2.4 Selection for thermostable viral mutants

### 2.4.1 Selection for thermostable viral mutants: reagents and materials

0.2 mL PCR tubes (Lab supply catalogue number: AXY321-01-102)

Bio-Rad T100$^{TM}$ Thermal Cycler (Bio-Rad, Hercules, California, USA)

50,000 MWCO centrifugal filters (Amicon reference number: UFC805024)

T25 25 cm$^2$ cell culture vessel (Greiner Bio-One CELLSTAR reference number: 690160)

### 2.4.2 Selection for thermostable viral mutants: protocol

Viral samples in 0.2 mL PCR tubes were heated to desired temperatures in thermocycler for 30 minutes and cooled back down to 12 °C. The viral titres of the heated samples, as well as unheated controls were enumerated using plaque formation assays (See: 2.2 Plaque formation assay). Virus from the heated sample was infected at an MOI of 0.1 through a confluent T25 containing approximately 1.72x10$^6$ H446 cells. The virus was allowed to infect the cells over 48 hours. The flasks were then collected and freeze-thawed three times at -80 °C to lyse the cells. The cell debris was separated from the supernatant by centrifugation for 5 minutes at 3,000 rpm. The supernatant was then passed through a 50,000 molecular weight cut-off filter. The bulk liquid that passed through the filter was discarded and the liquid that didn't pass through was resuspended in 100 µL R10 media + 2% FBS. This was further divided into two 0.2 mL PCR tubes, one which would then serve as the unheated control and one which would then be heated and titred as before.

## 2.5 Viral purification

### 2.5.1 Optiprep® viral purification: reagents and materials

R10 media (GibcoTM, Fischer scientific catalogue number: 11-875-127)

FBS: Foetal Bovine Serum. Moregate FCS, Lot#29827102

T175 175 cm$^2$ culture vessels (Greiner Bio-One CELLSTAR reference number: 660160)

60% Optiprep stock solution (Axis Shield product number: 1114542)

250 mL Nalgene bottles (ThermoFisher catalogue number: 2103-0008)

Beckman Coulter Avanti J-26 XP1 high-speed centrifuge (Beckman Coulter, Indianapolis, USA)

Fiberlite F250 rotor (ThermoFisher Scientific Waltham, Massachusetts, USA)

Beckman Coulter Optima XPN-80 ultracentrifuge (Beckman Coulter, Indianapolis, USA)

Beckman Coulter SW32.1 Ti rotor (Beckman Coulter, Indianapolis, USA)

Beckman 16.8 mL polypropylene tubes (Beckman Coulter reference number: 337986)

Beckman 36 mL polypropylene tubes (Beckman Coulter reference number: 326823)

### 2.5.2 Optiprep® viral purification: protocol

H446 cells were grown to confluence in six T175 culture vessels containing 35mL R10 + 10% FBS. The growth media in each culture vessel was replaced with 25 mL infection media containing 20 mL R10 + 2% FBS and 5mL R10 + 2% + 1 µL SVV 1:40 µL viral dilution in R10. The cells and virus were incubated at 37 °C + 5% $CO_2$ for 48 hours, or until complete cytopathic effect was observed. The cells were then freeze-thawed from -80 °C to room temperature repeatedly to lyse the cells. The media containing virus and cells from all of the culture vessels were combined in 250 mL Nalgene bottle(s) and balanced with Nalgene bottle(s) containing water. The Nalgene bottles were centrifuged at 10,000 g for 1 hour at room temperature using a Fiberlite F250 rotor in a Beckman Coulter Avanti J-26 XP1 high-speed centrifuge. The virus containing supernatant was collected and the cell debris pellet was stored at 4 °C. The virus containing supernatant was added to 36 mL tubes, balanced and placed in Beckman Coulter SW 32 buckets. They were then spun down for 2 hours at 28,500 rpm using a Beckman Coulter SW32.1 Ti rotor in a Beckman Coulter Optima XPN-80 ultracentrifuge. The supernatant was decanted and stored at 4 °C. The viral pellet was covered with 200 µL sterile PBS and stored overnight. The following day the viral pellet was vigorously resuspended and loaded into a 17 mL tube containing 25% optiprep solution, underlaid with 2mL 50% optiprep. The tubes were loaded into SW 32.1 buckets and centrifuged for 1 hour at 28,500 rpm using a Beckman Coulter Optima XPN-80 ultracentrifuge. The viral band on the interface of the 25% and 50% optiprep solutions was then disturbed by pipetting up and down, and the

tubes spun down for 18 hours at 28,500 rpm using a Beckman Coulter Optima XPN-80 ultracentrifuge. Virus from observed bands was then collected and visualised under transmission electron microscopy (see: 2.12: Transmission electron microscopy).

### 2.5.3 Caesium chloride viral purification: reagents and materials

R10 media (GibcoTM, Fischer scientific catalogue number: 11-875-127)

FBS: Foetal Bovine Serum. Moregate FCS, Lot#29827102

T175 175 $cm^2$ culture vessels (Greiner Bio-One CELLSTAR reference number: 660160)

Caesium Chloride (Serva product number: 15554)

250 mL Nalgene bottles (ThermoFisher catalogue number: 2103-0008)

Beckman Coulter Avanti J-26 XP1 high-speed centrifuge (Beckman Coulter, Indianapolis, USA)

Fiberlite F250 rotor (ThermoFisher Scientific Waltham, Massachusetts, USA)

Beckman Coulter Optima XPN-80 ultracentrifuge (Beckman Coulter, Indianapolis, USA)

Beckman Coulter SW32.1 Ti rotor (Beckman Coulter, Indianapolis, USA)

Beckman 16.8 mL polypropylene tubes (Beckman Coulter reference number: 337986)

Beckman 36 mL polypropylene tubes (Beckman Coulter reference number: 326823)

### 2.5.4 Caesium chloride viral purification: protocol

H446 cells were grown to confluence in ten T175 culture vessels containing 35mL R10 + 10% FBS. The growth media in each culture vessel was replaced with 25 mL infection media containing 20 mL R10 + 2% FBS and 5mL R10 + 2% + 1 MOI SVV in R10. The cells and virus were incubated at 37 °C + 5% $CO_2$ for 48 hours, or until complete cytopathic effect was observed. The cells were then freeze-thawed from -80 °C to room temperature repeatedly to lyse the cells. The media containing virus and cells from all of the culture vessels were combined in 250 mL Nalgene bottle(s) and balanced with Nalgene bottle(s) containing water. The Nalgene bottles were centrifuged at 10,000 g for 20 minutes at room temperature using a

Beckman Coulter Avanti J-26 XP1 high-speed centrifuge. The cell-free supernatant was then removed and the cell pellet stored at 4 °C. The cell-free supernatant was then divided between six 36 mL Beckman polypropylene tubes and centrifuged at 120,000 g for one hour and 10 minutes at 4 °C. This was done using SW32 buckets in a SW32.1 rotor. The supernatant was then collected and the viral pellets were allowed to resuspend overnight at 4 °C. The following day, the pellets were collected. CsCl gradients were formed by the addition of one part CsCl to two parts CsCl buffer. The density of the CsCl solution was measured by weighing a known volume and then checked for appropriateness against provided CsCl density vs. centrifugation speed graphs to prevent "bulleting". Beckman 16.8 mL polypropylene tubes were first loaded with 6 mL CsCl solution and then 4 mL of CsCl buffer. In one of the tubes, resuspended viral pellets in CsCl were added and the remainder of the tube was filled with CsCl buffer. This was balanced against another tube filled with just CsCl. The two tubes were then centrifuged at 22,000 rpm for 18 hours at room temperature. The CsCl around observed bands were collected and fractions were viewed under electron microscopy.

## 2.6 Viral RNA isolation

### 2.6.1 Viral RNA isolation: reagents and materials (Nucleospin)

Nucleospin® RNA virus kit (Macherey-Nagel reference number: 740956.250)

### 2.6.2 Viral RNA isolation: protocol (Nucleospin)

The viral RNA isolation protocol was performed according to the Nucleospin® RNA virus protocol as follows. 150 µL of purified virus sample was combined with 600 µL RAV1 and heated to 70 °C for 5 minutes. This was then combined with 600 µL ethanol, loaded into the Nucleospin® column and spun down at 8,000 g for 1 minute. 500 µL RAW was added to the column and this too was spun down at 8,000 g for 1 minute, the flow-through was then discarded. 600 µL RAV3 was added to the Nucleospin® column and the flow-through was discarded, this was repeated with 200 µL RAV. The column was then loaded into a new sterile

1.5 mL microcentrifuge tube. RNAse-free $H_2O$ was heated to 70 °C and 50 µL was added to the column. This was then centrifuged at 11,000 rpm for 1 minute and the flow-through was collected.

### 2.6.3 Viral RNA isolation: reagents and materials (QIAmp)

QIAmp® Viral RNA Mini Kit (QIAGEN catalogue number: 52904)

### 2.6.4 Viral RNA isolation: protocol (QIAmp)

SVV RNA isolation was performed according to the QIAmp® kit directions as follows:

560 µL buffer AVL with carrier RNA was combined with 140 µL sample in a 1.5 mL microcentrifuge tube. The microcentrifuge tube was then pulse-vortexed for 15 seconds and allowed to sit for 10 minutes at ambient temperature. This was then followed by centrifugation, addition of 560 µL ethanol, vortexing and another round of centrifugation. Two halves of the current solution (should be 630 µL) were added to two QIAmp mini columns inside two 2mL collection tubes. 560 µL of buffer AW1 was added to each of the tubes and they were centrifuged at 8,000 rpm for minute. The flow-through in the 2 mL collection tube was discarded and the same collection tube was replaced. 500 µL buffer AW2 was then added and centrifuged at full speed for 3 minutes. This step was then repeated as per kit recommendation. The 2 mL column was then replaced by a clean 1.5 mL microcentrifuge tubes and following the addition of 60 µL buffer AVE, were centrifuged for a final time for one minute at 8,000 rpm.

## 2.7 cDNA generation

### 2.7.1 cDNA generation: reagents and materials

High capacity cDNA reverse transcription kit (Applied Biosystems reference number: 4368814)

Bio-Rad T100$^{TM}$ Thermal Cycler (Bio-Rad, Hercules, California, USA)

0.2 mL PCR tubes (Lab supply catalogue number: AXY321-01-102)

Primers:

Pair 1 Forward TTTGAAATGGGGGGCTG

Pair 1 Reverse GATAGACGGGATCTGAAAGGGTG

Pair 2 Forward CTACCTCGGTAGACATAAAC

Pair 2 Reverse GCTATTTGGTTCCAGTCTTTG

### 2.7.2 cDNA generation: protocol

Reaction mixtures were generated according to the following proportions

- 2 µL RT buffer
- 0.8 µL dNTP's
- 1.5 µL random primers
- 0.5 µL specific primers
- 1 µL reverse transcriptase
- 4.2 µL $H_2O$

  = 20 µL reaction mix

Reaction mixtures were then heated according to the regime stipulated in Table 1.

**Table 1.** Thermocycler regimen for cDNA generation

| **Temperature** | 25 °C | 37 °C | 85 °C | 4 °C |
|---|---|---|---|---|
| **Time** | 10 minutes | 120 minutes | 5 minutes | ∞ |

## 2.8 PCR amplification

### 2.8.1 PCR amplification: reagents and materials

Bio-Rad T100$^{TM}$ Thermal Cycler (Bio-Rad, Hercules, California, USA)

0.2 mL PCR tubes (Lab supply catalogue number: AXY321-01-102)

Phision Hot Start II DNA Polymerase (ThermoFisher scientific catalogue number: F549L)

5X Phusion HF buffer (Included with Phusion Hot Start II DNA polymerase)

DMSO (Included with Phusion Hot Start II DNA polymerase)

50 mM $MgCl_2$ (Included with Phusion Hot Start II DNA polymerase)

Primers:

Pair 1 Forward GGCAACATCCAACCTGCTTTTG

Pair 1 Reverse TTTGTGAGGAGACCCGCTAATCC

Pair 2 Forward TTCAGTAGACTTCTCGACCTCCTC

Pair 2 Reverse AGGAGTTCTGTGTCTCTGAGGATTG

Pair 3 Forward GTCCCAATTTCATCAACCCCTATCAAG

Pair 3 Reverse TTGTGCAGGCTAAACCAACCATCAG

Pair 4 Forward CTACATCTCGCCCAGTGACTACC

Pair 4 Reverse TGTTTTACAGCGGTGCTTTTCTTCTC

Pair 5 Forward CATGCTGATTGGGGGACTATTTACG

Pair 5 Reverse GCAGCTATTTGGTTCCAGTCTTTGAC

2.8.2 PCR amplification: protocol

Reaction mixtures were generated according to the following proportions

- 12.4 µL $H_2O$
- 4 µL buffer
- 0.4 µL dTNP's (10mM)
- 0.2 µL Phusion Hot Start II DNA polymerase
- 1 µL forward primer
- 1 µL reverse primer
- 1 µL template cDNA

  = 20 µL reaction mix

**Table 2.** Thermocycler regimen for PCR amplification of wild-type and putative SVV-001 mutant genomes

| | | 40x Cycles | | | |
|---|---|---|---|---|---|
| **Temperature** | 98 °C | 98 °C | 55 °C | 72 °C | 12 °C |
| **Time** | 30 seconds | 7 seconds | 30 seconds | 45 seconds | ∞ |

### 2.8.3 Gel electrophoresis

PCR reaction mixes were combined with 1 µL 5X loading dye and subjected to electrophoresis through 2% agarose gels at 60 V until the dye fronts had migrated the length of the gel, taking somewhere between 75-90 minutes. Gels were visualised with a Cambridge Uvitec gel doc.

### 2.8.4 Gel extraction

Gel extraction of the PCR fragments of interest were performed using a QIAGEN MinElute® Gel extraction kit (QIAGEN catalogue number: 28604) according to the supplied protocol. This was as follows: DNA fragment was excised with a clean, sharp scalpel and placed in a 1.5 mL microcentrifuge tube. The gel fragment was then weighed and three parts buffer QG was added to one part gel slice. The contents of the microcentrifuge tube were then heated to 50 °C with regular stirring until the gel fragment was completely dissolved. One gel volume's worth of isopropanol was then added and mixed by inversion. The liquid was then added to a MinElute column inside a 2 mL collection tube and centrifuged for 1 minute at 13,000 rpm. 500 µL of buffer QG was added and the column was centrifuged for a further 1 minute at 13,000 rpm. This was followed by the addition of 750 µL of buffer PE and centrifugation at 13,000 rpm for 1 minute. The column was then allowed to stand for 2-5 minutes before being centrifuged again at 13,000 rpm. The MinElute column was then placed in a sterile 1.5 mL microcentrifuge tube, and 10 µL buffer EB was added to the column before a final centrifugation at 13,000 rpm for 1 minute. The column was then removed and the eluted DNA stored at -4 °C.

## 2.9 Sequencing

### 2.9.1 Sequencing: reagents and materials

MilliQ water

0.2 mL PCR tubes (Lab supply catalogue number: AXY321-01-102)

### 2.9.2 Sequencing: protocol

Gel extracted PCR products were measured for protein concentration using a Nanodrop. 5 µL reaction mixtures were made according to the following proportions.

- 1 ng per 100 bp PCR product per 5 µL
- 3.2 pmol primer per 5 µL

These samples were submitted to Genetic Analysis Services and the results were analysed using DNASTAR Seqman Pro software.

## 2.10 *In silico* analysis of putative thermostability mutations

### 2.10.1 Visualisation of viral capsid structures with UCSF Chimera

Viral structures were accessed using protein database accession numbers. Using in-built tools, the changes in internal binding were shown between the wild-type and mutant (Petterson et. al., 2004). Contacts between residues were defined by having a Van Der Waal overlap of -0.4 Å or greater.

### 2.10.2 Prediction of protein stability change using DUET

DUET utilises two methods to predict the change in protein stability due to mutation (Pires, Ascher & Blundell, 2014). The first is SDM, which utilises environment-specific substitution tables (ESSTs) to calculate change in thermal stability of proteins on mutation (Pandurangan et. al., 2017). The second is mCSM (Pires, Ascher & Blundell, 2013). The basis of mCSM protein stability prediction is the use of graph-based signatures representing the distance between atoms (Pires, Ascher & Blundell, 2013).

## 2.11 Transmission electron microscopy

### 2.11.1 Transmission electron microscopy: reagents and materials

1% Uranyl Acetate (pH 4)

Phosphotungstic acid

### 2.11.2 Transmission Electron Microscopy: protocol

#### 2.11.2.1 Sample preparation

Copper grids were glow-discharged. The copper grids were then treated with 5 µL sample and allowed to sit for 1 minute before being blotted off. The copper grids were then treated with 5 µL of either 1% Uranyl Acetate (pH 4) or Phosphotungstic Acid for 1 minute, before blotting the liquid off.

#### 2.11.2.2 Image collection

Philips CM100 BioTWIN transmission electron microscope with a LaB6 emitter (Philips/FEI Corporation, Eindhoven, Holland) running at 100 kV. Images were acquired using a MegaView lll digital camera (Olympus Soft Imaging Solutions GmbH, Münster, Germany).

## 2.12 SDS-PAGE gel analysis

### 2.12.1 SDS-PAGE gel analysis: reagents and materials

MilliQ water

100% Methanol

500 mM DTT (Dithiothreitol)

NuPAGE™ LDS Sample Buffer (ThermoFisher Scientific catalogue number NP0007)

Chloroform

Bolt™ 4-12% Bis-Tris Plus Gel (Invitrogen catalogue number: NW04120BOX)

ECL™ Rainbow™ Full Range Protein Marker (GE Healthcare product number: RPN800E)

SeeBlue™Plus2 Pre-stained Protein Standard (Thermofisher scientific catalogue number: LC5925)

Qubit™ protein assay kit (ThermoFisher Scientific catalogue number Q33211)

Qubit™ assay tubes (ThermoFisher Scientific catalogue number Q32856)

Qubit 1.0 flurometer (ThermoFisher Scientific Waltham, Massachusetts, USA)

### 2.12.2 SDS-PAGE gel analysis: protocol

#### 2.12.2.1 Protein Precipitation

In a 1.5 mL microcentrifuge tube, 150 µL of purified virus in solution was combined with 650 µL methanol and mixed well. This was combined with 150 µL chloroform and vortexed. 450 µL of milliQ water was also added and the microcentrifuge tube was vortexed again. The liquid was then centrifuged at 13,000 rpm for 5 minutes. This resulted in a white band between and upper and lower volumes. The upper volume was removed and a further 650 µL of methanol was added. The microcentrifuge tube was inverted 3 times and centrifuged at 13,000 rpm for 5 minutes. The pellet was resuspended overnight in 20 µL milliQ water.

#### 2.12.2.2 Sample preparations

The 20 µL of resuspended protein from the previous step was combined with 6.66µL NuPAGE™ LDS Sample buffer and 2.66 µL 500 mM DTT. The 1.5 mL microcentrifuge tube containing the resuspended protein was then heated to 90 °C for 10 minutes.

#### 2.12.2.3 Qubit assay

Qubit protein buffer was made by addition of 1 part Qubit™ protein reagent to 200 parts Qubit™ protein buffer. Protein standards were made by adding 10 µL of supplied protein solutions in 190 µL Qubit protein assay buffer. Samples were measured with 1 µL prepared protein sample in 199 µL Qubit protein buffer. The standards were first measured with a Qubit 1.0 fluorometer to generate Bradman curves. The fluorescence from the samples were then measured against the Bradman curves to derive the concentration of protein in the samples.

#### 2.12.2.4 Gel electrophoresis

Gel tanks were almost completely filled with 1X MES. The sticker on the reverse of a Bolt™ 4-12% Bis-Tris Plus Gel was removed and the gel itself inserted into the gel tank, fixed in place with the cassette clamps. The comb from the Bolt™ 4-12% Bis-Tris Plus Gel was removed and the tank filled to the indicated level so as to fill the wells of the Bolt™ 4-12% Bis-Tris

Plus Gel. Viral protein samples and ECL™ Rainbow™ Full Range Protein Marker were loaded into wells of the gel. Gels were run under a constant voltage of 70 V until dye fronts had migrated through the length of the gel (usually one and a half hours). The gels were removed from the tank and the plastic casing cracked open. The gel was placed in a plastic tray with coomassie blue colloidal stain and left to stain overnight. The stained gel was then destained and viewed under the Uvitec Cambridge gel doc.

#### 2.12.3 ImageJ: Fiji analysis

Image J is an extensible open-source program for the analysis of scientific images. Image J: Fiji contains a number of additional plugins particularly suited to the analysis of biological images based on common biology techniques (Schindelin et. al., 2012). Once SDS PAGE gels were photographed, Image J: Fiji was used to determine the varying ratios of capsid proteins present in the wild-type and thermally selected populations. For more information on how this was done, refer to (7.2 ImageJ Fiji analysis of SDS PAGE gels).

## 2.13 Mass spectrometry

### 2.13.1 Mass spectrometry protocol

Gel bands were extracted with a sterile scalpel and were submitted in sterile 1.5 mL microcentrifuge tubes to Otago's Centre for Protein Research (CPR). MALDI tandem Time-of-Flight (MALDI-TOF) Mass Spectrometry was used to analyse the submitted protein bands and the results were checked against MASCOT and SEQUEST search engines.

## 2.14 Particle Stability Thermal Release assay (PaSTRy)

### 2.14.1 PaSTRy: reagents and materials

Qubit™ protein assay kit (ThermoFisher Scientific catalogue number Q33211)

Qubit™ assay tubes (ThermoFisher Scientific catalogue number Q32856)

Qubit 1.0 flurometer (ThermoFisher Scientific Waltham, Massachusetts, USA)

MicroAmp® Fast Optical 96-well Reaction Plate (Applied Biosystems reference number: 4346906)

20X SYTO9 (ThermoFisher Scientific catalogue number: S34854)

30X SYPRO Orange (ThermoFisher Scientific catalogue number: S6650)

Applied Biosystems Viia7 qPCR (Applied Biosystems, Carlsbad, California, USA)

2.14.2 PaSTRy: protocol

Protein in virus solution was measured using a Qubit 1.0 fluorometer (see: 2.12.2.3: Qubit assay) to determine the volume necessary for 1 µg total viral protein. Wells of 96-well plates were filled with 20 µL reaction mixtures according to the proportions outlines in Table 3.

**Table 3:** Reaction mixtures for PaSTRy

| 56 °C resistant SVV + Nucleotide binding dye | SVV-001 + Nucleotide binding dye | 56 °C resistant SVV + hydrophobic residue binding dye | 56 °C resistant SVV + hydrophobic residue binding dye |
|---|---|---|---|
| 6 µL purified viral fraction<br>3 µL 20X SYTO9<br>11 µL PBS | 4 µL purified viral fraction<br>3 µL 20X SYTO9<br>13 µL PBS | 2 µL purified viral fraction<br>2 µL 30X SYPRO Orange<br>16 µL PBS | 2 µL purified viral fraction<br>2 µL 30X SYPRO Orange<br>16 µL PBS |

Reaction mixtures were heated from 25 °C to 95 °C in 0.5 °C increments with a 30 second resting step at each temperature. 2 minute holding steps were used at 25 °C to 95 °C, but fluorescence was not measured during these steps.

## 2.15 Cryo-electron microscopy

### 2.15.1 Cryo-electron microscopy reagents and materials

JEOL 2200FS Cryo-TEM (JEOL ltd., Tokyo, Japan)

FEI Vitrobot Mark IV (FEI, Hillsboro, Oregon, USA)

C-flat grids CF-2/1-2C-50 (Electron microscopy sciences catalogue number: E13557)

100,000 NMWL filters (Amicon reference number: UFC510024)

GloQube glow discharger (Quorum technologies, Lewes, UK)

### 2.15.2 Cryo-electron microscopy protocol

Sample Preparation

CsCl purified 56 °C resistant thermostable SVV-001 mutant was concentrated by passing isolated fractions through 100,000 NMWL filters and resuspension in PBS. C-flat grids were glow discharged for 60 seconds at a constant current of 5 mA using a GloQube glow discharger. 3.5 µL of purified thermostable SVV mutant in PBS was added to the C-flat grids and the excess liquid was blotted off with a FEI Vitrobot Mark IV at 100% humidity for 3.5 seconds with blot force 0. Immediately following blotting, grids were plunge frozen in liquid ethane at -180 °C. Frozen grids were transferred into grid storage boxes and stored in liquid nitrogen until imaging.

Image acquisition

Frozen grids were imaged at 20,000x or 25,000x magnification on a JEOL 2200FS Cryo-TEM operating at 200 kV. Movie frames were recorded with a DE-20 direct electron detector. Grid areas were selected on the basis of optimal ice thickness. Montages were taken of grid areas with thin ice, which provides a low-magnification overview of the available grid holes for imaging. Grid holes within grid areas containing vitreous ice and particles were manually labelled for image acquisition. Figure 8 below is included to distinguish between the some of the terminology used in describing areas and/or sub-areas within C-flat grids.

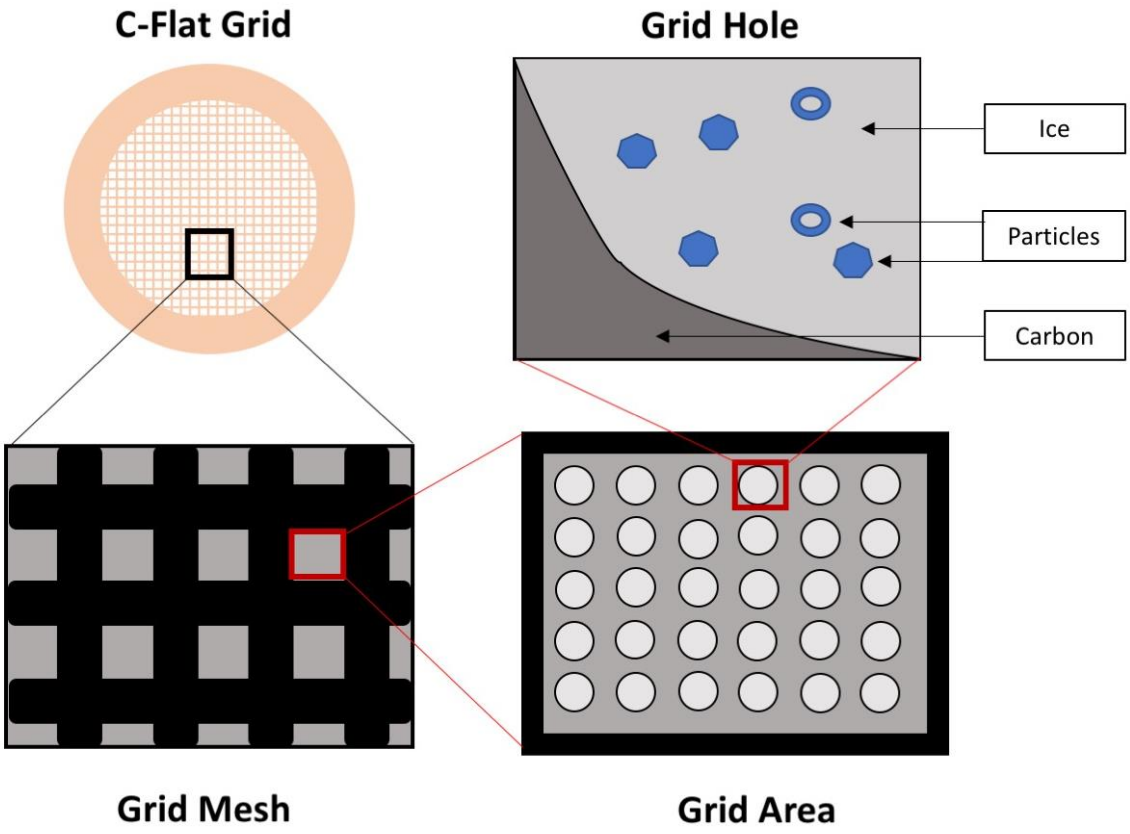


**Figure 8: C-flat grid structure.** C-flat grids as they appear under increasing magnification, from the whole grid, to a representation of how a grid hole appears in a micrograph taken at 20,000x magnification.

### 2.15.3 Single Particle Analysis

The data collected from cryo-electron microscopy investigation of 56 °C resistant SVV mutants was analysed using Relion 3.0 software. First, a total of 18 movie frames were aligned, a process which is performed to correct for motion of particles induced by agitation from the electron beam. Each movie frame had a total dose of 2.78 el/Å$^2$/frame, culminating in a total dose of 50 el/Å$^2$/image. Particles of interest were manually picked using in-built software tools. The picked particles were then Contrast Transfer Function (CTF) corrected. CTF correction is undertaken to adjust for sub-optimal imaging conditions using the Scherzer formula as below:

$$\gamma(k) = \pi/2\,(C_s\lambda^3k^4 - 2\Delta z\lambda k^2)$$

Where: γ(k) = Phase shift

k = Scattering vector

$C_S$ = Spherical aberration coefficient of the microscope

$\lambda$ = Wavelength of the electron beam

$\Delta z$ = Defocus

The Scherzer formula determines phase shift as a result of defocus and spherical aberration, which when corrected for provide an image that better represents the sample. After CTF correction, 2D classes of picked particles /were iteratively generated to filter out particles that were not examples of full, packaged virions. Once 2D classes were determined to be of sufficient quality, 3D classification was performed using a a low-pass filtered 30 Å structure of the SVV-001 (Electron Microscopy Data Bank accession number: 7110) and imposing I4 symmetry. A gold-standard fourier shell cut-off of 0.143 was then used to estimate the resolution of the generated 3D model.

# 3 Results

## 3.1 Thermal probe

### 3.1.1 Susceptibility of wild-type SVV to varying incubation temperatures.

Before attempting to select for a thermostable mutant, it was prudent to characterise the thermostability of wild-type SVV-001. This was to inform the temperature for the regime of heating and passage to select for the mutants, and provide a reference to which any generated mutants could be compared. Figure 3 shows SVV viral titres remained stable when heated for 30 minutes at temperatures between 37 °C and 55 °C, with SVV viral titre declining sharply with incubation temperature exceeding 56 °C. At 58.5 °C, there was a 100-fold decrease in viral titre which would be used in forthcoming experiments to select for thermostable SVV mutants.

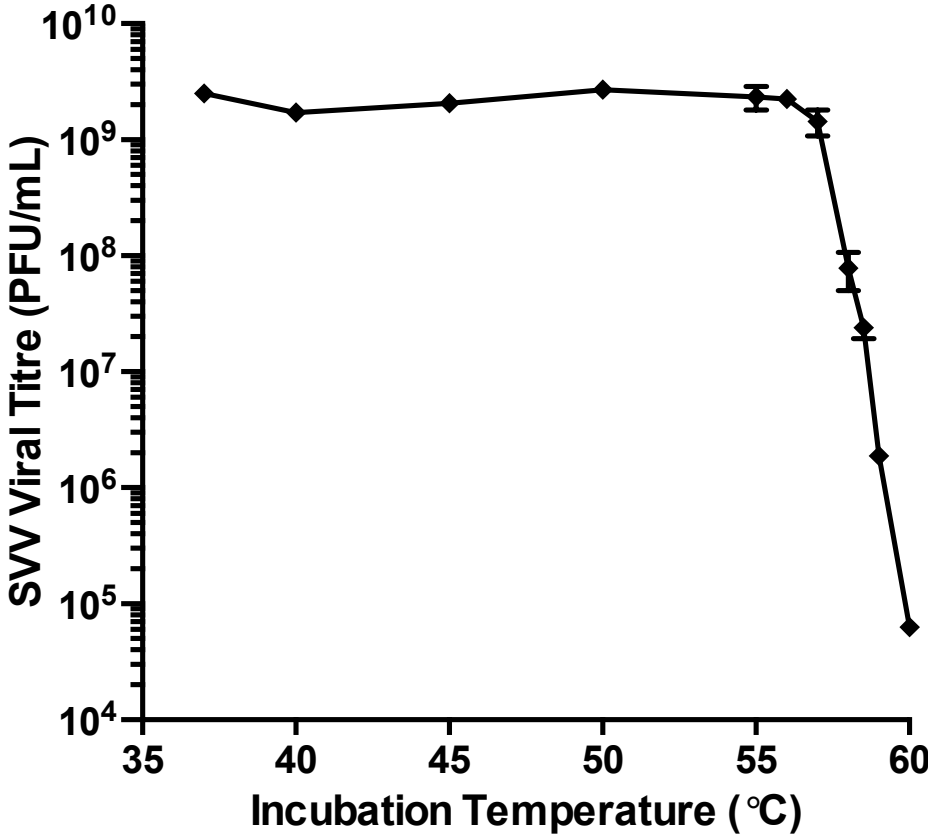

**Figure 9: Heating at 58.5 °C reduces SVV viral titre 100-fold.** From a $5x10^{11}$ PFU/mL stock of purified SVV, 1:50 µL dilutions were aliquoted and heated at various temperatures for 30 minutes before being cooled to 12 °C and titred by plaque assay.

3.1.2 Susceptibility of wild-type SVV to varying incubation temperatures (revised method)

To gain a clearer idea as to the temperature required to exert a significant pressure on wild-type SVV-001, the methodology was amended to include a comparison of the heated samples and analogous unheated controls, rather than comparing viral titres of the heated samples to the titre of the stock from which they were derived. This was done in light of conflicting results from the previously discussed thermal probe experiments and the initial thermal selection experiment (see: 3.2.1 Thermal selection of SVV-001). Figure 10 shows a statistically significant approximately 200-fold decrease in SVV viral titre when heated to 53.5 °C.

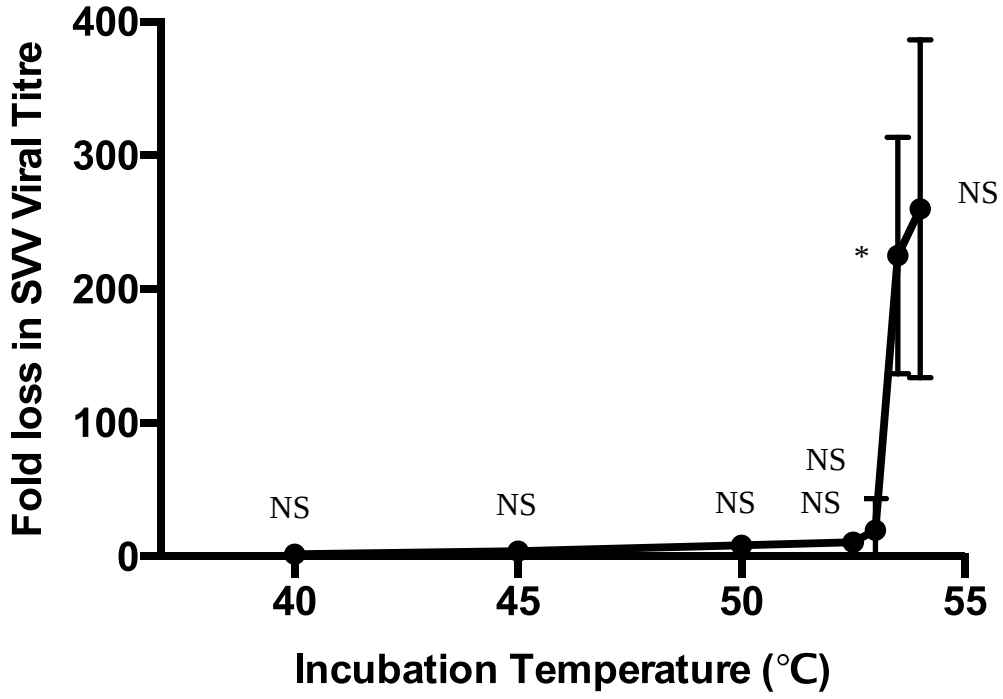


**Figure 10: Heating at 53.5 °C significantly reduces SVV viral titre.** Aliquots of SVV-001 in solution were added in equal volumes to PCR tubes and of paired samples, one was heated to the desired temperature for 30 minutes and the incubated other at room temperature for 30 minutes. The viral titres of the two samples were enumerated with plaque assays and the difference plotted above.

## 3.2 Thermal selection

### 3.2.1 Thermal selection of wild-type SVV-001

Following the initial temperature probe, wild-type SVV-001 was passaged through H446 cells and heated to 58.5 °C. Contrary to the results of the first temperature probe, Figure 11 shows that when heated to 58.5 °C for 30 minutes, SVV-001 viral titre would drop below the limits of detection, inferring much greater loss in viral titre than 100-fold. This experiment was the basis for the need to revise the method for the thermal probe (see: 3.1.2 Thermal probe). This experiment did show that SVV-001 titre could be maintained at similar levels when passaged without heating at 0.1 MOI.

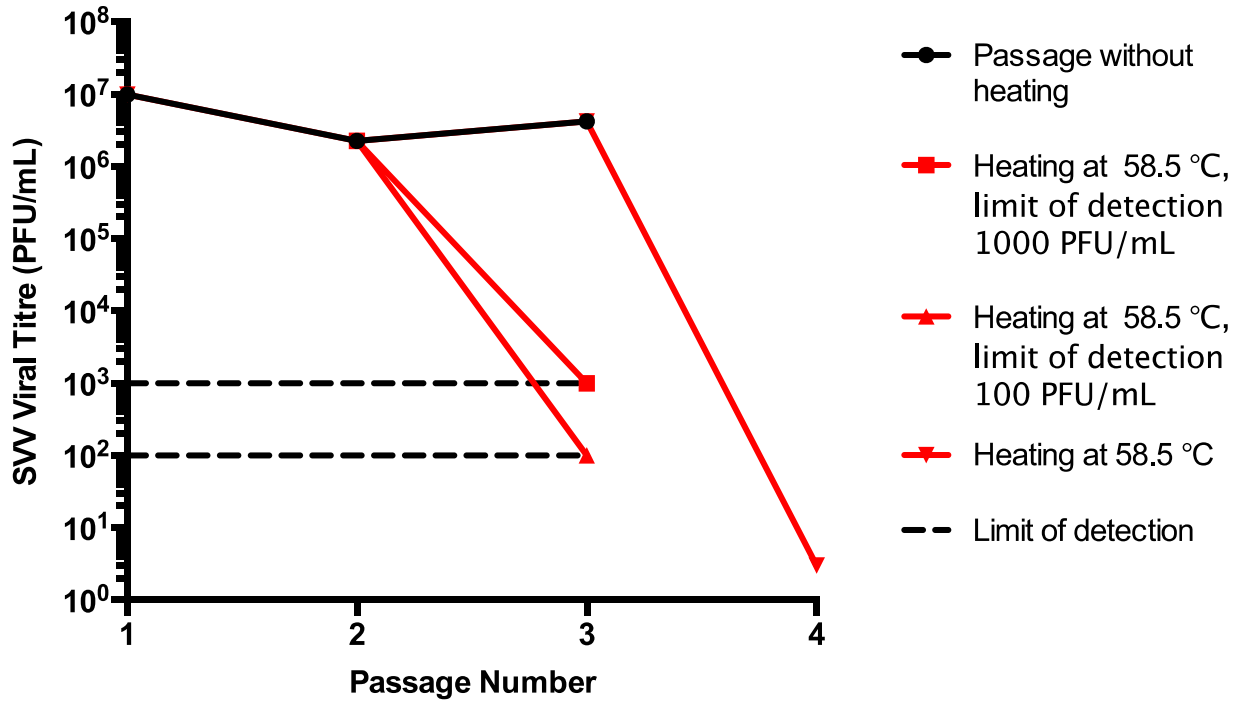


**Figure 11: Heating at 58.5 °C for 30 minutes produced a single SVV viral plaque.** SVV-001 was inoculated into a confluent T25 culture vessel of H446 cells (approximately 1.72 x $10^6$ cells) at MOI 0.1. After separation from cells by freeze-thawing and centrifugation, virus in solution were heated to 58.5 °C and titred with plaque assays. Passage without heating is shown in black, while red lines denote heating.

One viral plaque was observed in a plaque assay of the undiluted heated viral sample. As this plaque was thought to represent a uniquely thermostable viral population, the plaque was

extracted from the well using a 20 µL – 200 µL pipette tip and grown in a confluent T25 of H446 cells. The virus from this plaque will be referred to as the plaque purified viral population in forthcoming experiments.

### 3.2.2 Thermal selection for a 58.5 °C resistant mutant from plaque-purified viral population

As the plaque-purified viral population was initially derived from a plaque that remained after exposure of wild-type SVV-001 to incubation at 58.5 °C, we investigated whether this population remained resistant to heating at this temperature. Figure 12 shows that initially, this was not the case, though this plaque purified viral population was more resistant to heating at 58.5 °C than the wild-type, there still remained a significant difference between the pre- and post-heated viral titres. This trend continued for 10 cycles of heating and passage, with no apparent adaption of the plaque purified viral population to heating at 58.5 °C. At this time, attempts to select for increased thermal stability were ceased.

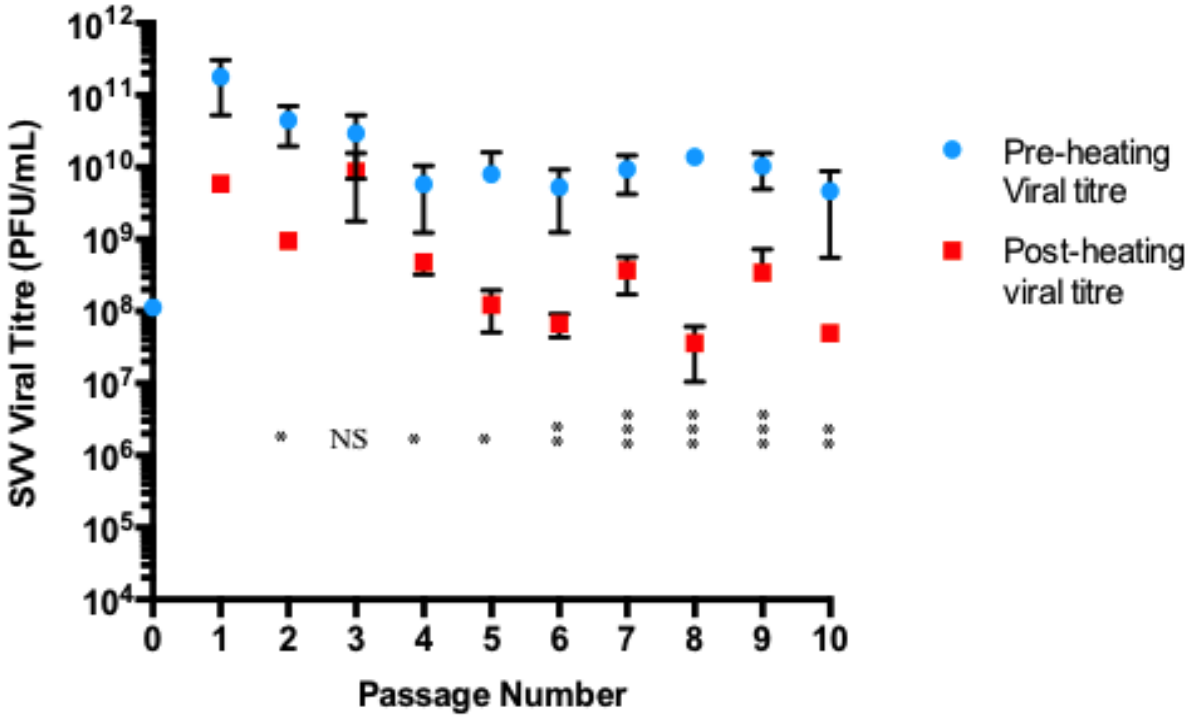


**Figure 12: Plaque purified virus showed no adaptation to heating at 58.5 °C.** Titres of pre- and post-heated virus were enumerated with plaque assays and surviving virus post-heating was passaged through H446 cells, forming the next passage's pre-heated virus. After the initial

passage, experiments were performed in triplicate and statistically analysed with paired student's T-test.

### 3.2.3 Thermal selection for a 56 °C resistant SVV-001 mutant from plaque-purified viral population

Though selection with the plaque purified viral population failed to produce a viral mutant that was completely resistant to heating at 58.5 °C, it was reasoned that as there was a similar loss in viral titre when heating the wild-type to 53.5 °C, that this plaque purified viral population might be completely resistant to heating at temperatures lower than 58.5 °C, but higher than 53.5 °C. Figure 13 shows that the plaque purified viral population remained stable across three successive passages after heating to 56 °C.

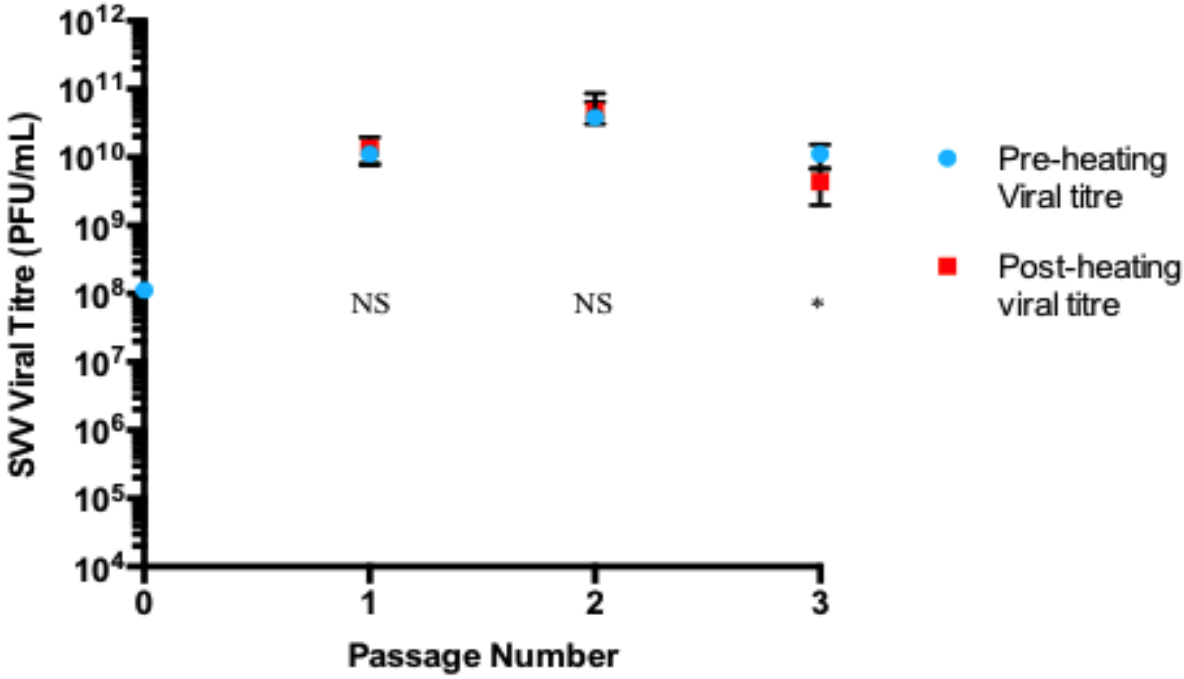


**Figure 13: Plaque purified virus was completely resistant to heating at 56 °C.** Titres of pre- and post-heated virus were enumerated with plaque assays and surviving virus post heating was passaged through H446 cells, forming the next passage's pre-heated virus. Experiments were performed in triplicate and statistically analysed with paired student's T-test.

## 3.3 Viral purifications

### 3.3.1 Viral purification by ultracentrifugation through Optiprep® gradient

The viral populations shown in the thermal selection experiments to have a higher tolerance to heating were grown to high titres in H446 cells before being purified by Optiprep® or caesium chloride gradient. Figure 14 below provides an example of a viral band, which is somewhat difficult to see, but lies between the interface (strong white band) and the point at which the curved and cylindrical portions of the Beckman tubes intersect. Figure 8 also shows electron micrographs taken from two separate purifications of the 56 °C resistant viral population and 58.5 °C selected viral population.

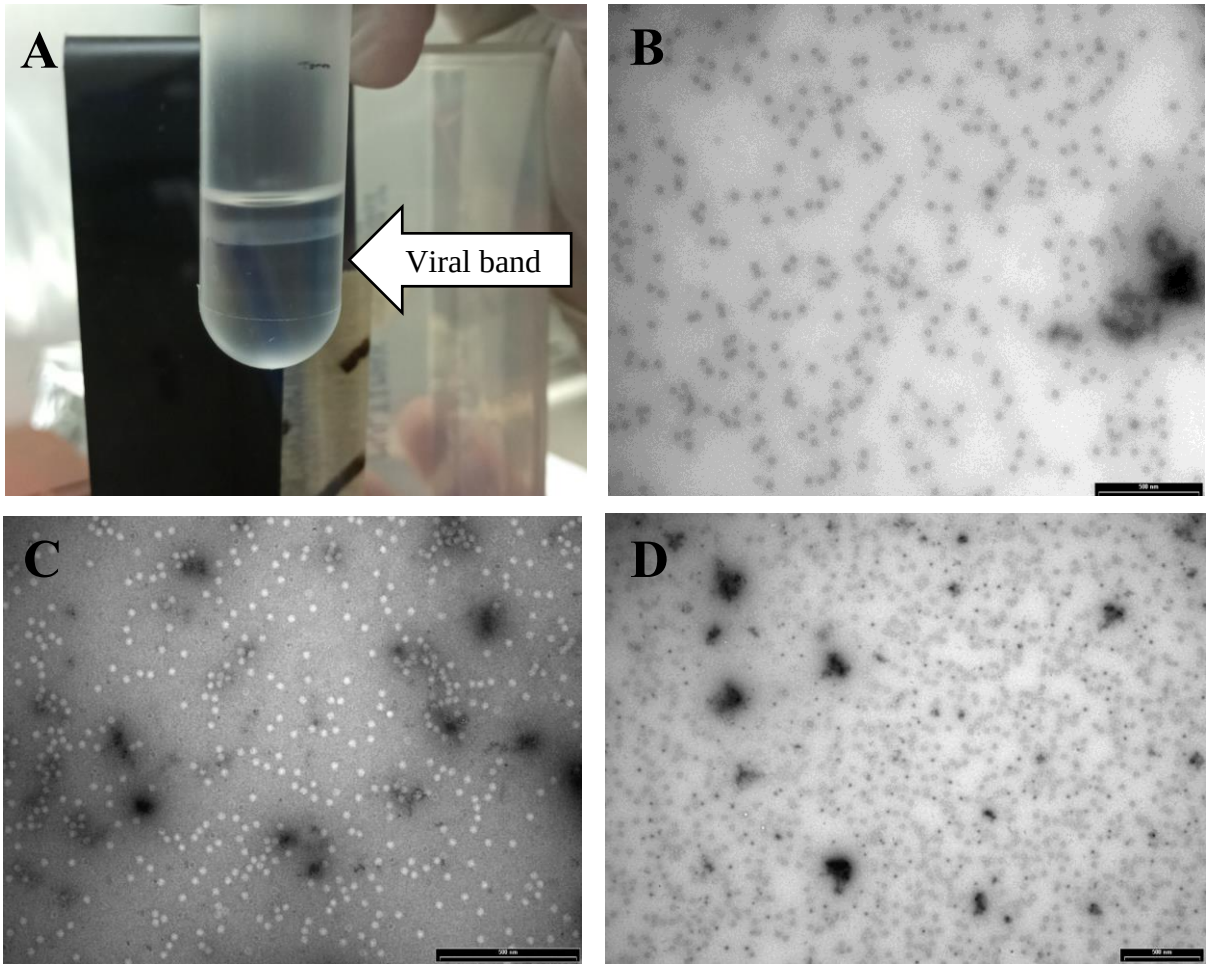


**Figure 14: Viral purification of 56 °C resistant and 58.5 °C selected viral populations. A)** An example of a viral band following the final step in viral purification. **B)** Electron micrograph of purified 56 °C resistant virus. **C)** Electron micrograph of purified 58.5 °C virus. **D)** Electron micrograph of purified 56 °C resistant virus. Scale bars 500 nm.

## 3.4 PCR amplification

### 3.4.1 SVV-001 and putative thermostable mutants

The RNA from wild-type SVV-001 and 56 °C resistant viral populations were extracted using a Nucleospin® RNA virus kit. This was used as the template for the generation of two cDNA products which together are analogous to P1, that included part of the 5’ UTR and part of P2 (See: 2.8 cDNA generation). This cDNA was then expanded in five separate PCR reactions as described in methods (See: 2.9 PCR amplification). As the third set of PCR primers targeted an area of overlap between the two cDNA constructs, either of the two could be used as a template for PCR. For this reason, both cDNA constructs were used as templates, generating similarly sized PCR products. Figure 11 shows the process of preparing the SVV capsid encoding region for sequencing, including gel electrophoresis of PCR reactions of wild-type SVV-001, 56 °C resistant and 58.5 °C selected viral populations.

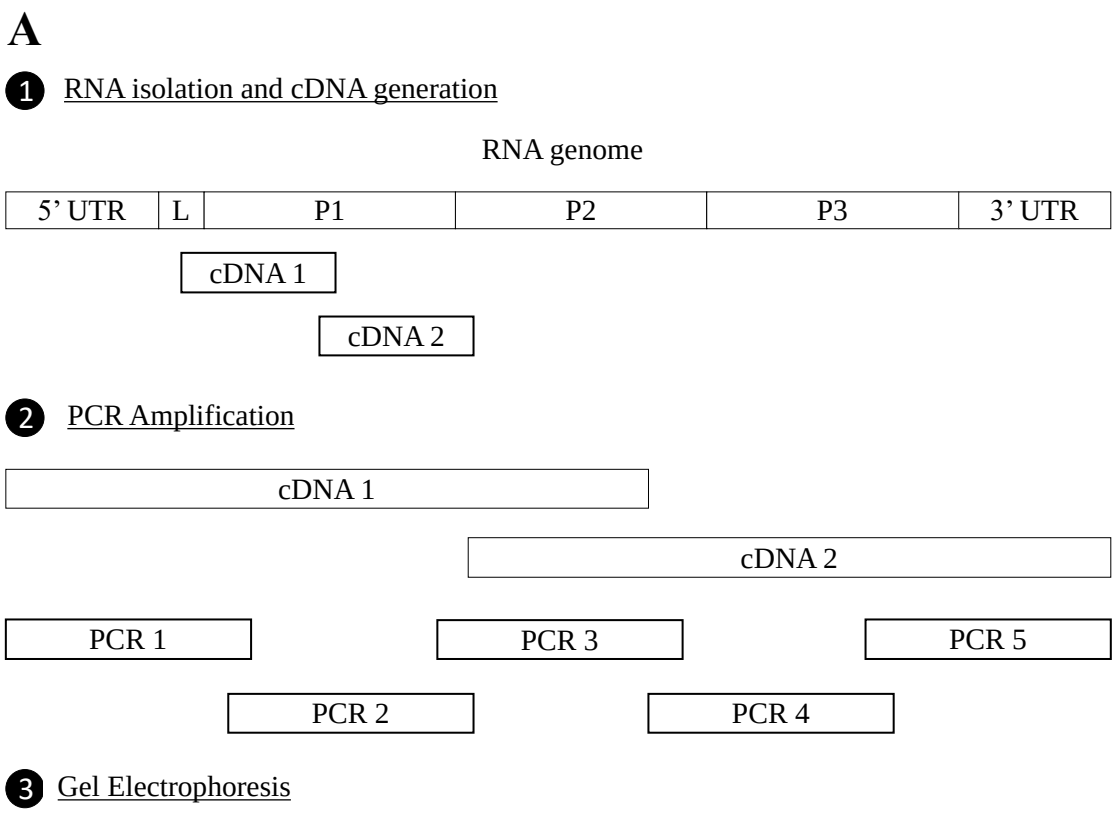

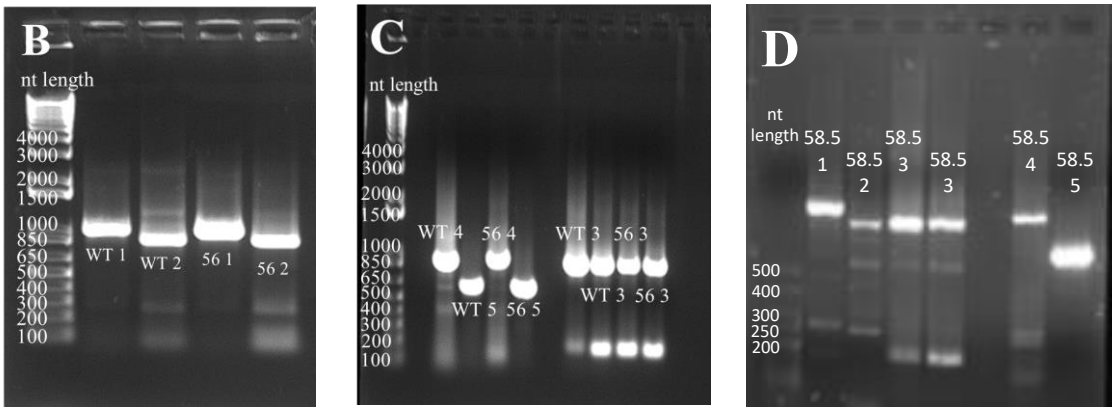


**Figure 15: Workflow of the preparation of the wild-type, 56 °C resistant and 58.5 °C selected viral populations for sequencing. A)** cDNA from the capsid coding region of SVV-001 and thermostable populations was generated in two halves. Using the two cDNA constructs as templates, the capsid coding region of SVV-001 and thermostable populations were expanded in five PCR reactions. **B)** PCR reactions expanding the first two segments of each of the 56 resistant and wild-type viral populations. **C)** PCR reactions expanding the remaining segments of each of the 56 resistant and wild-type viral populations. **D)** PCR reactions expanding 58.5 °C selected viral populations.

## 3.5 Observed mutations in thermostable viral populations

### 3.5.1 Synonymous and non-synonymous mutations

The results of sequencing the putative thermostable populations identified a number of mutations which were present in thermostable mutants but absent in the reference and sequenced SVV-001. These include synonymous and non-synonymous mutations. Figure 16 below lists the mutations within the sequenced DNA, these were present in both the 56 °C resistant and 58.5 °C selected viral populations, and their relative conservation across 96 aligned Senecavirus isolate genomes.

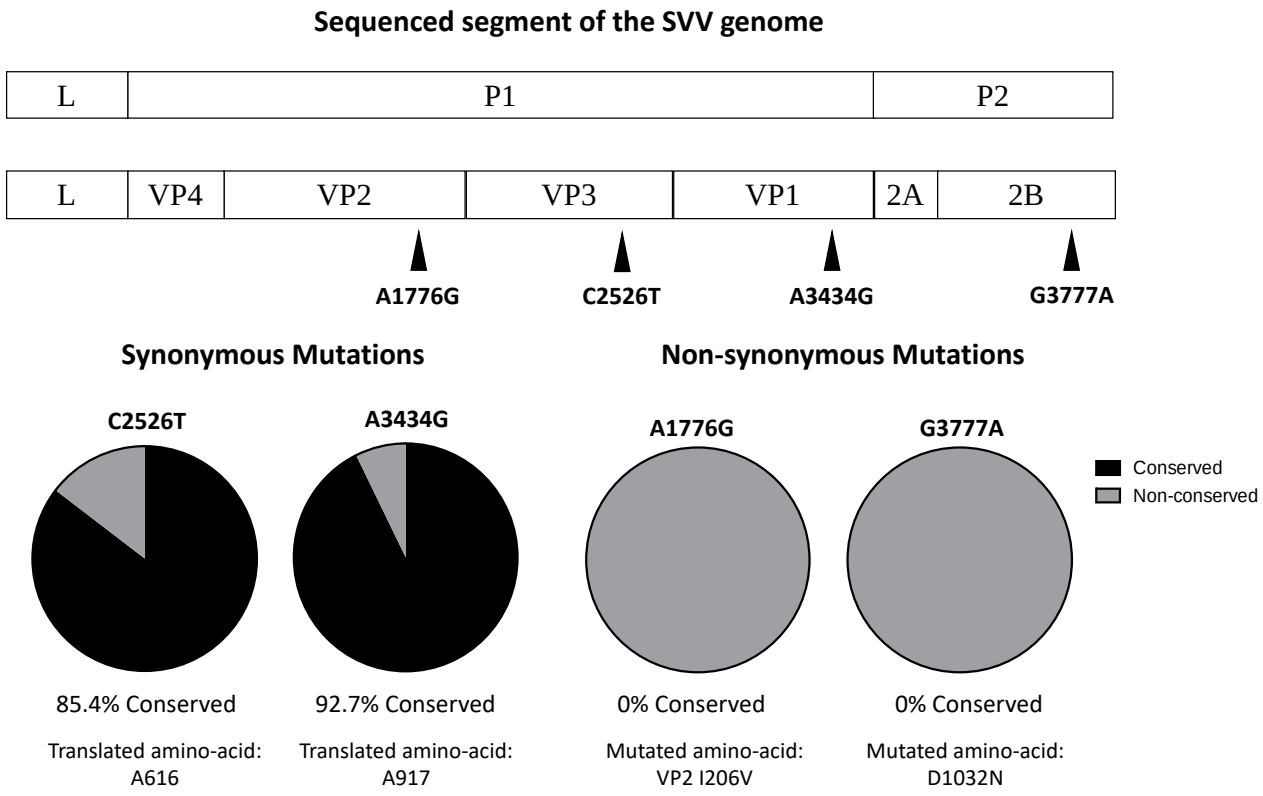


**Figure 16: Mutations observed in the thermostable SVV mutants.** Four mutations were identified in the sequenced portion of the mutant genomes, A1776G, C2526T, A3434G and G3777A. These were organised by effect on translated polyprotein and degree to which they are present in 96 sequenced Senecavirus isolates available in Genbank.

Among the four mutations in the sequenced region of the 56°C resistant and 58.5 °C selected viral populations there were two synonymous mutations, which were well conserved in 96 of the Senecavirus isolate full genomes accessible through Genbank. Conversely, the two non-synonymous mutations were not seen in any of the other 96 Senecavirus isolates.

### 3.5.2 Structural protein mutations

To gain insight into how the VP2 I206V mutation may affect thermostability, the SVV-001 protomer was modelled using UCSF Chimera. Using in-built tools, interactions between residues were shown based on defined parameters. For exact settings refer to 2.11.1. Figure 17

below provides a representation of the position of VP2 I206V mutation within the SVV-001 protomer, as well as potential interactions with nearby residues.

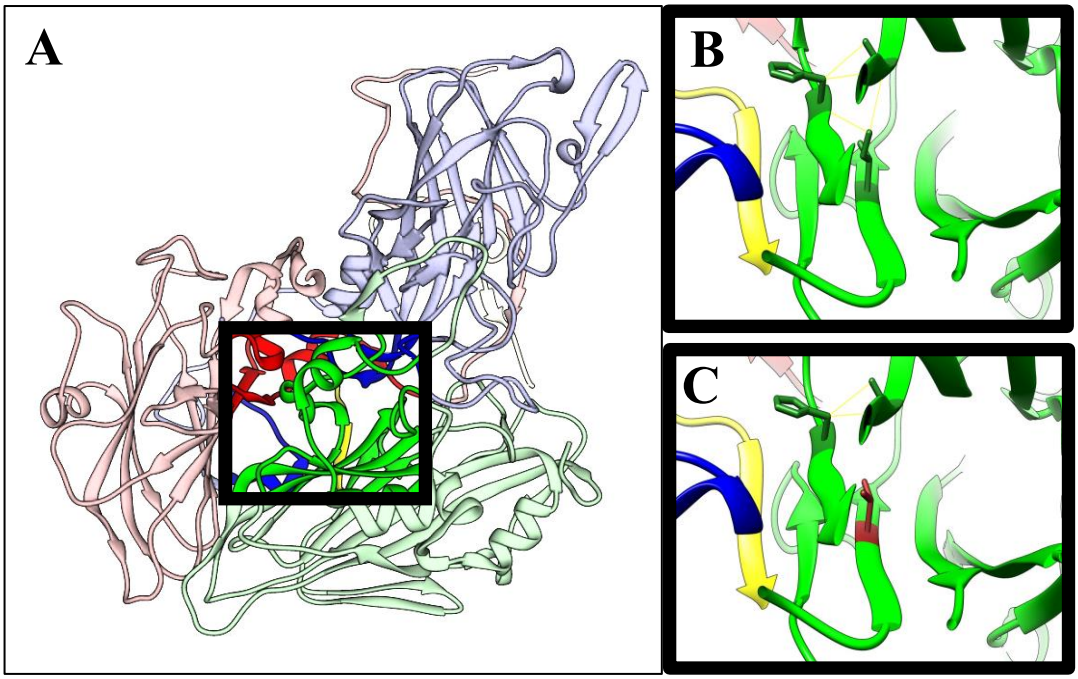


| D | mCSM Predicted Stability change (ΔΔG): | SDM Predicted Stability change (ΔΔG): | DUET Predicted Stability change (ΔΔG): |
|---|---|---|---|
| | -1.9 Kcal/mol (Destabilising) | -2.38 Kcal/mol (Destabilising) | -2.323 Kcal/mol (Destabilising) |

**Figure 17: VP2 I206V is predicted to decrease intraprotomeric binding. A)** The SVV-001 capsid protomer with area of interest highlighted was visualised using UCSF Chimera (accession number 3CJI). **B)** The highlighted area of A) showing the interactions (highlighted with yellow lines) between VP2 H204 and residues including VP2 I206 in the wild-type capsid as predicted by UCSF Chimera. **C)** The same highlighted area as in B) with the same parameters for internal binding applied but with the VP2 I206V residue shown in dark red. **D)** The results of mCSM, SDM, and DUET predictions of the change of stability as a result of the introduction of the I206V mutation.

### 3.5.3 Genomic RNA secondary structural mutations

To predict the effect of synonymous and non-synonymous mutations on the secondary structure of the SVV viral genome, the wild type and mutant sequences were entered into the RNA*fold* WebServer and the predicted structures shown below in Figure 18. The A1776G, C2526U and G3777A mutations are predicted to change the secondary structure of the RNA genome to a

noticeable degree. The A3434G mutation is not predicted to alter the secondary structure of the RNA genome.

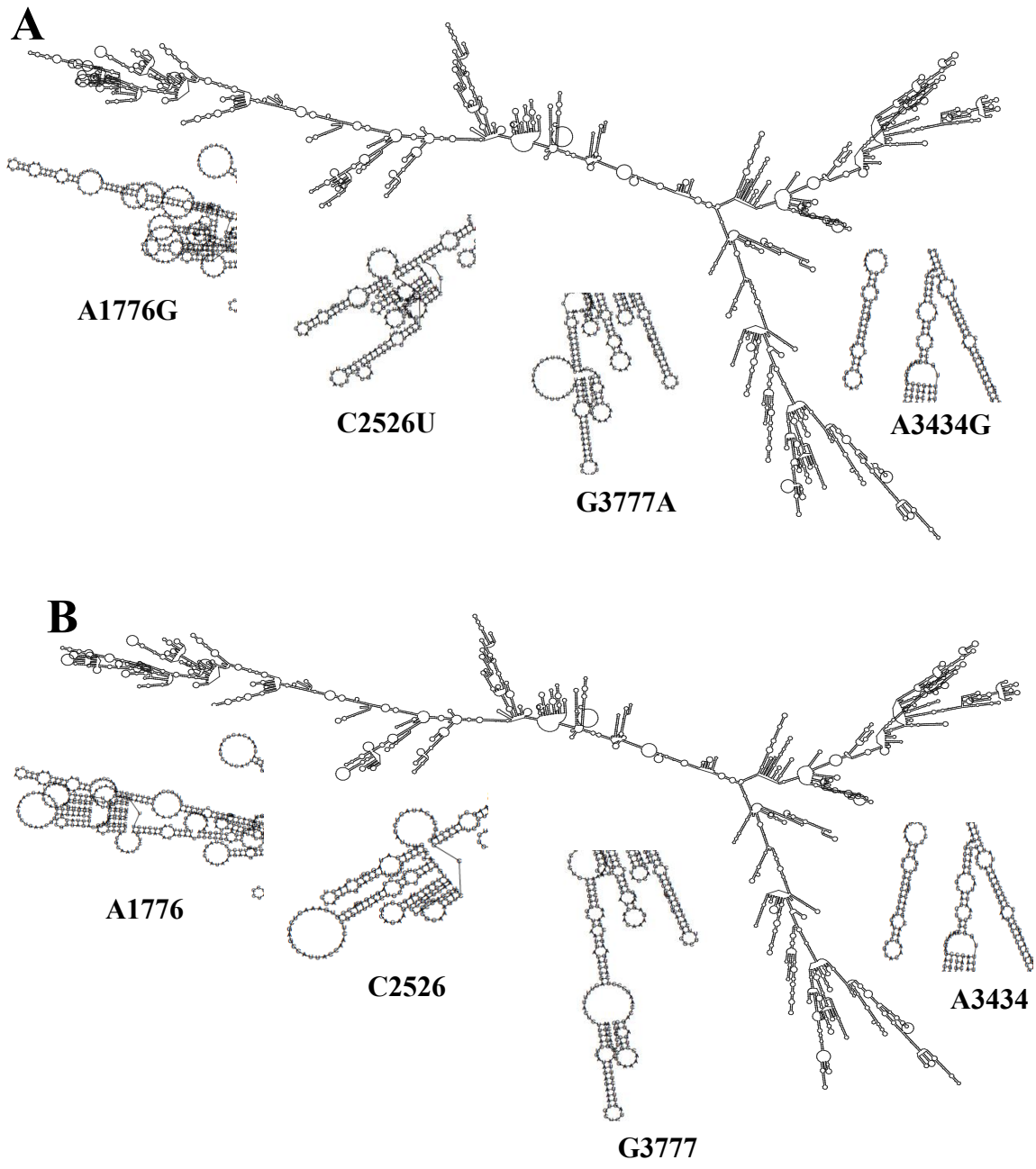


**Figure 18: Predicted secondary structures of wild type and mutant genomic RNA. A)** The thermostable mutant genome structure as predicted by RNA*fold* WebServer. **B)** The SVV-001 genome structure as predicted by the RNA*fold* WebServer. In A) and B), areas of interest of the wild-type and mutant are cropped and shown separate from the full genome.

## 3.6 SDS-PAGE analysis

### 3.6.1 SDS PAGE analysis of wild type and mutant SVV structural proteins

As the VP2 I206V mutation is predicted to ablate interaction with H204, the residue essential for the cleavage of VP0 to VP2 and VP4, it was hypothesised that this would manifest in a difference in the proportion of precursor and cleaved structural proteins present in the wild-type vs. mutant virus. To investigate whether this was the case, protein from wild-type and mutant virus was extracted and run on SDS-PAGE gels, with results as shown in Figure 19 below.

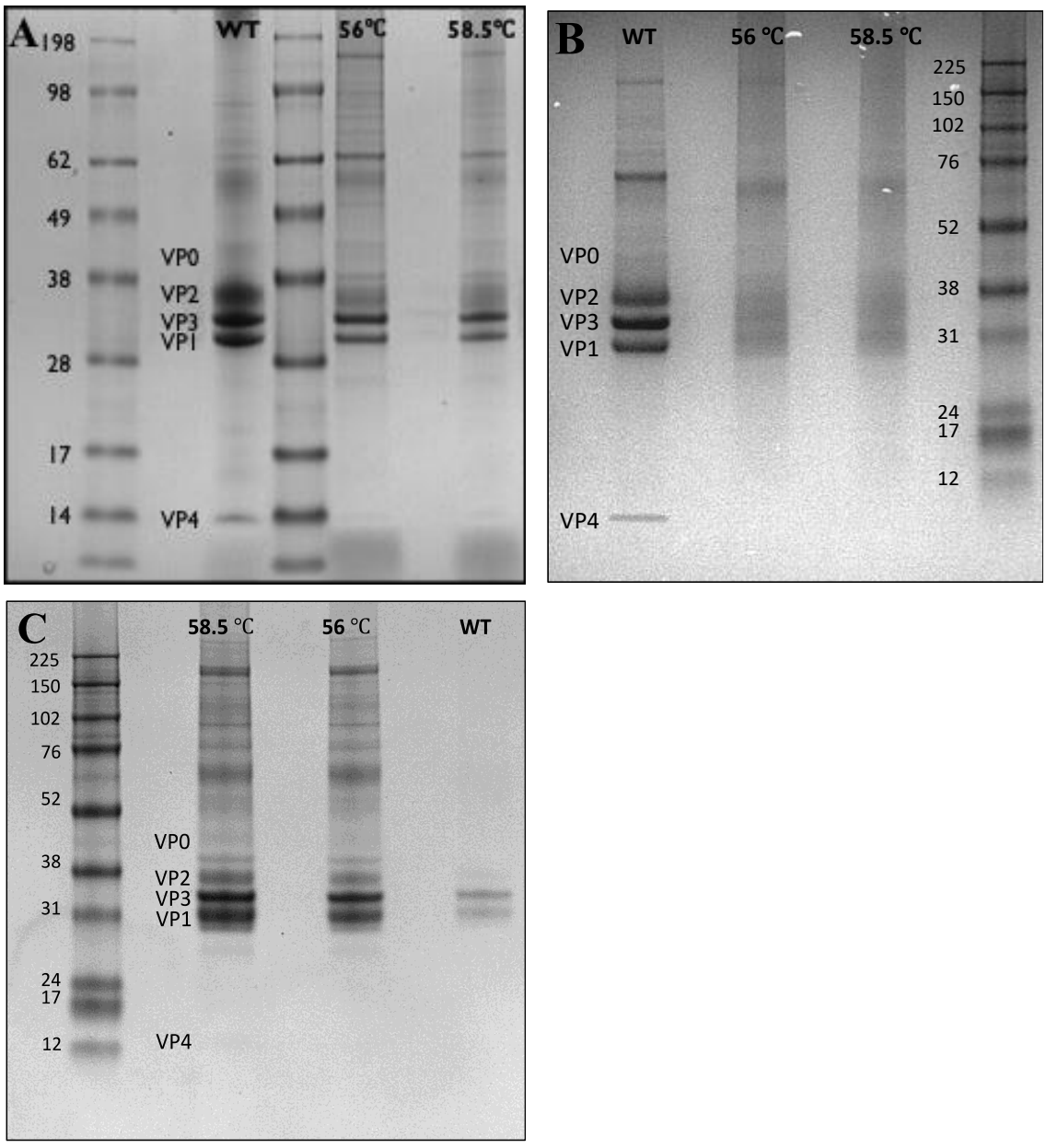

**Figure 19: Protein bands observed in SVV-001 lane appear different to those in the 56 °C resistant and 58.5 °C selected viral mutants' lanes. A)** As well as appearing better defined than the wild-type bands, the mutant lanes also had two strong bands at around 62 kDa and 130 kDa. **B)** A later SDS-PAGE gel using wild-type SVV-001 purified by Optiprep® gradient also showed bands at around 62 kDa and 130 kDa, note that the 56 resistant and 58.5 selected mutant lanes were not considered in further analysis. **C)** A repeated gel where the wild-type lane was not used in further analysis

### 3.6.2 *In silico* analysis of SDS-PAGE gels

ImageJ: Fiji (Schindlen et. al., 2012) was used to quantify the relative intensities of the bands corresponding to structural proteins in the SDS-PAGE gels (see: Figure 19). The relative intensities of VP2 and VP4 with respect to the precursor VP0 for the wild-type, 56 °C resistant and 58.5 selected mutants were measured, with results as shown below in Figure 20.

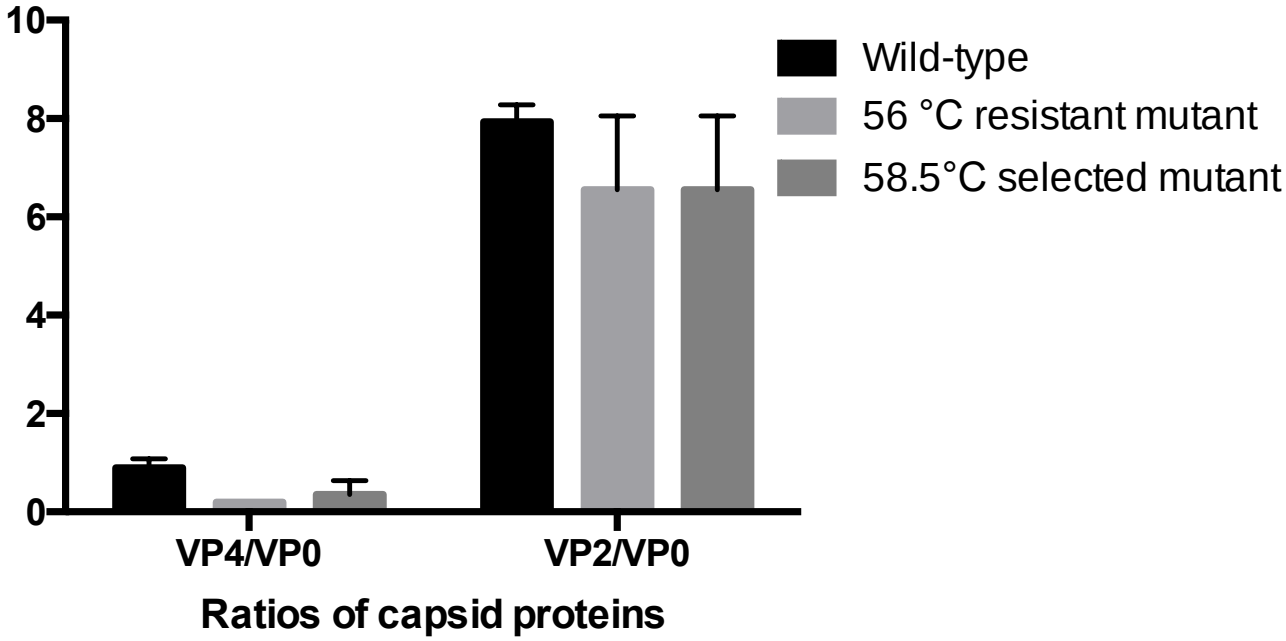


**Figure 20: Wild-type SVV-001 has a greater ratio of VP2 and VP4 with respect to VP0 than the thermostable mutants.** Ratios of ImageJ Fiji analysed structural protein bands from SDS-PAGE gels were compared between wild-type and thermostable mutants.

## 3.7 Mass Spectrometry

### 3.7.1 MASCOT database search results of analysed protein bands

The results of the SDS-PAGE gel raised a number of questions, for instance, the nature of the two strong bands that were not present in the wild-type, but that were present in the mutant lanes. To determine what exactly these are, they were excised from the gel and submitted to Otago's Centre for Protein Research (CPR). Figure 21 indicates those bands that were submitted to CPR, as well as the results of database searches following Matrix-Assisted Laser Desorption Ionisation-Time of Flight (MALDI-TOF) mass spectrometry.

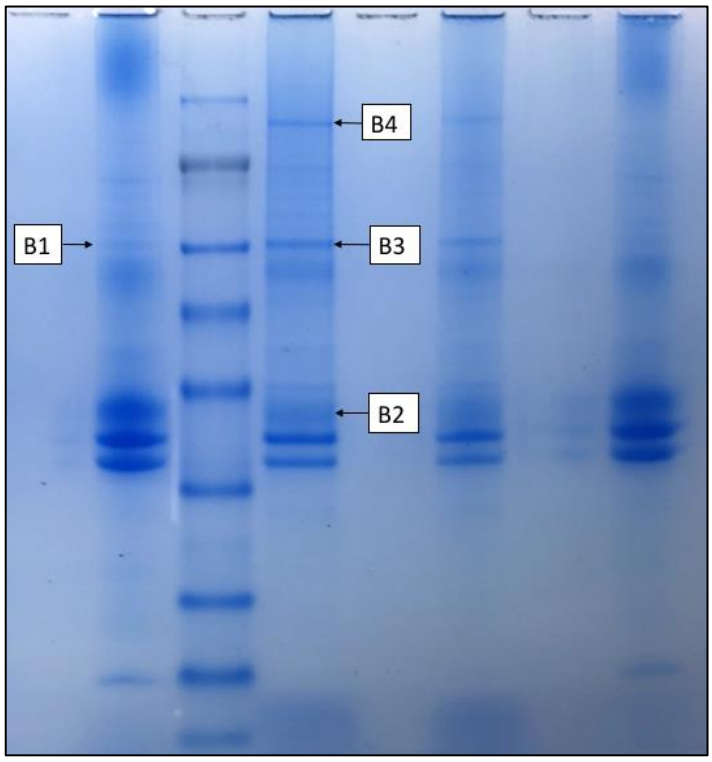


**Sample**: B1
**Database**: SwissProt tryptic search
**Protein hits**: ALBU BOVIN Serum albumin OS=Bos Taurus OX=9913 GN=ALB PE=1 SV=4

**Sample**: B2
**Database**: SwissProt tryptic search
**Protein hits**: 3CJI C Chain C, Structure of Seneca Valley Virus-001

**Sample**: B3
**Database**: SwissProt tryptic search
**Protein hits**: ALBU BOVIN Serum albumin OS=Bos Taurus OX=9913 GN=ALB PE=1 SV=4

**Sample**: B4
**Database**: SwissProt tryptic search
**Protein hits**: A2MG BOVIN Alpha-2-macroglobulin OS=Bos Taurus OX=9913 GN=A2M PE=1 SV=2

**Figure 21: Four bands of interest from an SDS-PAGE gel were investigated with mass spectrometry.** Bands submitted for MALDI-TOF mass spectrometry are denoted "B" (for "band") 1 through 4 and results with respect to database searches are displayed.

Mass spectrometry revealed that the 62 kDa and 130 kDa bands in the initial SDS-PAGE experiment were most likely bovine serum proteins. Taken in light of later SDS-PAGE gels, these were most likely the result of Optiprep® gradient co-purification. As an internal control, the band "B2" was determined, as predicted, to be VP2 of SVV.

## 3.8 Particle Stability Thermal Release assay (PaSTRy)

To directly contrast the thermal stability SVV-001 and 56 °C resistant viral populations, Particle Stability Thermal Release assays (PaSTRy) were performed with CsCl purified viral fractions. Figure 22 below demonstrates capsid destruction as a result of incubation at high temperature, using concentration of free RNA and exposure of protein hydrophobic residues as metrics.

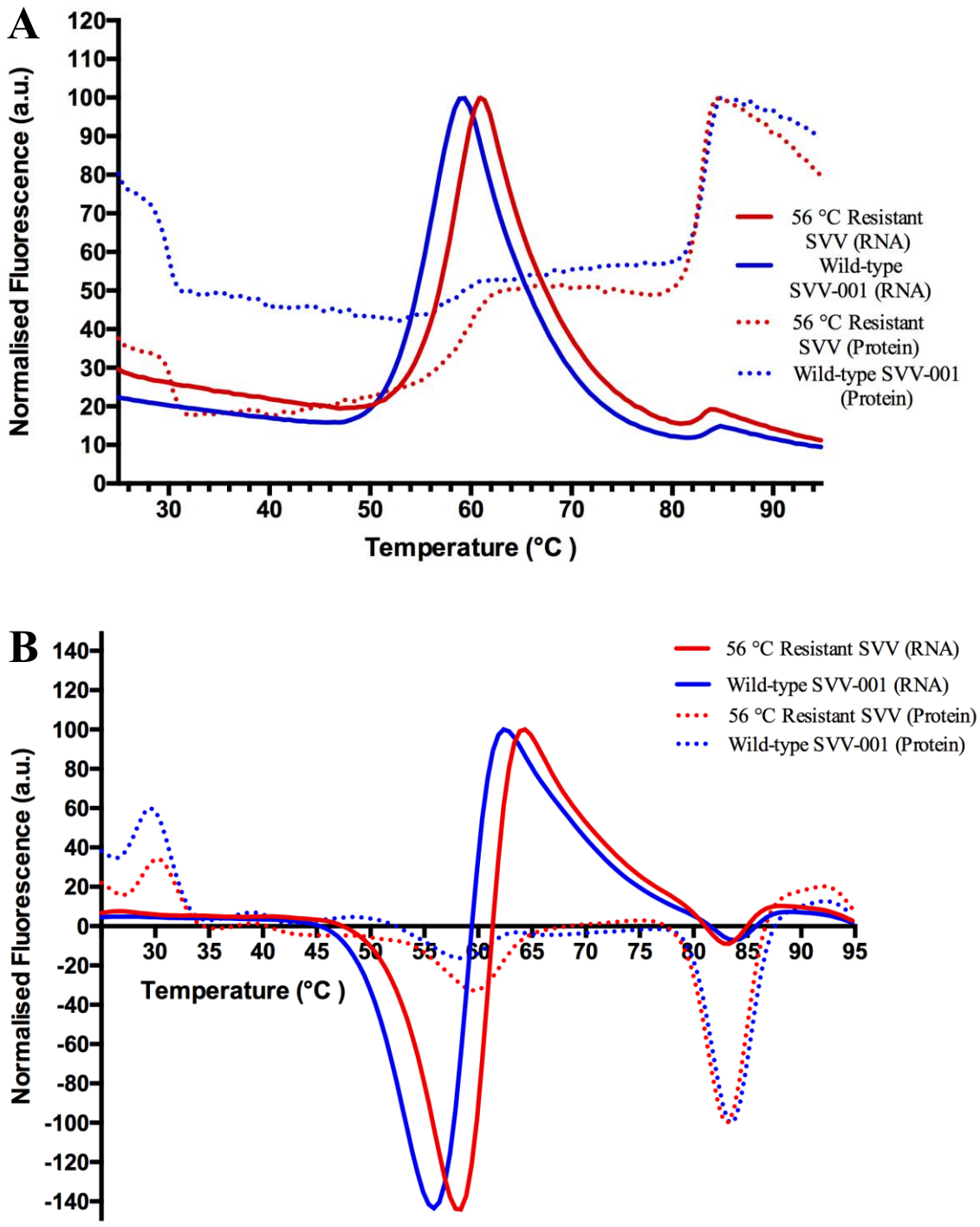


**Figure 22: PaSTRy comparing wild-type SVV-001 with thermostable mutant.** Release of viral RNA and exposure of hydrophobic residues from capsids in response to heating was monitored by SYTO9 and SYPRO Orange dyes respectively, with wild-type shown in dark blue, and 56 °C resistant viral population shown in red. In the RNA experiments, thermostable virus was assayed three times with triplicate values, and wild-type virus was assayed three times as internal controls. The protein experiments were performed with duplicate values. **A**) Normalised curve derived from melt curve actual values **B)** Derivative plot of melt curves

Results from the RNA-based PaSTRy assays showed an approximate positive 2 °C shift in the point of maximal fluorescence between the wild-type (59 °C) and thermostable mutants (61 °C), confirming the thermostable phenotype of the 56 °C resistant viral population. In the hydrophobic residue-based PaSTRy assays, there was a similar difference between the first peaks of the wild-type (61 °C) and thermostable virus (63.5 °C), while the secondary peaks were near-identical at approximately 84.5 °C. The first peaks correspond to the dissociation of virus from full capsids to pentamers, and the secondary peaks correspond to the denaturation of pentamers.

## 3.9 Cryo-electron microscopy

The 56 °C resistant mutant virus was prepared for cryo-electron microscopy, and a low-resolution structure was derived using the equipment readily available to Otago Micro and Nano Imaging (OMNI), including a JEOL 2200FS and RELION 3.0 software (Scheres, S. H., 2018). Note that this work was only made possible with assistance from Nadishka Jayawardena, who provided supervision and technical support with the JEOL 2200FS microscope, as well as invaluable assistance with single particle analysis.

### 3.9.1 Image collection

C-flat grids were visualised at 200 kV using a JEOL 2200FS cryo-electron microscope. First, grid areas to be examined were chosen based on ice quality. Montages were taken of chosen grid areas using in-built software tool Serial EM. From these montages, grid holes were labelled and images were acquired of the grid holes and particles therein. Figure 23 provides insight into this process.

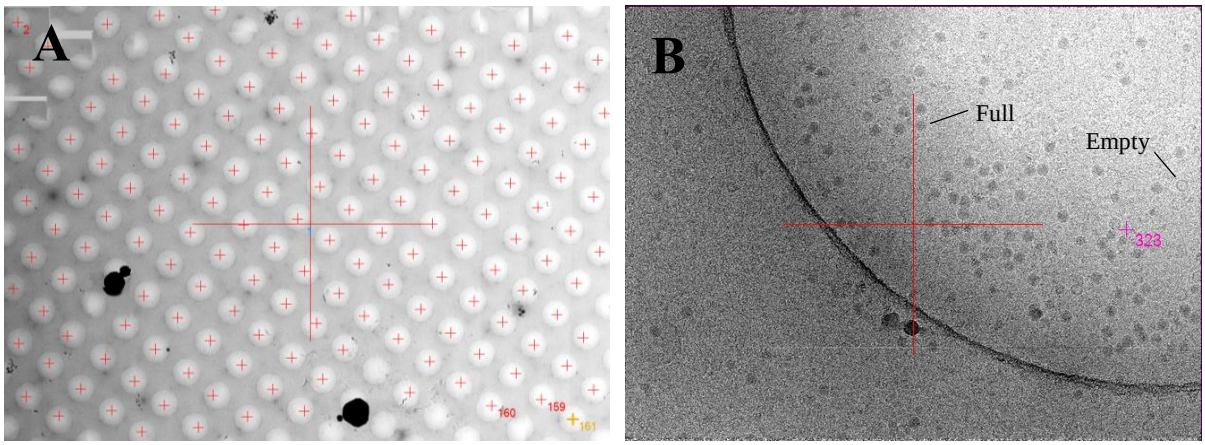


**Figure 23: Cryo-electron microscopy micrograph acquisition**. **A)** A completed montage of a grid area with red crosses indicating those grid holes to be imaged **B)** Image of a grid hole with both full and empty capsids visible.

### 3.9.2 Single particle analysis

Single particle analysis describes a process by which three-dimensional structures are derived from the data collected during cryo-electron microscopy. First image stacks are aligned to correct for motion during the exposure of the sample to the electron beam. Particles of interest in aligned images were manually picked. Particles that were picked were CTF corrected (see: 2.16.3 Single particle analysis) and 2D classes were generated to filter out broken and/or junk particles and ensure only intact, full viral capsids were to be analysed. Once the 2D classes were determined to be of sufficient quality, an initial 3D class was generated using SVV cryo-EM map as a reference and by imposing icosahedral symmetry (I4). Figure 24 below demonstrates results from important steps within the process of single particle analysis.

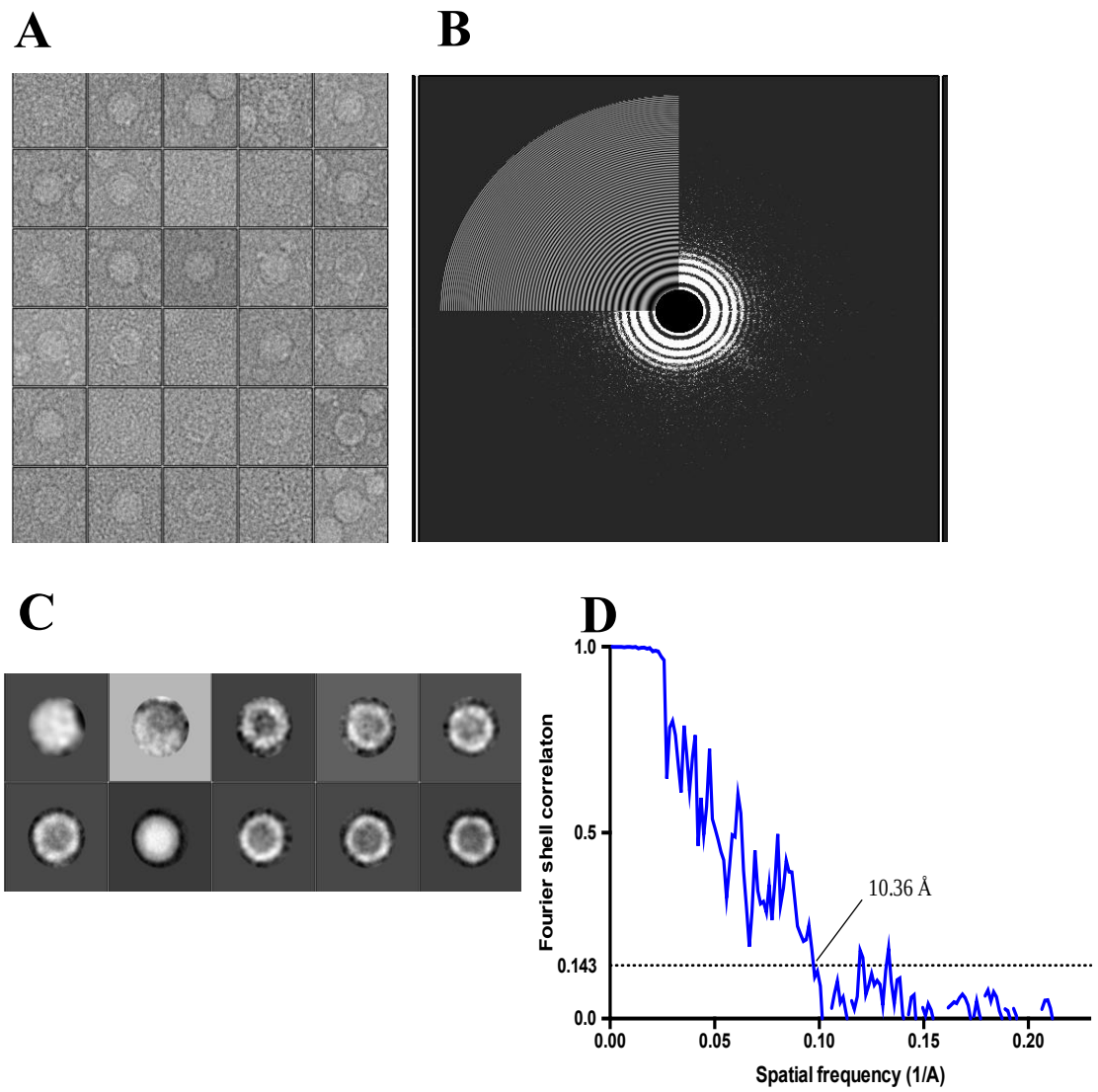


**Figure 24: Single particle analysis of the 56 °C resistant mutant. A)** Examples of particles picked from micrographs collected using the JEOL 2200FS electron microscope. **B)** CTF correction of motion corrected micrographs with simulated power spectrum (grey) and experimental power spectrum (black). **C)** 2D classes generated from picked particles including intact, broken and/or junk particles. **D)** 3D reconstruction produced a 10.36 Å resolution structure according to the gold standard fourier shell correlation cut-off of 0.143.

### 3.9.3 Cryo-electron microscopy derived structure of the 56 °C resistant mutant

Single particle analysis of collected micrographs culminated in a 10.36 Å structure of the 56 °C resistant mutant, as shown in Figure 21 alongside a 5.9 Å structure of the wild-type SVV-

001. This structure was derived from 404 out of 412 initially selected particles.

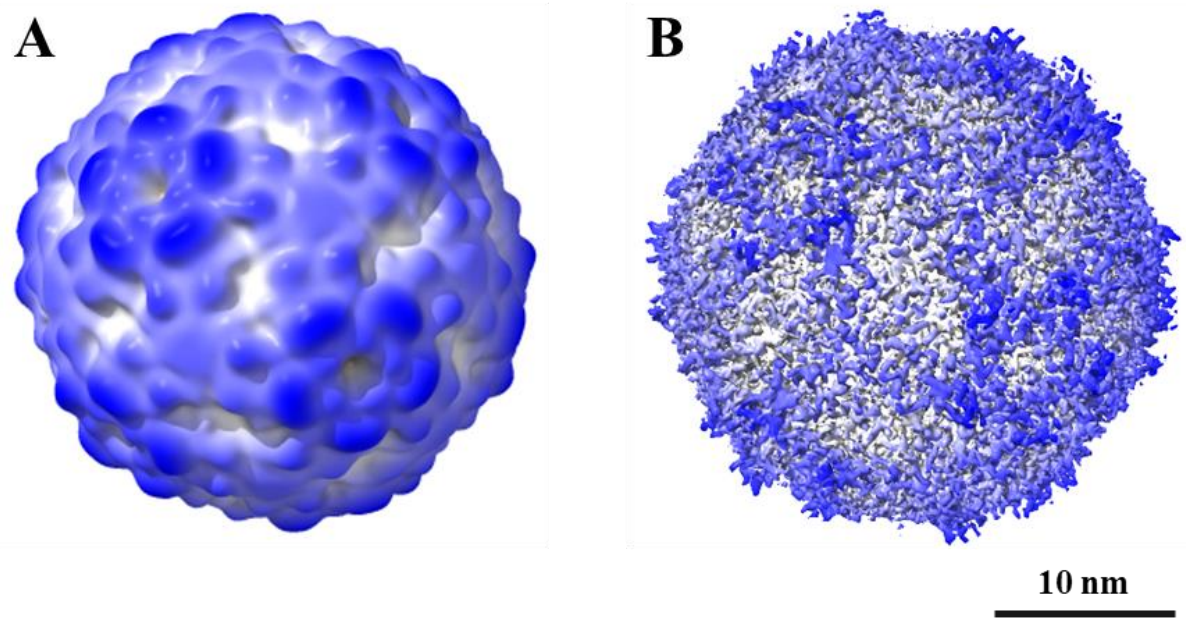


**Figure 25: Cryo-EM determined structure of the 56°C resistant mutant**. Structures of the 56 °C resistant mutant **(A)** at 10.36 Å resolution and of SVV-001 at 3.8 Å resolution **(B)** are shown on the left and right respectively. The scale bar shown represents 10 nm.

# 4 Discussion

## 4.1 Thermostability of wild-type SVV-001

While there are a variety of means to select for viral mutants with increased stability, for example exposure to extreme pH, the application of heat for this purpose was chosen for this work as it has a precedence in the literature (Adeyemi et. al., 2017). Successful SVV infection of susceptible cells requires binding to ANTXR1, more specifically the binding of the BC loop & loop II of VP1, the "puff" of VP2 and the "knob" of VP3, to ANTXR1 (Jayawardena et. al., 2018). Heat denatures the bonds between the viral proteins that comprise the viral capsid, thereby altering the delicate steric relationship of viral proteins and allowing the RNA genome to leak out of the capsid and in turn preventing successful infection. With heat selected as the means to derive stable mutants, the thermal probe experiments were performed for two reasons. Firstly, this was to characterise the thermostability of the SVV-001 viral capsid to provide a reference to which any mutant could be compared. Secondly, this was to inform an appropriate temperature to be used in a regimen of heating and passage to select for thermostable mutants. The first method that was used to determine this was taking aliquots of an SVV-001 stock of known viral titre, and measuring the viral titre after exposure to heating for 30 minutes. The initial experiments performed showed no appreciable loss in viral titre after incubation for 30 minutes between 40 °C and 55 °C, with a sharp decrease between 55 °C and 60 °C. After heating at 58.5 °C, there was an approximately 99% decrease in viral titre, and so this temperature was deemed appropriate for thermal selection going ahead. In light of the results of the thermal selection, which will be discussed later, there was a need to return to the thermal probe experiments. The method was therefore changed from comparing heated virus to the titre of a known stock, to include paired, equal aliquots of unheated and heated virus of a more dilute solution. This indicated that heating at 53.5 °C for 30 minutes causes a statistically significant approximately 99% decrease in SVV-001 viral titre. It is not immediately clear for

what reason the results from the two sets of experiments were so different. It could be that in first method the higher concentration of virus in sample would aggregate, thereby shielding some virus from complete exposure to heat.

## 4.2 Selection for thermostable SVV-001 mutants

The idea of the thermal selection experiments was to change the fundamental representation of SVV-001 virions with thermostable capsids from a minority to a majority, while still preserving qualities important for oncolytic activity, such as the ability to productively infect susceptible cells. The first thermal selection experiment, wherein wild-type SVV-001 was exposed to heating at 58.5 °C for 30 minutes, produced drastically different results than expected. Rather than losing approximately 99%, as the first thermal probe experiment would suggest, the SVV viral titre would fall over 99.99% and 99.999%, falling below the limit of detection. When the limit was sufficiently changed, there was a measurable 6 log decrease in viral titre down to the observation of a single viral plaque post-heating. Though the initial idea was not to plaque-purify putative thermostable mutants, this single plaque was the only one to come from the undiluted sample of the heated viral solution, and was therefore thought to represent a maximally and uniquely thermostable population. The single viral plaque was isolated from the plaque formation assay and was grown in a confluent T25 culture vessel of H446 cells. The concentrated cell lysate from this culture vessel was the "passage zero" for the forthcoming 56 °C and 58.5 °C thermal selection experiments. The difference between the expected results from the thermal probe and the observed results from the first thermal selection experiment was the basis for the revision of the method of the thermal probe. An important but minor finding from this experiment was that infection of susceptible cells with a known MOI of SVV-001 reliably produced similar titres of progeny virus.

As the single viral plaque was originally isolated from a wild-type SVV population heated to 58.5 °C, it was pertinent to determine whether this population was completely resistant to heating at this temperature. As it would turn out, it was not, and repeated passage and heating over 10 successive passages was not sufficient to select for a population that was completely resistant to heating at 58.5 °C. This finding was not entirely unexpected however, as literature on related viruses provides insight as to why this may be. In poliovirus, thermostable virus could be selected for that would be completely resistant to heating at 53 °C for 30 minutes, but a population that was completely resistant to heating at 57 °C for 30 minutes could not be selected for (Adeyemi et. al., 2017). This is consistent with findings in foot-and-mouth disease virus (FMDV) that capsid instability, as determined in the case of FMDV by mutually repellent charged residues on the interpentameric axis, is a property necessary for preserving infectivity (Lopez-Agruello et. al., 2019). Both of those studies suggest the pursuit of selection for thermostable mutants with conserved infectivity is inherently a self-limiting process.

While there was no discernible trend of adaptation of the plaque purified viral population to heating at 58.5 °C, the amount of viral titre produced after every passage gradually decreased over the course of the experiment. This is despite infection at a constant MOI. It was reasoned that the virus that has been through 10 successive passages may have developed additional, or alternative, mutations conferring thermostability, as was the case in poliovirus after 10 successive passages at 57 °C (Adeyemi et. al., 2017). For these reasons it would be purified and the capsid coding region sequenced.

As the plaque purified viral population was similarly resistant to heating at 58.5 °C as the wild-type SVV-001 was to heating at 53.5 °C, it was reasonable to expect that the plaque purified population would be resistant to heating at a temperature less than 58.5 °C but higher than 53.5

°C. The plaque purified viral population was evaluated for resistance to 56 °C, the average of the two values, and was shown to be completely resistant to heating at this temperature across three successive passages. The virus from the final passage of each of the 58.5 °C and 56 °C thermal selection experiments were used in forthcoming purification and sequencing experiments.

Though the thermostable phenotype of the mutant virus could be inferred from the results of the plaque formation assays, it is important to remember that plaque formations assays are, by nature, based on infectivity. SVV infectivity is based in large part on receptor binding, a property which would necessarily be conserved in any thermostable mutants from which VLPs are to be derived. For this reason, plaque assays are valuable in selecting for thermostable virus with conserved functionality. Conversely, plaque assays comparing the heated and unheated populations do not strictly measure the effect of heating on capsid integrity, rather they measure the effect of heating on infectivity. This is where PaSTRy becomes advantageous. PaSTRy utilises fluorescent dyes to monitor the levels of indicators of molecule denaturation in response to heat, such as exposure of protein hydrophobic residues, or levels of free RNA accessible to the dye. As PaSTRy does not rely on successful infection and lysis of prey cells, comparison between the wild-type and thermostable mutant response to heating using PaSTRy is a direct comparison of capsid stability. The results of the PaSTRy experiments showed an approximate 2 °C difference between in the fluorescence associated with capsid degradation of the wild-type and thermostable mutants, as measured by release of free RNA and exposure of hydrophobic residues. For the RNA measurements, the wild-type showed maximal fluorescence at approximately 59 °C and the 56 °C resistant mutant displayed maximal fluorescence at 61 °C. The protein results were somewhat different, with the wild-type plateauing after 61 °C and the 56 °C resistant mutant plateauing after heating to 63.5 °C. This

would suggest that RNA release precedes exposure of hydrophobic residues. This would be consistent with the RNA evacuating the capsid before dye can penetrate and bind the hydrophobic residues on the inside of the capsids. This may also speak to why rather than discreet peaks as seen in the RNA PaSTRy experiments, the increase in fluorescence in the protein PaSTRy has a much flatter curve. Whereas the RNA release conceivably occurs rapidly, due to the pressure difference across the capsid, hydrophobic residues may be continually exposed as the heat denatures viral capsids. The difference between the two viral populations as measured by PaSTRy would appear slight, especially when compared to plaque assay results, highlighting the importance of using both.

Aside from the RNA fluorescence peaks at around 59 °C and 61 °C for the wild-type and mutant respectively, there were smaller, secondary peaks were seen at higher temperatures. These smaller peaks were at approximately 84 °C for the thermostable mutant and 85 °C for the wild-type. Similar results were observed in another picornavirus, Equine Rhinitis A virus (ERAV), using another RNA-binding dye, SYBRgreen2 (Walter et. al., 2012). In the case of ERAV, smaller peaks were seen around 81 °C. The exact nature of these smaller peaks was not commented on (Walter et. al., 2012). Due to the extreme nature of the temperatures at which the secondary peaks are observed, it is unlikely that they represent capsid degradation of a viral sub-population. Most likely, the secondary peaks represent the denaturation of RNA secondary structures, which would free up additional nucleotide lengths for dye-binding. If the secondary structures of the genome have indeed changed between the wild-type and thermostable SVV, this may then be reflected in a difference in the temperature that produces the secondary fluorescence peaks.

## 4.3 Altered capsid maturation as the likely modality granting thermostability to mutant SVV-001

The explicit intent of this project was to determine mutations conferring stability to the SVV capsid, for the production of Virus-Like Particles. This means that the mutations that are of the greatest interest to this project are non-synonymous mutations in the SVV structural proteins. Investigations into both thermally selected mutants only found one such mutation, VP2 I206V. It was not immediately obvious how, if at all, this mutation may confer thermostability to the SVV viral capsid. Commonly, mutations conferring thermostability to picornaviral capsids increase the internal binding of these capsids, either within protomers (Adeyemi et. al., 2017) or between pentamers (Lopez-Arguello et. al., 2019). This appears not to be the case with VP2 I206V, as modelling with DUET software indicated that the mutation itself is decreases the overall internal binding of the SVV protomer. VP2 I206V is not positioned at either the inter-protomeric or interpentameric interfaces, and so most likely does not act to strengthen binding between capsid subunits. Further *in silico* analysis of the VP2 I206V mutation with UCSF Chimera predicted that the substitution of isoleucine with the shorter valine is predicted to ablate interaction with VP2 H204. VP2 H204 is an amino-acid previously identified as being integral to the cleavage of VP0 to VP2 and VP4 in SVV, with homologues in other picornaviruses, including VP2 H195 in PV and VP2 H145 in FMDV (Strauss et. al., 2018). If the interaction with VP2 I206 is important for the positioning and/or function of VP2 H204, then this would manifest as a change in the relative proportions of VP0 to VP2 and VP4 observed between the wild-type and mutants. For this reason, we isolated the structural proteins from wild-type and mutant SVV and analysed these with SDS-PAGE gel electrophoresis. The bands seen in the mutant and wild-type lanes were quite different, with strong, distinct bands at approximately 62 kDa and 130 kDa in the mutant lane that were not present in the wild-type lane. As these seemed to be rough multiples of the 36 kDa VP2 protein, or fusions of multiple

capsid proteins, we hypothesised that perhaps there may have been altered capsid protein translation in the thermostable mutants. These would be investigated with mass spectrometry. For mass spectrometry, bands of interest were extracted from SDS-PAGE gels and submitted to Otago's Centre for Protein Research, where analysis and database referencing revealed that the approximately 62 and 138 kDa bands were bovine serum proteins. These were most likely co-purified with SVV during optiprep gradient purification. As in the original SDS-PAGE gel the wild-type SVV-001 was purified with caesium chloride gradient, this would likely explain why those bovine serums were not present in the wild-type. Repeated gels with wild-type SVV-001 likewise purified by Optiprep® gradient revealed similar higher kDa bands to those seen in the thermostable mutant lanes, precluding the conclusion that these bands were in some way related to the thermostable phenotype of the mutants. Though identical protein amounts were loaded in the initial SDS-PAGE experiment, the presence of bovine serum proteins in the Optiprep® purified samples would have contributed to the measured protein concentration, and thus direct comparison of the band intensities of the structural proteins of the wild-type and thermostable virus would have been inappropriate. For this reason, the band intensities for structural proteins were compared to each other within their own lanes. The initial gel that was run suggested that the ratio of VP2 and VP4 when compared to VP0 was non-significantly lower in the thermostable mutants than in the wild-type. This supports the idea the VP2 I206V mutation impacts the cleavage of precursor structural proteins. Work from within this lab has shown that as well as the genome packaged capsid, the SVV procapsid has cleaved VP0 (Strauss et. al., 2018). This means that whatever degree of thermostability that VP2 I206V confers, any SVV VLP's produced also stand to benefit from. It is worth mentioning as well that the A1776G mutation is predicted to alter the secondary structure of the SVV-001 genome, and as the RNA genome interacts with the interior of the capsid, this may play a role in improving the thermostability of the mutant virion (Shakeel et. al., 2016).

While technically in the structural proteins coding sequences, the C2526U and A3434G mutations are synonymous mutations, and so do not alter the translated structural proteins. This does not necessarily mean that they do not have any impact on thermostability. As previously mentioned, the RNA bound within picornaviral capsids can interact with the interior of the capsid structural proteins (Shakeel et. al., 2016). The C2526U mutation is predicted to change the secondary structure of the RNA genome, which may alter the interactions between the genome and the capsid interior. The A3434G mutation however, is not predicted to appreciably change the secondary structure of the viral genome, and so may simply be a chance mutation, that does not contribute to the thermostable phenotype.

Finally, the G3777A mutation is an interesting one, as it is outside the capsid-encoding P1 region of SVV-001 and therefore cannot have an impact on the capsid protein stability. It is located in the sequence encoding the viral 2B protein, which in most picornaviruses is a viroporin. Viroporins are relatively small proteins which oligomerise and permeabilise lipid membranes (Nieva et. al., 2012). Picornaviral 2B proteins localise to the endoplasmic reticulum and Golgi complex, where mulitmers form pores through which small solutes can leak out (Nieva et. al. 2003). This raises questions as to how, if at all, the G3777A mutation might contribute to the replication of the thermostable selected mutants. Hypothesis generation is further complicated by the low degree of primary sequence identity between picornaviral 2B proteins, as shown by the initial study reporting the discovery of SVV-001, where no picornaviral species shared an excess of 20% sequence identity with SVV-001 (Hales et. al., 2008). Despite low sequence identity, picornaviral 2B proteins are thought to have a high degree of structural similarity with each other, sharing a helix-turn-helix motif that is responsible for the membrane binding activity. G3777A is predicted to have an effect on the

secondary structure of the RNA genome, which presents a much clearer way in which it might contribute to the thermostable phenotype.

Cryo-electron microscopy was undertaken to discern any changes to the structure of the thermostable mutant virus as a result of mutations in the structural proteins and/or RNA genome. From CsCl purified fractions, a 10.36 Å structure was derived of the 56 °C resistant mutant. Unfortunately, as 10.36 Å is relatively low resolution, the conclusions that can be drawn from this structure are limited. At this resolution, it would appear that the thermostable mutant is not appreciably different to a 3.8 Å structure of the SVV-001 capsid.

## 4.4 Summary

This work sought to determine residues and mutations thereof that confer thermal stability to the SVV-001 capsid, to inform the production of thermostable VLPs. First, the temperature sufficient to exert a significant selection pressure on SVV-001 was investigated. Early results from this investigation lead to the heating of SVV-001 to 58.5 °C for 30 minutes, which when enumerated produced a single viral plaque. This single viral plaque was extracted and grown in H446 cells while the method for determining an appropriate selection temperature was amended. With the amended method, roughly 99% of wild-type SVV-001 was shown to be inactivated as a consequence of heating at 53.5 °C for 30 minutes. When tested similarly, the plaque purified viral population was completely resistant to heating at 56 °C for 30 minutes, and could not be successfully be selected to be fully resistant to heating at 58.5 °C after 30 minutes. Wild-type SVV-001, as well as viral populations that were resistant to heating at 56 °C, and that had undergone 10 successive passages with heating at 58.5 °C, were then expanded, purified and sequenced. This revealed a number of mutations inside and outside of the capsid coding region of the genome which were present in the 56 °C resistant and 58.5 °C

selected viral populations that were not present in wild-type SVV-001. These mutations were then modelled *in silico*. One mutation in particular, VP2 I206V, was reasoned to alter the relative amounts of the capsid proteins VP2 and VP4 versus their precursor VP0. Protein from purified viral fractions was precipitated out and analysed using SDS-PAGE. This suggested that there was a non-significantly increased proportion of VP0 in the thermostable mutants than in the wild-type SVV-001. The SDS-PAGE results also showed two bands in the thermostable mutant lanes at approximately 62 kDa and 130 kDa, which were confirmed by mass-spectrometry to be bovine serum proteins. Repeated SDS-PAGE with SVV-001 purified by Optiprep® gradient also showed two similar bands. The wild-type and 56 °C resistant viral populations were then directly contrasted with PaSTRy. PaSTRy demonstrated that the capsids of wild-type virus dissociate and release RNA from around 59 °C, whereas capsids of 56 °C resistant virus dissociate do the same from 61 °C onwards. Finally, CsCl purified 56 °C resistant SVV was prepared for cryo-electron microscopy, producing a 10.36 Å structure of the full capsid.

# 5 Future Work

This work identified mutations present in thermally selected populations of the novel oncolytic virus, Seneca Valley Virus. Though four mutations were initially identified, it would seem that only one of these would likely be of utility of the production of thermostable VLPs, as was the express purpose of undertaking this project. This was the VP2 I206V mutation. Naturally, future work would involve the introduction of the VP2 I206V mutation in to the wild-type SVV-001 and the verification of the presence or absence of the thermostable phenotype.

Continuing on the assumption that VP2 I206V is experimentally demonstrated to confer increased structural stability to the SVV-001 capsid, the next objective would be to determine if the VP2 I206V mutation would similarly increase the structural stability of the empty capsid of SVV-001 compared to the wild-type empty capsid. As the VLP is non-infectious, VLP titres post-heating would have to be measured using a different method than the plaque assays used for determining SVV viral titres. Looking further in to the development of stable VLP's, strategies would have to be developed for the successful packaging of cytotoxic drugs into the SVV-001 VLP. As in FMDV there has been putative packaging signals identified within the secondary structures of the genome (Logan et. al., 2018), it stands to reason SVV may have similar packaging signals. At the time of this writing, this lab is undertaking work to determine the presence of packaging signals within the SVV genome. If they are discovered, they will present a likely route by which cytotoxic drugs can be introduced into the SVV VLP.

This project also resulted in solving the structure of the 56 °C resistant SVV to a resolution of 10.36 Å. Further work would entail solving the structure to a much higher resolution so as to draw much more meaningful conclusions as to the effect of the mutations on the viral structure.

# 6 References


1. Adachi, M., Brooks, S. E., Stein, M. R., Franklin, B. E., & Caccavo, F. A. (2006). Destruction of human retinoblastoma after treatment by the E variant of encephalomyocarditis virus. *Journal of neuro-oncology*, *77*(3), 233-240.

2. Adams, M.J.; King, A.M.; Carstens, E.B. Ratification vote on taxonomic proposals to the International Committee on Taxonomy of Viruses (2013). *Arch Virol* 2013, *158*, 2023-2030, doi:10.1007/s00705-013-1688-5.

3. Adams, M. J., Lefkowitz, E. J., King, A. M. Q., Bamford, D. H., Breitbart, M., Davison, A. J., Ghabrial S. A., Gorbalenya, A. E., Knowles, N. J., Krell, P., Lavigne, R., Prangshevilli, D., Sanfaçon¸H., Siddell, S. G., Simmonds P. & Carstens, E. B. (2015). Ratification vote on taxonomic proposals to the International Committee on Taxonomy of Viruses (2015). *Archives of virology*, *160*(7), 1837-1850.

4. Adeyemi, O. O., Nicol, C., Stonehouse, N. J., & Rowlands, D. J. (2017). Increasing type 1 poliovirus capsid stability by thermal selection. *Journal of virology*, *91*(4), e01586-16.

5. Alberts, P.; Olmane, E.; Brokane, L.; Krastina, Z.; Romanovska, M.; Kupcs, K.; Isajevs, S.; Proboka, G.; Erdmanis, R.; Nazarovs, J., et al. Long-term treatment with the oncolytic ECHO-7 virus Rigvir of a melanoma stage IV M1c patient, a small cell lung cancer stage IIIA patient, and a histiocytic sarcoma stage IV patient-three case reports. *APMIS* 2016, *124*, 896-904, doi:10.1111/apm.12576

6. Alberts, P.; Tilgase, A.; Rasa, A.; Bandere, K.; Venskus, D. The advent of oncolytic virotherapy in oncology: The Rigvir(R) story. *Eur J Pharmacol* 2018, *837*, 117-126, doi:10.1016/j.ejphar.2018.08.042.

7. Andtbacka, R.H.I.; Curti, B.D.; Hallmeyer, S.; Feng, Z.; Paustian, C.; Bifulco, C.; Fox, B.; Grose, M.; Shafren, D. Phase II calm extension study: Coxsackievirus A21 delivered intratumorally to patients with advanced melanoma induces immune-cell infiltration in the tumor microenvironment. *Journal for ImmunoTherapy of Cancer* 2015, *3*, doi:10.1186/2051-1426-3-s2-p343

8. Andtbacka, R.H.I.; Curti, B.; Hallmeyer, S.; Feng, Z.; Paustian, C.; Bifulco, C.; Fox, B.; Grose, M.; Davies, B.; Karpathy, R., et al. Phase II CALM extension study: Enhanced immune-cell infiltration within the tumour micro-environment of patients with advanced melanoma following intralesional delivery of Coxsackievirus A21. *Eur J Cancer* 2015, *51*, S677-S677, doi:Doi 10.1016/S0959-8049(16)31854-8.

9. Annels, N.E.; Arif, M.; Simpson, G.R.; Denyer, M.; Moller-Levet, C.; Mansfield, D.; Butler, R.; Shafren, D.; Au, G.; Knowles, M., et al. Oncolytic Immunotherapy for

Bladder Cancer Using Coxsackie A21 Virus. *Mol Ther Oncolytics* 2018, *9*, 1-12, doi:10.1016/j.omto.2018.02.001.

10. Ansardi, D. C., Porter, D. C., Jackson, C. A., Gillespie, G. Y., & Morrow, C. D. (2001). RNA replicons derived from poliovirus are directly oncolytic for human tumor cells of diverse origins. *Cancer research*, *61*(23), 8470-8479.

11. Asada, T. (1974). Treatment of human cancer with mumps virus. *Cancer*, *34*(6), 1907-1928.

12. Atsumi, S., Matsumine, A., Toyoda, H., Niimi, R., Iino, T., Nakamura, T., Matsubara, T., Asanuma, K., Komada, Y., Uchida, A., & Sudo, A. (2012). Oncolytic virotherapy for human bone and soft tissue sarcomas using live attenuated poliovirus. *International journal of oncology*, *41*(3), 893-902.

13. Au, G.G.; Lincz, L.F.; Enno, A.; Shafren, D.R. Oncolytic Coxsackievirus A21 as a novel therapy for multiple myeloma. *Brit J Haematol* 2007, *137*, 133-141, doi:10.1111/j.1365-2141.2007.06550.x.

14. Au, G.G.; Beagley, L.G.; Haley, E.S.; Barry, R.D.; Shafren, D.R. Oncolysis of malignant human melanoma tumors by Coxsackieviruses A13, A15 and A18. *Virol J* 2011, *8*, 22, doi:10.1186/1743-422X-8-22

15. Babiker, H.M.; Riaz, I.B.; Husnain, M.; Borad, M.J. Oncolytic virotherapy including Rigvir and standard therapies in malignant melanoma. *Oncolytic Virother* 2017, *6*, 11-18, doi:10.2147/OV.S100072.

16. Banerjee, R., & Dasgupta, A. (2001). Interaction of picornavirus 2C polypeptide with the viral negative-strand RNA. *Journal of General Virology*, *82*(11), 2621-2627.

17. Barnard, M. E., Boeke, C. E., & Tamimi, R. M. (2015). Established breast cancer risk factors and risk of intrinsic tumor subtypes. *Biochimica et Biophysica Acta (BBA)-Reviews on Cancer*, *1856*(1), 73-85.

18. Bedard, K. M., & Semler, B. L. (2004). Regulation of picornavirus gene expression. *Microbes and Infection*, *6*(7), 702-713.

19. Bell, M. P., & Pavelko, K. D. (2016). Enhancing the tumor selectivity of a picornavirus virotherapy promotes tumor regression and the accumulation of infiltrating CD8+ T cells. *Molecular cancer therapeutics*, *15*(3), 523-530.

20. Bell, M. P., Renner, D. N., Johnson, A. J., & Pavelko, K. D. (2014). A CD8 T-cell epitope variant enhances immune targeting to a recombinant picornavirus vaccine antigen. *Viral immunology*, *27*(7), 361-366.

21. Bostwick, D. G., Burke, H. B., Djakiew, D., Euling, S., Ho, S. M., Landolph, J., Morrison, H., Sonewane, B., Shiflett, T., Waters D. J., & Timms, B. (2004). Human

prostate cancer risk factors. *Cancer: Interdisciplinary International Journal of the American Cancer Society*, *101*(S10), 2371-2490.

22. Bradley, S., Jakes, A. D., Harrington, K., Pandha, H., Melcher, A., & Errington-Mais, F. (2014). Applications of coxsackievirus A21 in oncology. *Oncolytic virotherapy*, *3*, 47.

23. Bray, F., Ferlay, J., Soerjomataram, I., Siegel, R. L., Torre, L. A., & Jemal, A. (2018). Global cancer statistics 2018: GLOBOCAN estimates of incidence and mortality worldwide for 36 cancers in 185 countries. *CA: a cancer journal for clinicians*, *68*(6), 394-424.

24. Brown, M. C., & Gromeier, M. (2015). Cytotoxic and immunogenic mechanisms of recombinant oncolytic poliovirus. *Current opinion in virology*, *13*, 81-85.

25. Brown, M. C., Holl, E., Boczkowski, D., Walton, R., Bigner, D. D., Gromeier, M., & Nair, S. K. (2015). Oncolytic poliovirus directs tumor antigen presentation and T cell activation in vitro. *Journal for immunotherapy of cancer*, *3*(2), P332.

26. Brown, M. C., Holl, E. K., Boczkowski, D., Dobrikova, E., Mosaheb, M., Chandramohan, V., Bigner, D. D., & Nair, S. K. (2017). Cancer immunotherapy with recombinant poliovirus induces IFN-dominant activation of dendritic cells and tumor antigen–specific CTLs. *Science translational medicine*, *9*(408), eaan4220.

27. Bruvere, R., Heisele, O., Ferdats, A., Rupais, A., & Muceniece, A. (2002). Echovirus-mediated biotherapy for malignant tumours: 40 years of investigation. *Acta Med Litu*, *9*(Suppl 9), 97-100.

28. Buckland, F. E., Bynoe, M. L., & Tyrrell, D. A. J. (1965). Experiments on the spread of colds: II. Studies in volunteers with coxsackievirus A21. *Epidemiology & Infection*, *63*(3), 327-343.

29. Burke, M. J. (2016). Oncolytic Seneca Valley Virus: past perspectives and future directions. *Oncolytic virotherapy*, *5*, 81.

30. Burke, M. J., Ahern, C., Weigel, B. J., Poirier, J. T., Rudin, C. M., Chen, Y., Cripe, T. P., Bernhart, M. B., & Blaney, S. M. (2015). Phase I trial of Seneca Valley Virus (NTX-010) in children with relapsed/refractory solid tumors: A report of the Children's Oncology Group. *Pediatric blood & cancer*, *62*(5), 743-750.

31. Cameron, C. E., Suk Oh, H., & Moustafa, I. M. (2010). Expanding knowledge of P3 proteins in the poliovirus lifecycle. *Future microbiology*, *5*(6), 867-881.

32. Carocci, M., & Bakkali-Kassimi, L. (2012). The encephalomyocarditis virus. *Virulence*, *3*(4), 351-367.

33. Carstens, E. B. (2010). Ratification vote on taxonomic proposals to the International Committee on Taxonomy of Viruses (2009). *Archives of virology*, *155*(1), 133-146.

34. Cello, J., Toyoda, H., DeJesus, N., Dobrikova, E. Y., Gromeier, M., & Wimmer, E. (2008). Growth phenotypes and biosafety profiles in poliovirus-receptor transgenic mice of recombinant oncolytic polio/human rhinoviruses. *Journal of medical virology*, *80*(2), 352-359.

35. Dalldorf, G., & Sickles, G. M. (1948). An Unidentified, Filtrable Agent Isolated From the Feces of Children With Paralysis. *Science (Washington)*, 61-4.

36. Dethlefs, S., Escriou, N., Brahic, M., van der Werf, S., & Larsson-Sciard, E. L. (1997). Theiler's virus and Mengo virus induce cross-reactive cytotoxic T lymphocytes restricted to the same immunodominant VP2 epitope in C57BL/6 mice. *Journal of virology*, *71*(7), 5361-5365.

37. Desjardins, A., Sampson, J. H., Peters, K. B., Ranjan, T., Vlahovic, G., Threatt, S., & Herndon, J. E. (2014). Oncolytic polio/rhinovirus recombinant (PVSRIPO) in recurrent glioblastoma (GBM): first Phase I clinical trial evaluating the intratumoral administration. *Neuro-oncology*, *16*(Suppl 3), iii43.

38. Desjardins, A., Gromeier, M., Herndon, J. E., Beaubier, N., Bolognesi, D. P., Friedman, A. H., McSherry, F., Muscat, A. M., Nair, S., & Peters, K. B. (2018). Recurrent glioblastoma treated with recombinant poliovirus. *New England Journal of Medicine*, *379*(2), 150-161.

39. Dick, G. W. A. (1948). Mengo encephalomyelitis virus: pathogenicity for animals and physical properties. *British journal of experimental pathology*, *29*(6), 559.

40. Dobrikova, E. Y., Broadt, T., Poiley-Nelson, J., Yang, X., Soman, G., Giardina, S., Harris. R., & Gromeier, M. (2008). Recombinant oncolytic poliovirus eliminates glioma in vivo without genetic adaptation to a pathogenic phenotype. *Molecular therapy*, *16*(11), 1865-1872.

41. Dobrikova, E. Y., Goetz, C., Walters, R. W., Lawson, S. K., Peggins, J. O., Muszynski, K., Ruppel. S., Poole, K., Giardina, S. L., Vela, E. M., & Estep, J. E. (2012). Attenuation of neurovirulence, biodistribution, and shedding of a poliovirus: rhinovirus chimera after intrathalamic inoculation in Macaca fascicularis. *Journal of virology*, *86*(5), 2750-2759.

42. Domingo, E., Sheldon, J., & Perales, C. (2012). Viral quasispecies evolution. Microbiol. Mol. Biol. Rev., 76(2), 159-216.

43. Donina, S.; Strele, I.; Proboka, G.; Auzins, J.; Alberts, P.; Jonsson, B.; Venskus, D.; Muceniece, A. Adapted ECHO-7 virus Rigvir immunotherapy (oncolytic virotherapy) prolongs survival in melanoma patients after surgical excision of the tumour in a retrospective study. *Melanoma Res* 2015, *25*, 421-426, doi:10.1097/CMR.0000000000000180

44. Eisenhauer, E. A., Therasse, P., Bogaerts, J., Schwartz, L. H., Sargent, D., Ford, R., Arbuck, S., Gwyther, S., Mooney, M., & Rubinstein, L. (2009). New response evaluation criteria in solid tumours: revised RECIST guideline (version 1.1). *European journal of cancer*, *45*(2), 228-247.

45. Fallaux, F. J., Bout, A., van der Velde, I., van den Wollenberg, D. J., Hehir, K. M., Keegan, J., Augur, C., Cramer, S. J., Van Ormondt, H., Van Der Eb, A. J., Valerio, D. & Hoeben, R. C. (1998). New helper cells and matched early region 1-deleted adenovirus vectors prevent generation of replication-competent adenoviruses. *Human gene therapy*, *9*(13), 1909-1917.

46. Fukuhara, H., Ino, Y., & Todo, T. (2016). Oncolytic virus therapy: a new era of cancer treatment at dawn. *Cancer science*, *107*(10), 1373-1379.

47. Garber, K. China approves world's first oncolytic virus therapy for cancer treatment. *J Natl Cancer Inst* 2006, *98*, 298-300, doi:10.1093/jnci/djj111

48. Gerber, D. E. (2008). Targeted therapies: a new generation of cancer treatments. *American family physician*, *77*(3).

49. Georgiades, J., Zielinski, T., Cicholska, A., & Jordan, E. (1959). Research on the oncolytic effect of APC viruses in cancer of the cervix uteri; preliminary report. *Biuletyn Instytutu Medycyny Morskiej w Gdansku*, *10*, 49-57.

50. Ghadirian, P., Cadotte, M., Lacroix, A., & Perret, C. (1991). Family aggregation of cancer of the prostate in Quebec: the tip of the iceberg. *The prostate*, *19*(1), 43-52.

51. Ghoncheh, M., Pournamdar, Z., & Salehiniya, H. (2016). Incidence and mortality and epidemiology of breast cancer in the world. *Asian Pac J Cancer Prev*, *17*(S3), 43-46.

52. Glover Jr, F. E., Coffey, D. S., Douglas, L. L., Russell, H., Cadigan, M., Tulloch, T., Wedderburn, K., Wan, R. L., Baker, T. D., & Walsh, P. C. (1998). Familial study of prostate cancer in Jamaica. *Urology*, *52*(3), 441-443.

53. Greig, S.L. Talimogene Laherparepvec: First Global Approval. *Drugs* 2016, *76*, 147-154, doi:10.1007/s40265-015-0522-7.

54. Gromeier, M., Alexander, L., & Wimmer, E. (1996). Internal ribosomal entry site substitution eliminates neurovirulence in intergeneric poliovirus recombinants. *Proceedings of the National Academy of Sciences*, *93*(6), 2370-2375.

55. Haggar, F. A., & Boushey, R. P. (2009). Colorectal cancer epidemiology: incidence, mortality, survival, and risk factors. *Clinics in colon and rectal surgery*, *22*(04), 191-197.

56. Hales, L. M., Knowles, N. J., Reddy, P. S., Xu, L., Hay, C., & Hallenbeck, P. L. (2008). Complete genome sequence analysis of Seneca Valley virus-001, a novel oncolytic picornavirus. *Journal of General Virology*, *89*(5), 1265-1275.

57. Hambardzumyan, D., Becher, O. J., Rosenblum, M. K., Pandolfi, P. P., Manova-Todorova, K., & Holland, E. C. (2008). PI3K pathway regulates survival of cancer stem cells residing in the perivascular niche following radiation in medulloblastoma in vivo. *Genes & development*, *22*(4), 436-448.

58. Hazini, A.; Pryshliak, M.; Bruckner, V.; Klingel, K.; Sauter, M.; Pinkert, S.; Kurreck, J.; Fechner, H. Heparan Sulfate Binding Coxsackievirus B3 Strain PD: A Novel Avirulent Oncolytic Agent Against Human Colorectal Carcinoma. *Hum Gene Ther* 2018, *29*, 1301-1314, doi:10.1089/hum.2018.036.

59. Helwig, F. C., & Schmidt, E. C. H. (1945). A filter-passing agent producing interstitial myocarditis in anthropoid apes and small animals. *Science*, *102*(2637), 31-33.

60. Hodes, M.E.; Morgan, S.; Hubbard, J.D.; Yu, P.L.; Lukemeyer, J.W. Tissue culture and animal studies with an oncolytic bovine enterovirus (bovine enterovirus 1). *Cancer Res* 1973, *33*, 2408-2414.

61. Holl, E. K., Brown, M. C., Boczkowski, D., McNamara, M. A., George, D. J., Bigner, D. D., Gromeier, M., & Nair, S. K. (2016). Recombinant oncolytic poliovirus, PVSRIPO, has potent cytotoxic and innate inflammatory effects, mediating therapy in human breast and prostate cancer xenograft models. *Oncotarget*, *7*(48), 79828.

62. Hoster, H.A.; Zanes, R.P., Jr.; Von Haam, E. Studies in Hodgkin's syndrome; the association of viral hepatitis and Hodgkin's disease; a preliminary report. *Cancer Res* 1949, *9*, 473-480.

63. Huse, J. T., & Holland, E. C. (2010). Targeting brain cancer: advances in the molecular pathology of malignant glioma and medulloblastoma. *Nature reviews cancer*, *10*(5), 319.

64. International Agency for Research on Cancer (2019). World cancer statistics fact sheet. Retrieved from gco.iarc.fr

65. Jahan, N., Wimmer, E., & Mueller, S. (2011). A host-specific, temperature-sensitive translation defect determines the attenuation phenotype of a human rhinovirus/poliovirus chimera, PV1 (RIPO). *Journal of virology*, *85*(14), 7225-7235.

66. Jayawardena, N., Burga, L. N., Easingwood, R. A., Takizawa, Y., Wolf, M., & Bostina, M. (2018). Structural basis for anthrax toxin receptor 1 recognition by Seneca Valley Virus. Proceedings of the National Academy of Sciences, 115(46), E10934-E10940.

67. Johnson, L. A., Morgan, R. A., Dudley, M. E., Cassard, L., Yang, J. C., Hughes, M. S., Kammula, U. S., Royal, R. E., Sherry, R. M., Wunderlich, J. R., & Lee, C. C. R. (2009). Gene therapy with human and mouse T-cell receptors mediates cancer regression and targets normal tissues expressing cognate antigen. *Blood*, *114*(3), 535-546.

68. June, C. H., O'Connor, R. S., Kawalekar, O. U., Ghassemi, S., & Milone, M. C. (2018). CAR T cell immunotherapy for human cancer. *Science*, *359*(6382), 1361-1365.

69. Kuwata, T. (1965). Infection of tumour cells by extraneous viruses. *GANN Japanese Journal of Cancer Research*, *56*(5), 467-475.

70. Leme, R. A., Zotti, E., Alcantara, B. K., Oliveira, M. V., Freitas, L. A., Alfieri, A. F., & Alfieri, A. A. (2015). Senecavirus A: an emerging vesicular infection in Brazilian pig herds. *Transboundary and emerging diseases*, *62*(6), 603-611.

71. Li, L., Fan, H., Song, Z., Liu, X., Bai, J., & Jiang, P. (2019). Encephalomyocarditis virus 2C protein antagonizes interferon-β signaling pathway through interaction with MDA5. *Antiviral research*, *161*, 70-84.

72. Lin, Y.; Wang, W.; Wan, J.; Yang, Y.; Fu, W.; Pan, D.; Cai, L.; Cheng, T.; Huang, X.; Wang, Y. Oncolytic activity of a coxsackievirus B3 strain in human endometrial cancer cell lines. *Virol J* 2018, *15*, 65, doi:10.1186/s12985-018-0975-x.

73. Liu, Z., Zhao, X., Mao, H., Baxter, P. A., Huang, Y., Yu, L., Wadhwa, L., Su, J. M., Adesina, A., Perlaky, L., Hurwitz, M., Idamakanti, N., Reddy, P. S., Hallenbeck, P. L., Hurwitz, R. L., Lau, C. C., Chintagumpala, M., Blaney, S. M., & Li, X. N. (2013). Intravenous injection of oncolytic picornavirus SVV-001 prolongs animal survival in a panel of primary tumor–based orthotopic xenograft mouse models of pediatric glioma. *Neuro-oncology*, *15*(9), 1173-1185.

74. Liu, T., Li, X., Wu, M., Qin, L., Chen, H., & Qian, P. (2019). Seneca Valley virus 2C and 3Cpro induce apoptosis via mitochondrion-mediated intrinsic pathway. *Frontiers in Microbiology*, *10*, 1202.

75. Logan, G., Newman, J., Wright, C. F., Lasecka-Dykes, L., Haydon, D. T., Cottam, E. M., & Tuthill, T. J. (2018). Deep sequencing of foot-and-mouth disease virus reveals RNA sequences involved in genome packaging. *Journal of virology*, *92*(1), e01159-17.

76. López-Argüello, S., Rincón, V., Rodríguez-Huete, A., Martínez-Salas, E., Belsham, G. J., Valbuena, A., & Mateu, M. G. (2019). Thermostability of the Foot-and-Mouth Disease Virus Capsid Is Modulated by Lethal and Viability-Restoring Compensatory Amino Acid Substitutions. *Journal of virology*, JVI-02293.

77. Malo, C.S.; Renner, D.N.; Kelcher, A.M.H.; Jin, F.; Hansen, M.J.; Pavelko, K.D.; Johnson, A.J. The Effect of Vector Silencing during Picornavirus Vaccination against Experimental Melanoma and Glioma. *Plos One* 2016, *11*, doi:ARTN e0162064

78. Martner, A., Östman, S., Lundin, S., Rask, C., Björnsson, V., Telemo, E., Collins, V., & Wold, A. E. (2013). Stronger T cell immunogenicity of ovalbumin expressed intracellularly in Gram-negative than in Gram-positive bacteria. *PloS one*, *8*(5), e65124.

79. McPherson, K., Steel, C., & Dixon, J. M. (2000). ABC of breast diseases: breast cancer—epidemiology, risk factors, and genetics. *BMJ: British Medical Journal*, *321*(7261), 624.

80. Mehndiratta, M. M., Mehndiratta, P., & Pande, R. (2014). Poliomyelitis: historical facts, epidemiology, and current challenges in eradication. *The Neurohospitalist*, *4*(4), 223-229.

81. Merrill, M. K., Bernhardt, G., Sampson, J. H., Wikstrand, C. J., Bigner, D. D., & Gromeier, M. (2004). Poliovirus receptor CD155-targeted oncolysis of glioma. *Neuro-oncology*, *6*(3), 208-217.

82. Miles, L. A., Burga, L. N., Gardner, E. E., Bostina, M., Poirier, J. T., & Rudin, C. M. (2017). Anthrax toxin receptor 1 is the cellular receptor for Seneca Valley virus. *The Journal of clinical investigation*, *127*(8), 2957-2967.

83. Miyamoto, S.; Inoue, H.; Nakamura, T.; Yamada, M.; Sakamoto, C.; Urata, Y.; Okazaki, T.; Marumoto, T.; Takahashi, A.; Takayama, K., et al. Coxsackievirus B3 is an oncolytic virus with immunostimulatory properties that is active against lung adenocarcinoma. *Cancer Res* 2012, *72*, 2609-2621, doi:10.1158/0008-5472.CAN-11-3185

84. Molina, J. R., Mandrekar, S. J., Dy, G. K., Aubry, M. C., Allen Ziegler, K. L., Dakhil, S. R., Sachs, B. A., Nieva, J. J., Schild, S. E., Burroughs, K., & Williams, A. (2013). A randomized double-blind phase II study of the Seneca Valley virus (NTX-010) versus placebo for patients with extensive stage SCLC (ES-SCLC) who were stable or responding after at least four cycles of platinum-based chemotherapy: Alliance (NCCTG) N0923 study.

85. Morton, C. L., Houghton, P. J., Kolb, E. A., Gorlick, R., Reynolds, C. P., Kang, M. H., Maris, J. M., Keir, S. T., Wu, J., & Smith, M. A. (2010). Initial testing of the replication competent Seneca Valley virus (NTX-010) by the pediatric preclinical testing program. *Pediatric blood & cancer*, *55*(2), 295-303.

86. Nieva, J. L., Agirre, A., Nir, S., & Carrasco, L. (2003). Mechanisms of membrane permeabilization by picornavirus 2B viroporin. *FEBS letters*, *552*(1), 68-73.

87. Nieva, J. L., Madan, V., & Carrasco, L. (2012). Viroporins: structure and biological functions. Nature Reviews Microbiology, 10(8), 563-574.

88. Ochiai, H., Moore, S. A., Archer, G. E., Okamura, T., Chewning, T. A., Marks, J. R., Sampson, J. H., & Gromeier, M. (2004). Treatment of intracerebral neoplasia and

neoplastic meningitis with regional delivery of oncolytic recombinant poliovirus. *Clinical cancer research*, *10*(14), 4831-4838.

89. Ochiai, H., Campbell, S. A., Archer, G. E., Chewning, T. A., Dragunsky, E., Ivanov, A., Gromeier, M., & Sampson, J. H. (2006). Targeted therapy for glioblastoma multiforme neoplastic meningitis with intrathecal delivery of an oncolytic recombinant poliovirus. *Clinical cancer research*, *12*(4), 1349-1354.

90. Pandha, H.; Harrington, K.; Ralph, C.; Melcher, A.; Grose, M.; Shafren, D. Phase I/II storm study: Intravenous delivery of a novel oncolytic immunotherapy agent, Coxsackievirus A21, in advanced cancer patients. *Journal for ImmunoTherapy of Cancer* 2015, *3*, doi:10.1186/2051-1426-3-s2-p341.

91. Pandha, H.S.; Annels, N.; Arif, M.; Mostafid, H.; Sandhu, S.; Harrington, K.; Melcher, A.; Mansfield, D.; Au, G.; Grose, M. Phase I/II CANON study: oncolytic immunotherapy for the treatment of non-muscle invasive bladder (NMIBC) cancer using intravesical coxsackievirus A21. *Ann Oncol* 2016, *27*.

92. Pandha, H.S.; Harrington, K.; Ralph, C.; Melcher, A.; Schmidt, E.; Kaufman, D.R.; Grose, M.; Karpathy, R.; Shafren, D. Intravenous coxsackievirus A21 in combination with pembrolizumab in advanced cancer patients: phase Ib KEYNOTE 200 study. *Annals of Oncology* 2016, *27*, doi:10.1093/annonc/mdw378.57.

93. Pandha, H.S.; Ralph, C.; Harrington, K.; Curti, B.D.; Sanborn, R.E.; Akerley, W.L.; Gupta, S.; Rudin, C.M.; Rosenberg, J.E.; Kaufman, D.R. Keynote-200 phase 1b: A novel combination study of intravenously delivered coxsackievirus A21 and pembrolizumab in advanced cancer patients. American Society of Clinical Oncology: 2017.

94. Pandurangan, A. P., Ochoa-Montaño, B., Ascher, D. B., & Blundell, T. L. (2017). SDM: a server for predicting effects of mutations on protein stability. *Nucleic acids research*, *45*(W1), W229-W235.

95. Pasma, T., Davidson, S., & Shaw, S. L. (2008). Idiopathic vesicular disease in swine in Manitoba. *The Canadian Veterinary Journal*, *49*(1), 84.

96. Paul, A. V. (2002). Possible unifying mechanism of picornavirus genome replication. In *Molecular Biology of Picornavirus* (pp. 227-246). American Society of Microbiology.

97. Paun, B. C., Cassie, S., MacLean, A. R., Dixon, E., & Buie, W. D. (2010). Postoperative complications following surgery for rectal cancer. *Annals of surgery*, *251*(5), 807-818.

98. Pavelko, K. D., Girtman, M. A., Mitsunaga, Y., Mendez-Fernandez, Y. V., Bell, M. P., Hansen, M. J., Allen, K. S., Rodriguez, M., & Pease, L. R. (2011). Theiler's murine encephalomyelitis virus as a vaccine candidate for immunotherapy. *PloS one*, *6*(5), e20217.

99. Pavelko, K. D., Bell, M. P., Karyampudi, L., Hansen, M. J., Allen, K. S., Knutson, K. L., & Pease, L. R. (2013). The epitope integration site for vaccine antigens determines virus control while maintaining efficacy in an engineered cancer vaccine. *Molecular Therapy*, *21*(5), 1087-1095.

100. Pelner, L.; Fowler, G.A.; Nauts, H.C. Effects of concurrent infections and their toxins on the course of leukemia. *Acta Med Scand Suppl* 1958, *338*, 1-47.

101. Pettersen, E. F., Goddard, T. D., Huang, C. C., Couch, G. S., Greenblatt, D. M., Meng, E. C., & Ferrin, T. E. (2004). UCSF Chimera—a visualization system for exploratory research and analysis. *Journal of computational chemistry*, *25*(13), 1605-1612.

102. Ping, Y., Liu, C., & Zhang, Y. (2018). T-cell receptor-engineered T cells for cancer treatment: current status and future directions. *Protein & cell*, *9*(3), 254-266.

103. Pires, D. E., Ascher, D. B., & Blundell, T. L. (2013). mCSM: predicting the effects of mutations in proteins using graph-based signatures. *Bioinformatics*, *30*(3), 335-342.

104. Pires, D. E., Ascher, D. B., & Blundell, T. L. (2014). DUET: a server for predicting effects of mutations on protein stability using an integrated computational approach. *Nucleic acids research*, *42*(W1), W314-W319.

105. Poirier, J. T., Dobromilskaya, I., Moriarty, W. F., Peacock, C. D., Hann, C. L., & Rudin, C. M. (2013). Selective tropism of Seneca Valley virus for variant subtype small cell lung cancer. *Journal of the National Cancer Institute*, *105*(14), 1059-1065.

106. Porter, A. G. (1993). Picornavirus nonstructural proteins: emerging roles in virus replication and inhibition of host cell functions. *Journal of virology*, *67*(12), 6917.

107. Porter, D. L., Levine, B. L., Kalos, M., Bagg, A., & June, C. H. (2011). Chimeric antigen receptor–modified T cells in chronic lymphoid leukemia. *New England Journal of Medicine*, *365*(8), 725-733.

108. Proboka, G.; Tilgase, A.; Isajevs, S.; Rasa, A.; Alberts, P. Melanoma Unknown Primary Brain Metastasis Treatment with ECHO-7 Oncolytic Virus Rigvir: A Case Report. *Front Oncol* 2018, *8*, 43, doi:10.3389/fonc.2018.00043

109. Reddy, P. S., Burroughs, K. D., Hales, L. M., Ganesh, S., Jones, B. H., Idamakanti, N., Hay, C., Li, S. S., Skele, K. L., Vasko, A. J., Yang, J., Watkins, D., Rudin, C. M., & Hallenbeck, P. L. (2007). Seneca Valley virus, a systemically deliverable oncolytic picornavirus, and the treatment of neuroendocrine cancers. *Journal of the National Cancer Institute*, *99*(21), 1623-1633.

110. Renner, D.N.; Jin, F.; Litterman, A.J.; Balgeman, A.J.; Hanson, L.M.; Gamez, J.D.; Chae, M.; Carlson, B.L.; Sarkaria, J.N.; Parney, I.F., et al. Effective Treatment of Established GL261 Murine Gliomas through Picornavirus Vaccination-Enhanced Tumor Antigen-Specific CD8+ T Cell Responses. *PLoS One* 2015, *10*, e0125565, doi:10.1371/journal.pone.0125565.

111. Rood, B. R., MacDonald, T. J., & Packer, R. J. (2004, October). Current treatment of medulloblastoma: recent advances and future challenges. In *Seminars in oncology* (Vol. 31, No. 5, pp. 666-675). WB Saunders.

112. Roos, F. C., Roberts, A. M., Hwang, I. I., Moriyama, E. H., Evans, A. J., Sybingco, S., Watson, I. R., Carneiro, C. G., Gedye, C., Girardin S. E., & Ailles, L. E. (2010). Oncolytic targeting of renal cell carcinoma via encephalomyocarditis virus. *EMBO molecular medicine*, *2*(7), 275-288.

113. Rosenberg, S. A., & Restifo, N. P. (2015). Adoptive cell transfer as personalized immunotherapy for human cancer. *Science*, *348*(6230), 62-68.

114. Rudin, C. M., Poirier, J. T., Senzer, N. N., Stephenson, J., Loesch, D., Burroughs, K. D., Reddy, P. S., Hann, C. L., & Hallenbeck, P. L. (2011). Phase I clinical study of Seneca Valley Virus (SVV-001), a replication-competent picornavirus, in advanced solid tumors with neuroendocrine features. *Clinical Cancer Research*, *17*(4), 888-895.

115. Ruiz, A. J., Hadac, E. M., Nace, R. A., & Russell, S. J. (2016). MicroRNA-detargeted mengovirus for oncolytic virotherapy. *Journal of virology*, *90*(8), 4078-4092.

116. Saeng-Chuto, K., Rodtian, P., Temeeyasen, G., Wegner, M., & Nilubol, D. (2018). The first detection of Senecavirus A in pigs in Thailand, 2016. *Transboundary and emerging diseases*, *65*(1), 285-288.

117. Samet, J. M., Avila-Tang, E., Boffetta, P., Hannan, L. M., Olivo-Marston, S., Thun, M. J., & Rudin, C. M. (2009). Lung cancer in never smokers: clinical epidemiology and environmental risk factors. *Clinical Cancer Research*, *15*(18), 5626-5645

118. Sciubba, J. J., & Goldenberg, D. (2006). Oral complications of radiotherapy. *The lancet oncology*, *7*(2), 175-183.

119. Scheres, S. H. (2018). Single-particle processing in relion-3.0.

120. Schindelin, J., Arganda-Carreras, I., Frise, E., Kaynig, V., Longair, M., Pietzsch, T., Rueden, C., Saalfeld, S., Schmid, B., & Tinevez, J. Y. (2012). Fiji: an open-source platform for biological-image analysis. *Nature methods*, *9*(7), 676.

121. Ségales, J., Barcellos, D., Alfieri, A., Burrough, E., & Marthaler, D. (2017). Senecavirus A: an emerging pathogen causing vesicular disease and mortality in pigs?. *Veterinary pathology*, *54*(1), 11-21.

122. Shafren, D.R.; Au, G.G.; Nguyen, T.; Newcombe, N.G.; Haley, E.S.; Beagley, L.; Johansson, E.S.; Hersey, P.; Barry, R.D. Systemic therapy of malignant human melanoma tumors by a common cold-producing enterovirus, coxsackievirus a21. *Clin Cancer Res* 2004, *10*, 53-60

123. Shafren, D., Smithers, B. M., & Formby, M. (2011). A phase I, open-label, cohort study of two doses of coxsackievirus A21 given intratumorally in stage IV melanoma. *Journal of Clinical Oncology*, *29*(15_suppl), 8573-8573.

124. Shafren, D.; Quah, M.; Wong, Y.; Andtbacka, R.H.I.; Kaufman, H.L.; Au, G.G. Combination of a novel oncolytic immunotherapeutic agent, CAVATAK (coxsackievirus A21) and immune-checkpoint blockade significantly reduces tumor growth and improves survival in an immune competent mouse melanoma model. *Journal for ImmunoTherapy of Cancer* 2014, *2*, doi:10.1186/2051-1426-2-s3-p125.

125. Shakeel, S., Westerhuis, B. M., Domanska, A., Koning, R. I., Matadeen, R., Koster, A. J., Bakker, A. Q., Beaumont, T., Wolthers, K. C., & Butcher, S. J. (2016). Multiple capsid-stabilizing interactions revealed in a high-resolution structure of an emerging picornavirus causing neonatal sepsis. *Nature communications*, *7*, 11387.

126. Shingu, M.; Chinami, M.; Taguchi, T.; Shingu, M., Jr. Therapeutic effects of bovine enterovirus infection on rabbits with experimentally induced adult T cell leukaemia. *J Gen Virol* 1991, *72 ( Pt 8)*, 2031-2034, doi:10.1099/0022-1317-72-8-2031.

127. Sievers, F., Wilm, A., Dineen, D., Gibson, T. J., Karplus, K., Li, W., Lopez, R., McWilliam, H., Remmert, M., Soding, J., & Thompson, J. D. (2011). Fast, scalable generation of high-quality protein multiple sequence alignments using Clustal Omega. *Molecular systems biology*, *7*(1).

128. Singh, K., Corner, S., Clark, S. G., Scherba, G., & Fredrickson, R. (2012). Seneca Valley virus and vesicular lesions in a pig with idiopathic vesicular disease. *J Vet Sci Technol*, *3*(6), 1-3.

129. Skelding, K.A.; Barry, R.D.; Shafren, D.R. Systemic targeting of metastatic human breast tumor xenografts by Coxsackievirus A21. *Breast Cancer Res Treat* 2009, *113*, 21-30, doi:10.1007/s10549-008-9899-2.

130. Smyth, M.; Symonds, A.; Brazinova, S.; Martin, J. Bovine enterovirus as an oncolytic virus: foetal calf serum facilitates its infection of human cells. *Int J Mol Med* 2002, *10*, 49-53.

131. Southam, C. M., & Moore, A. E. (1952). Clinical studies of viruses as antineoplastic agents, with particular reference to Egypt 101 virus. *Cancer*, *5*(5), 1025-1034.

132. Stern A, Bianco S, Yeh MT, Wright C, Butcher K, Tang C, Nielsen R, Andino R. 2014. Costs and Benefits of Mutational Robustness in RNA Viruses. Cell Reports 8:1026-1036.

133. Stoner, G. D., Williams, B., Kniazeff, A., & Shimkin, M. B. (1973). Effect of neuraminidase pretreatment on the susceptibility of normal and transformed mammalian cells to bovine enterovirus 261. *Nature*, *245*(5424), 319.

134. Strauss, M., Filman, D. J., Belnap, D. M., Cheng, N., Noel, R. T., & Hogle, J. M. (2015). Nectin-like interactions between poliovirus and its receptor trigger conformational changes associated with cell entry. *Journal of virology*, *89*(8), 4143-4157.

135. Strauss, M., Jayawardena, N., Sun, E., Easingwood, R. A., Burga, L. N., & Bostina, M. (2018). Cryo-electron microscopy structure of Seneca Valley virus procapsid. *Journal of virology*, *92*(6), e01927-17.

136. Sun, D., Vannucci, F., Knutson, T. P., Corzo, C., & Marthaler, D. G. (2017). Emergence and whole-genome sequence of Senecavirus A in Colombia. *Transboundary and emerging diseases*, *64*(5), 1346-1349.

137. Svitkin, Y. V., Imataka, H., Khaleghpour, K., Kahvejian, A., Liebig, H. D., & Sonenberg, N. (2001). Poly (A)-binding protein interaction with eIF4G stimulates picornavirus IRES-dependent translation. *Rna*, *7*(12), 1743-1752.

138. Svyatchenko, V.A.; Ternovoy, V.A.; Kiselev, N.N.; Demina, A.V.; Loktev, V.B.; Netesov, S.V.; Chumakov, P.M. Bioselection of coxsackievirus B6 strain variants with altered tropism to human cancer cell lines. *Archives of Virology* 2017, *162*, 3355-3362, doi:10.1007/s00705-017-3492-0

139. Taylor, M.W.; Cordell, B.; Souhrada, M.; Prather, S. Viruses as an aid to cancer therapy: regression of solid and ascites tumors in rodents after treatment with bovine enterovirus. *Proc Natl Acad Sci U S A* 1971, *68*, 836-840.

140. Tilgase, A.; Patetko, L.; Blake, I.; Ramata-Stunda, A.; Boroduskis, M.; Alberts, P. Effect of the oncolytic ECHO-7 virus Rigvir(R) on the viability of cell lines of human origin in vitro. *J Cancer* 2018, *9*, 1033-1049, doi:10.7150/jca.23242.

141. Tilgase, A.; Olmane, E.; Nazarovs, J.; Brokāne, L.; Erdmanis, R.; Rasa, A.; Alberts, P. Multimodality Treatment of a Colorectal Cancer Stage IV Patient with FOLFOX-4, Bevacizumab, Rigvir Oncolytic Virus, and Surgery. *Case Reports in Gastroenterology* 2018, *12*, 457-465, doi:10.1159/000492210.

142. Torre, L. A., Siegel, R. L., Ward, E. M., & Jemal, A. (2016). Global cancer incidence and mortality rates and trends—an update. Cancer Epidemiology and Prevention Biomarkers, 25(1), 16-27.

143. Toyoda, H., Yin, J., Mueller, S., Wimmer, E., & Cello, J. (2007). Oncolytic treatment and cure of neuroblastoma by a novel attenuated poliovirus in a novel poliovirus-susceptible animal model. *Cancer research*, *67*(6), 2857-2864.

144. Toyoda, H., Wimmer, E., & Cello, J. (2011). Oncolytic poliovirus therapy and immunization with poliovirus-infected cell lysate induces potent antitumor immunity against neuroblastoma in vivo. *International journal of oncology*, *38*(1), 81-87.

145. Trotti, A., Colevas, A. D., Setser, A., Rusch, V., Jaques, D., Budach, V., Langer, C., Murphy, B., Cumberlin, R., Coleman, C. N., & Rubin, P. (2003). CTCAE v3. 0: development of a comprehensive grading system for the adverse effects of cancer treatment. In *Seminars in radiation oncology* (Vol. 13, No. 3, pp. 176-181). WB Saunders.

146. Venkataraman, S., Reddy, S. P., Loo, J., Idamakanti, N., Hallenbeck, P. L., & Reddy, V. S. (2008). Structure of Seneca Valley Virus-001: an oncolytic picornavirus representing a new genus. *Structure*, *16*(10), 1555-1561.

147. Verstappen, C. C., Heimans, J. J., Hoekman, K., & Postma, T. J. (2003). Neurotoxic complications of chemotherapy in patients with cancer. *Drugs*, *63*(15), 1549-1563.

148. Wadhwa, L., Hurwitz, M. Y., Chévez-Barrios, P., & Hurwitz, R. L. (2007). Treatment of invasive retinoblastoma in a murine model using an oncolytic picornavirus. *Cancer research*, *67*(22), 10653-10656.

149. Walter, T. S., Ren, J., Tuthill, T. J., Rowlands, D. J., Stuart, D. I., & Fry, E. E. (2012). A plate-based high-throughput assay for virus stability and vaccine formulation. *Journal of virological methods*, *185*(1), 166-170.

150. Xia, Z.J.; Chang, J.H.; Zhang, L.; Jiang, W.Q.; Guan, Z.Z.; Liu, J.W.; Zhang, Y.; Hu, X.H.; Wu, G.H.; Wang, H.Q., et al. [Phase III randomized clinical trial of intratumoral injection of E1B gene-deleted adenovirus (H101) combined with cisplatin-based chemotherapy in treating squamous cell cancer of head and neck or esophagus]. *Ai Zheng* 2004, *23*, 1666-1670

151. Yang, X., Chen, E., Jiang, H., Muszynski, K., Harris, R. D., Giardina, S. L., Gromeier, M., Mitra, G., & Soman, G. (2009). Evaluation of IRES-mediated, cell-type-specific cytotoxicity of poliovirus using a colorimetric cell proliferation assay. *Journal of virological methods*, *155*(1), 44-54.

152. Yu, L., Baxter, P. A., Zhao, X., Liu, Z., Wadhwa, L., Zhang, Y., Su, J. M. F., Tan, X., Yang, J., Adesina, A., Perlaky, L., Hurwitz, M., Idamakanti, N., Police, S. R., Hallenback, P. L., Blaney, S. M., Chintagumpala, M., Hurwitz, R. L., & Li, X. N (2010). A single intravenous injection of oncolytic picornavirus SVV-001 eliminates medulloblastomas in primary tumor-based orthotopic xenograft mouse models. *Neuro-oncology*, *13*(1), 14-27.

153. Yuan, M., Wong, Y., Au, G., & Shafren, D. (2015). Combination of intravenously delivered cavatak (coxsackievirus A21) and immune-checkpoint blockade significantly reduces tumor growth and tumor rechallenge. *Journal for immunotherapy of cancer*, *3*(S2), P342.

154. Zhang, J., Piñeyro, P., Chen, Q., Zheng, Y., Li, G., Rademacher, C., Derscheid, R., Guo, B., Yoon, K. J., Madson, D., & Gauger, P. (2015). Full-length genome sequences of Senecavirus A from recent idiopathic vesicular disease outbreaks in US swine. *Genome Announc.*, *3*(6), e01270-15.

155. Zhang, X., Zhu, Z., Yang, F., Cao, W., Tian, H., Zhang, K., Zheng, H. & Liu, X. (2018). Review of Seneca Valley Virus: A Call for Increased Surveillance and Research. *Frontiers in Microbiology*, *9*, 940.

156. Zhao, X., Wu, Q., Bai, Y., Chen, G., Zhou, L., Wu, Z., Yang, H. & Ma, J. (2017). Phylogenetic and genome analysis of seven Senecavirus A isolates in China. *Transboundary and emerging diseases*, *64*(6), 2075-2082.

157. Zisman, A. L., Nickolov, A., Brand, R. E., Gorchow, A., & Roy, H. K. (2006). Associations between the age at diagnosis and location of colorectal cancer and the use of alcohol and tobacco: implications for screening. *Archives of internal medicine*, *166*(6), 629-634.

# 7 Supplementary Figures

## 7.1 Alignments of the thermostable SVV mutants against 96 Senecavirus isolates

### 7.1.1 Conservation of A1776G mutation across analogous sites in 96 Senecavirus isolates

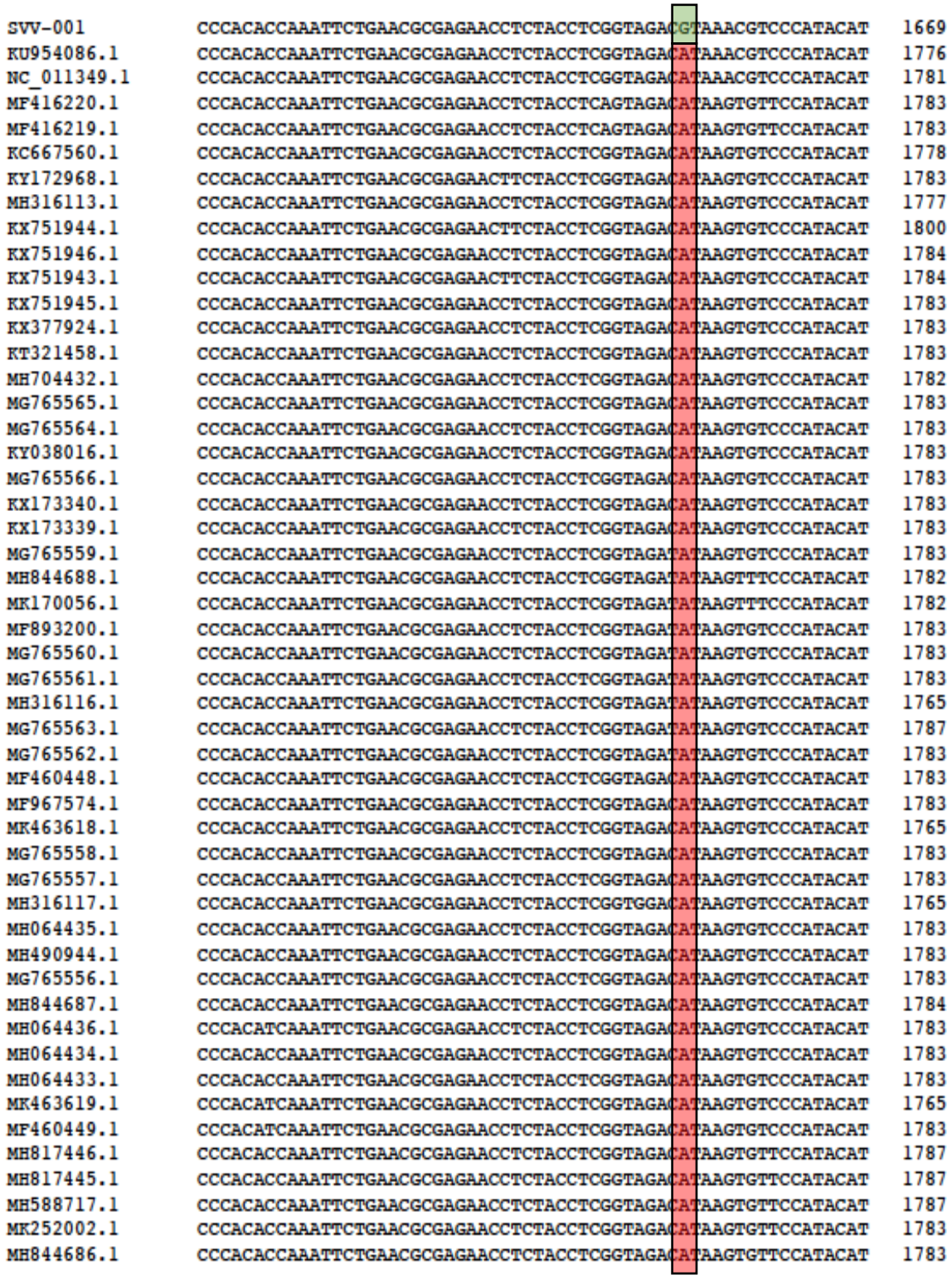

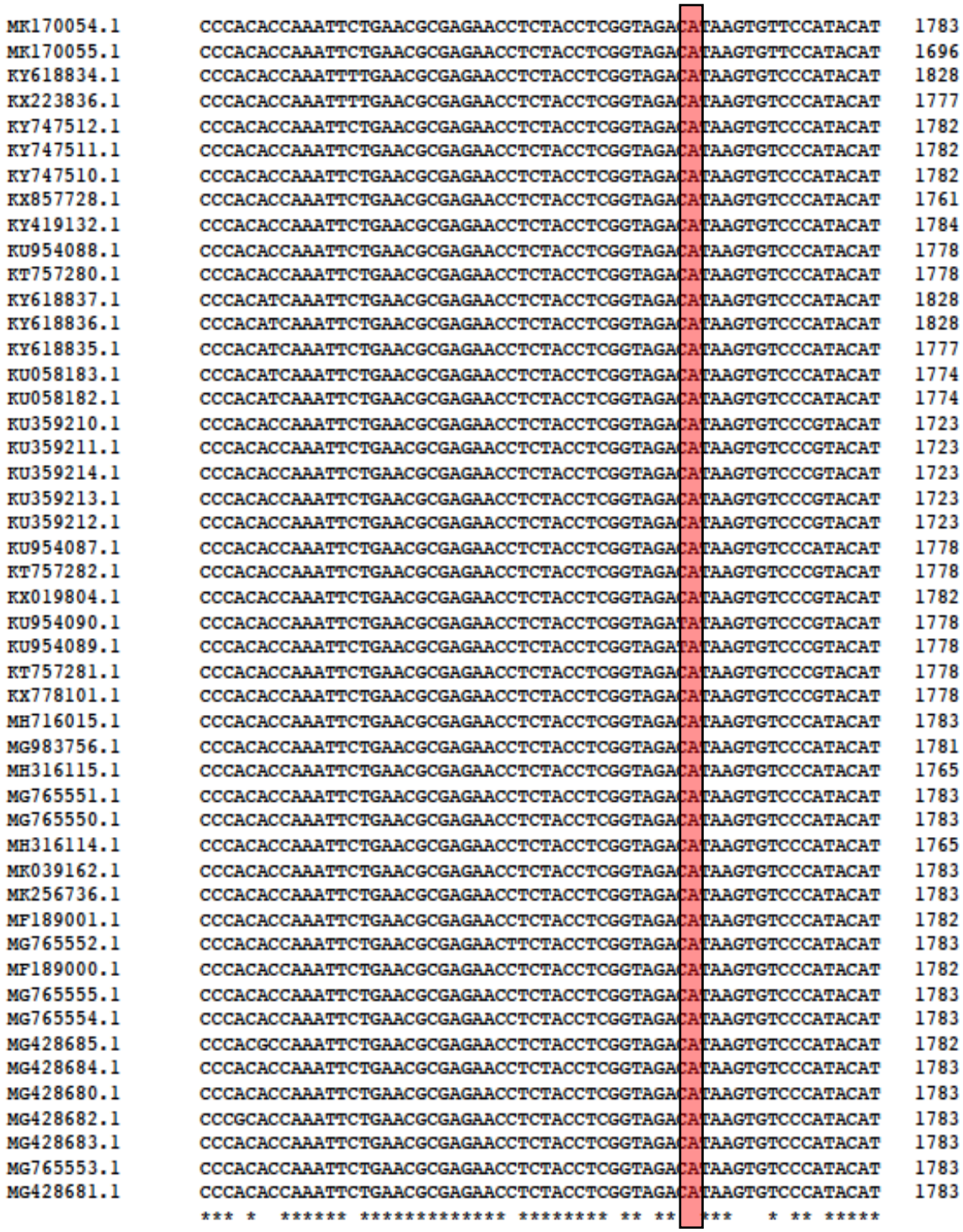


**Figure 26: Clustal omega alignment of the A1776G mutation against analogous sites in 96 Senecavirus A isolates.** SVV-001 thermostable mutant sequence is shown on the top row (shortened to SVV-001), with the rest annotated with their genbank accession numbers. Senecavirus isolates that share the mutation are shown in in green, with those that don't shown in red. The A1776G mutation does not appear in any of the Senecavirus isolates tested.

7.1.2 Conservation of C2526U mutation across analogous sites in 96 Senecavirus isolates


**Figure 27: Clustal omega alignment of the C2527U mutation against analogous sites in 96 Senecavirus A isolates.** Senecavirus isolates that share the mutation are shown in in green, with those that don't shown in red. The C2527T mutation is well conserved appearing in 85.4% of tested Senecavirus isolates.

### 7.1.3 Conservation of A3434G mutation across analogous sites in 96 Senecavirus isolates

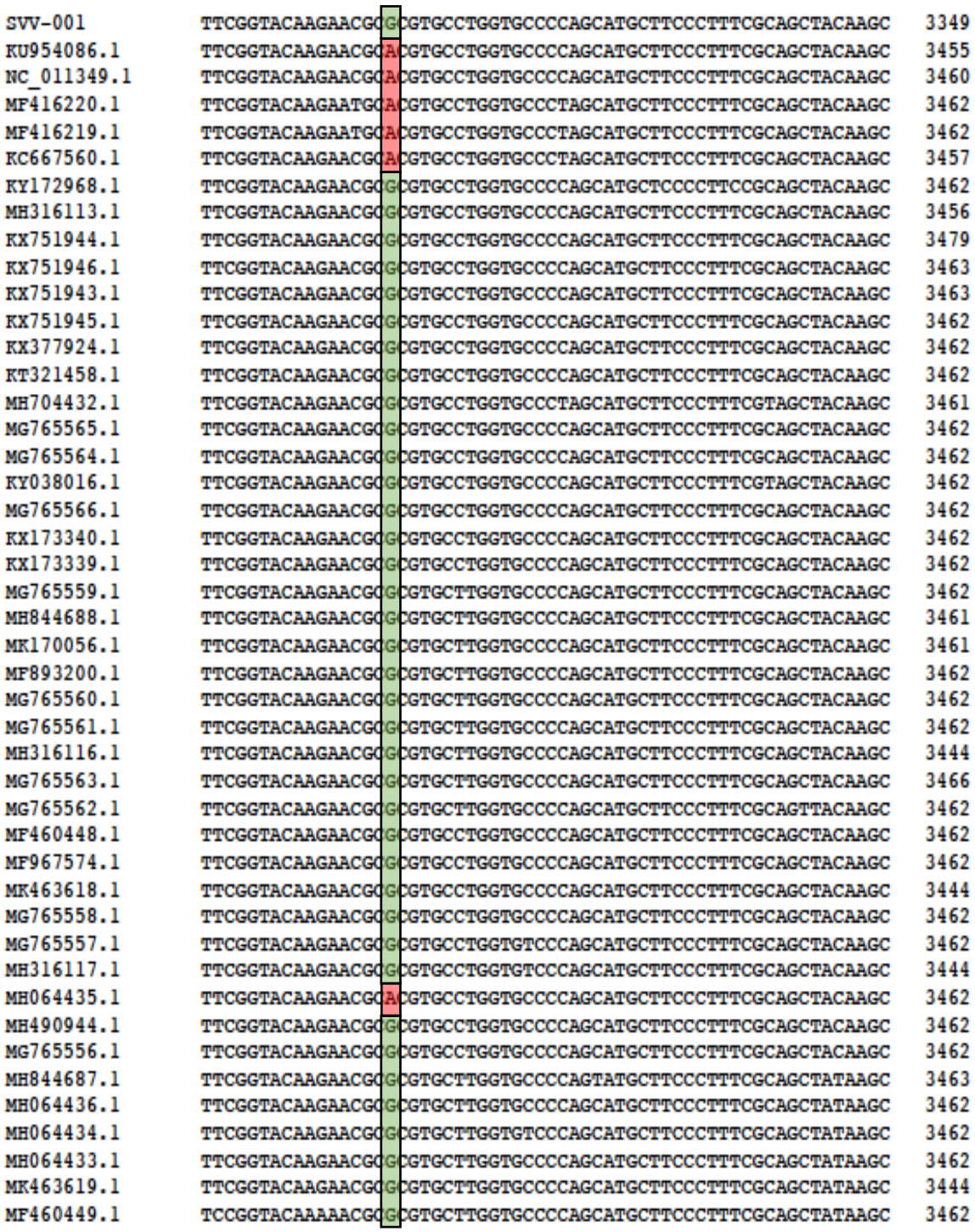

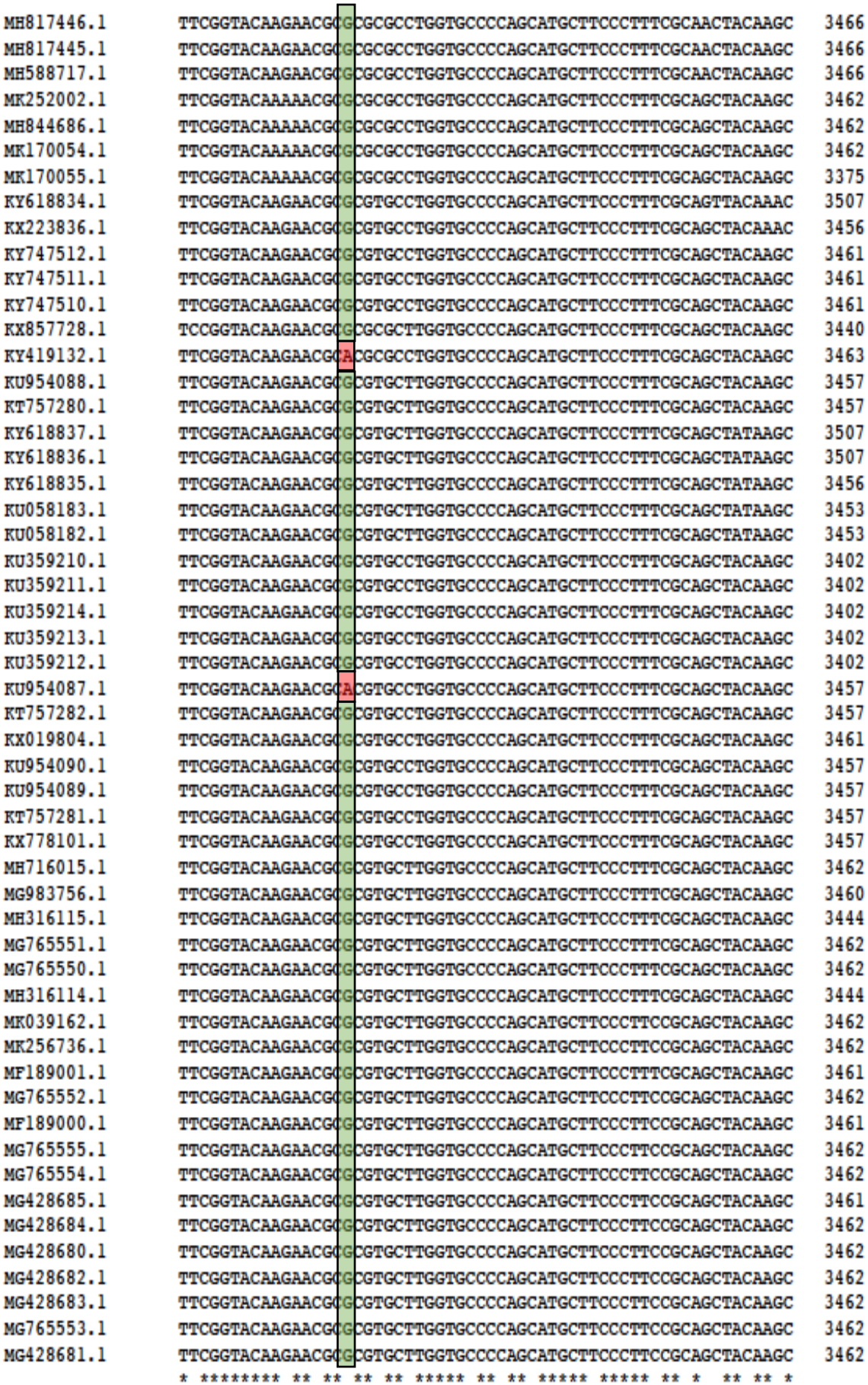
MH817446.1 TTCGGTACAAGAACGGGCGCGCCTGGTGCCCCAGCATGCTTCCCTTTCGCAACTACAAGC 3466
MH817445.1 TTCGGTACAAGAACGGGCGCGCCTGGTGCCCCAGCATGCTTCCCTTTCGCAACTACAAGC 3466
MH588717.1 TTCGGTACAAGAACGGGCGCGCCTGGTGCCCCAGCATGCTTCCCTTTCGCAACTACAAGC 3466
MK252002.1 TTCGGTACAAAAACGGGCGCGCCTGGTGCCCCAGCATGCTTCCCTTTCGCAGCTACAAGC 3462
MH844686.1 TTCGGTACAAAAACGGGCGCGCCTGGTGCCCCAGCATGCTTCCCTTTCGCAGCTACAAGC 3462
MK170054.1 TTCGGTACAAAAACGGGCGCGCCTGGTGCCCCAGCATGCTTCCCTTTCGCAGCTACAAGC 3462
MK170055.1 TTCGGTACAAAAACGGGCGCGCCTGGTGCCCCAGCATGCTTCCCTTTCGCAGCTACAAGC 3375
KY618834.1 TTCGGTACAAGAACGGGCGTGCCTGGTGCCCCAGCATGCTTCCCTTTCGCAGTTACAAAC 3507
KX223836.1 TTCGGTACAAGAACGGGCGTGCCTGGTGCCCCAGCATGCTTCCCTTTCGCAGCTACAAAC 3456
KY747512.1 TTCGGTACAAGAACGGGCGTGCCTGGTGCCCCAGCATGCTTCCCTTTCGCAGCTACAAGC 3461
KY747511.1 TTCGGTACAAGAACGGGCGTGCCTGGTGCCCCAGCATGCTTCCCTTTCGCAGCTACAAGC 3461
KY747510.1 TTCGGTACAAGAACGGGCGTGCCTGGTGCCCCAGCATGCTTCCCTTTCGCAGCTACAAGC 3461
KX857728.1 TCCGGTACAAGAACGGGCGCGCTTGGTGCCCCAGCATGCTTCCCTTTCGCAGCTACAAGC 3440
KY419132.1 TTCGGTACAAGAACGGCACGCGCCTGGTGCCCCAGCATGCTTCCCTTTCGCAGCTACAAGC 3463
KU954088.1 TTCGGTACAAGAACGGGCGTGCTTGGTGCCCCAGCATGCTTCCCTTTCGCAGCTACAAGC 3457
KT757280.1 TTCGGTACAAGAACGGGCGTGCTTGGTGCCCCAGCATGCTTCCCTTTCGCAGCTACAAGC 3457
KY618837.1 TTCGGTACAAGAACGGGCGTGCTTGGTGCCCCAGCATGCTTCCCTTTCGCAGCTATAAGC 3507
KY618836.1 TTCGGTACAAGAACGGGCGTGCTTGGTGCCCCAGCATGCTTCCCTTTCGCAGCTATAAGC 3507
KY618835.1 TTCGGTACAAGAACGGGCGTGCTTGGTGCCCCAGCATGCTTCCCTTTCGCAGCTATAAGC 3456
KU058183.1 TTCGGTACAAGAACGGGCGTGCTTGGTGCCCCAGCATGCTTCCCTTTCGCAGCTATAAGC 3453
KU058182.1 TTCGGTACAAGAACGGGCGTGCTTGGTGCCCCAGCATGCTTCCCTTTCGCAGCTATAAGC 3453
KU359210.1 TTCGGTACAAGAACGGGCGTGCCTGGTGCCCCAGCATGCTTCCCTTTCGCAGCTACAAGC 3402
KU359211.1 TTCGGTACAAGAACGGGCGTGCCTGGTGCCCCAGCATGCTTCCCTTTCGCAGCTACAAGC 3402
KU359214.1 TTCGGTACAAGAACGGGCGTGCCTGGTGCCCCAGCATGCTTCCCTTTCGCAGCTACAAGC 3402
KU359213.1 TTCGGTACAAGAACGGGCGTGCCTGGTGCCCCAGCATGCTTCCCTTTCGCAGCTACAAGC 3402
KU359212.1 TTCGGTACAAGAACGGGCGTGCCTGGTGCCCCAGCATGCTTCCCTTTCGCAGCTACAAGC 3402
KU954087.1 TTCGGTACAAGAACGGCACGTGCCTGGTGCCCCAGCATGCTTCCCTTTCGCAGCTACAAGC 3457
KT757282.1 TTCGGTACAAGAACGGGCGTGCCTGGTGCCCCAGCATGCTTCCCTTTCGCAGCTACAAGC 3457
KX019804.1 TTCGGTACAAGAACGGGCGTGCCTGGTGCCCCAGCATGCTTCCCTTTCGCAGCTACAAGC 3461
KU954090.1 TTCGGTACAAGAACGGGCGTGCCTGGTGCCCCAGCATGCTTCCCTTTCGCAGCTACAAGC 3457
KU954089.1 TTCGGTACAAGAACGGGCGTGCCTGGTGCCCCAGCATGCTTCCCTTTCGCAGCTACAAGC 3457
KT757281.1 TTCGGTACAAGAACGGGCGTGCCTGGTGCCCCAGCATGCTTCCCTTTCGCAGCTACAAGC 3457
KX778101.1 TTCGGTACAAGAACGGGCGTGCCTGGTGCCCCAGCATGCTTCCCTTTCGCAGCTACAAGC 3457
MH716015.1 TTCGGTACAAGAACGGGCGTGCTTGGTGCCCCAGCATGCTTCCCTTTCGCAGCTACAAGC 3462
MG983756.1 TTCGGTACAAGAACGGGCGTGCTTGGTGCCCCAGCATGCTTCCCTTTCGCAGCTACAAGC 3460
MH316115.1 TTCGGTACAAGAACGGGCGTGCTTGGTGCCCCAGCATGCTTCCCTTTCGCAGCTACAAGC 3444
MG765551.1 TTCGGTACAAGAACGGGCGTGCTTGGTGCCCCAGCATGCTTCCCTTTCGCAGCTACAAGC 3462
MG765550.1 TTCGGTACAAGAACGGGCGTGCTTGGTGCCCCAGCATGCTTCCCTTTCGCAGCTACAAGC 3462
MH316114.1 TTCGGTACAAGAACGGGCGTGCTTGGTGCCCCAGCATGCTTCCCTTTCGCAGCTACAAGC 3444
MK039162.1 TTCGGTACAAGAACGGGCGTGCTTGGTGCCCCAGCATGCTTCCCTTCCGCAGCTACAAGC 3462
MK256736.1 TTCGGTACAAGAACGGGCGTGCTTGGTGCCCCAGCATGCTTCCCTTCCGCAGCTACAAGC 3462
MF189001.1 TTCGGTACAAGAACGGGCGTGCTTGGTGCCCCAGCATGCTTCCCTTTCGCAGCTACAAGC 3461
MG765552.1 TTCGGTACAAGAACGGGCGTGCTTGGTGCCCCAGCATGCTTCCCTTCCGCAGCTACAAGC 3462
MF189000.1 TTCGGTACAAGAACGGGCGTGCTTGGTGCCCCAGCATGCTTCCCTTCCGCAGCTACAAGC 3461
MG765555.1 TTCGGTACAAGAACGGGCGTGCTTGGTGCCCCAGCATGCTTCCCTTCCGCAGCTACAAGC 3462
MG765554.1 TTCGGTACAAGAACGGGCGTGCTTGGTGCCCCAGCATGCTTCCCTTCCGCAGCTACAAGC 3462
MG428685.1 TTCGGTACAAGAACGGGCGTGCTTGGTGCCCCAGCATGCTTCCCTTCCGCAGCTACAAGC 3461
MG428684.1 TTCGGTACAAGAACGGGCGTGCTTGGTGCCCCAGCATGCTTCCCTTCCGCAGCTACAAGC 3462
MG428680.1 TTCGGTACAAGAACGGGCGTGCTTGGTGCCCCAGCATGCTTCCCTTCCGCAGCTACAAGC 3462
MG428682.1 TTCGGTACAAGAACGGGCGTGCTTGGTGCCCCAGCATGCTTCCCTTCCGCAGCTACAAGC 3462
MG428683.1 TTCGGTACAAGAACGGGCGTGCTTGGTGCCCCAGCATGCTTCCCTTCCGCAGCTACAAGC 3462
MG765553.1 TTCGGTACAAGAACGGGCGTGCTTGGTGCCCCAGCATGCTTCCCTTCCGCAGCTACAAGC 3462
MG428681.1 TTCGGTACAAGAACGGGCGTGCTTGGTGCCCCAGCATGCTTCCCTTCCGCAGCTACAAGC 3462

**Figure 28: Clustal omega alignment of the A3434G mutation against analogous sites in 96 Senecavirus A isolates.** Senecavirus isolates that share the mutation are shown in in green, with those that don't shown in red. The A3434G mutation is well conserved appearing in 92.7% of tested Senecavirus isolates.

### 7.1.4 Conservation of G3777A mutation across analogous sites in 96 Senecavirus isolates

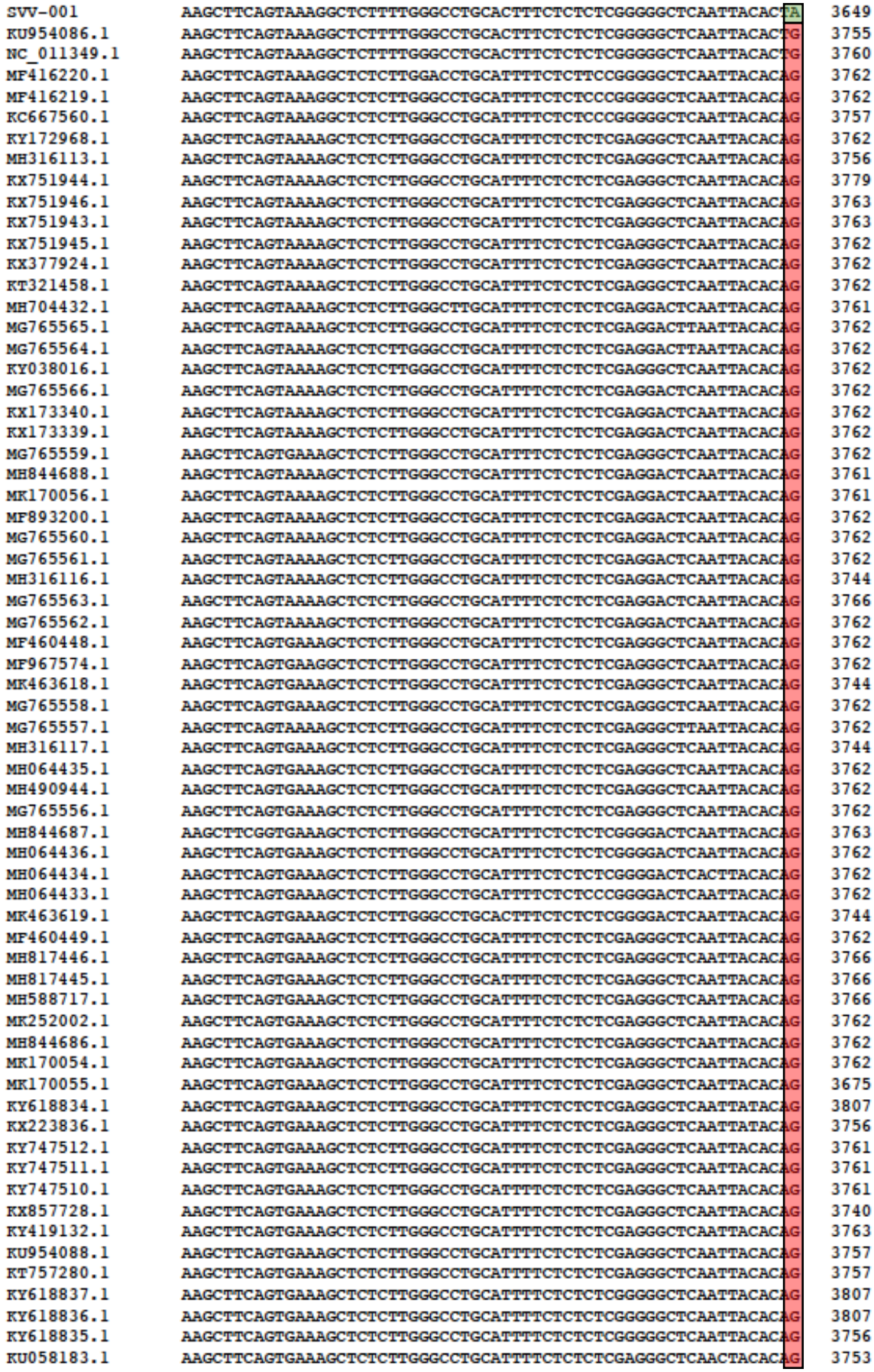

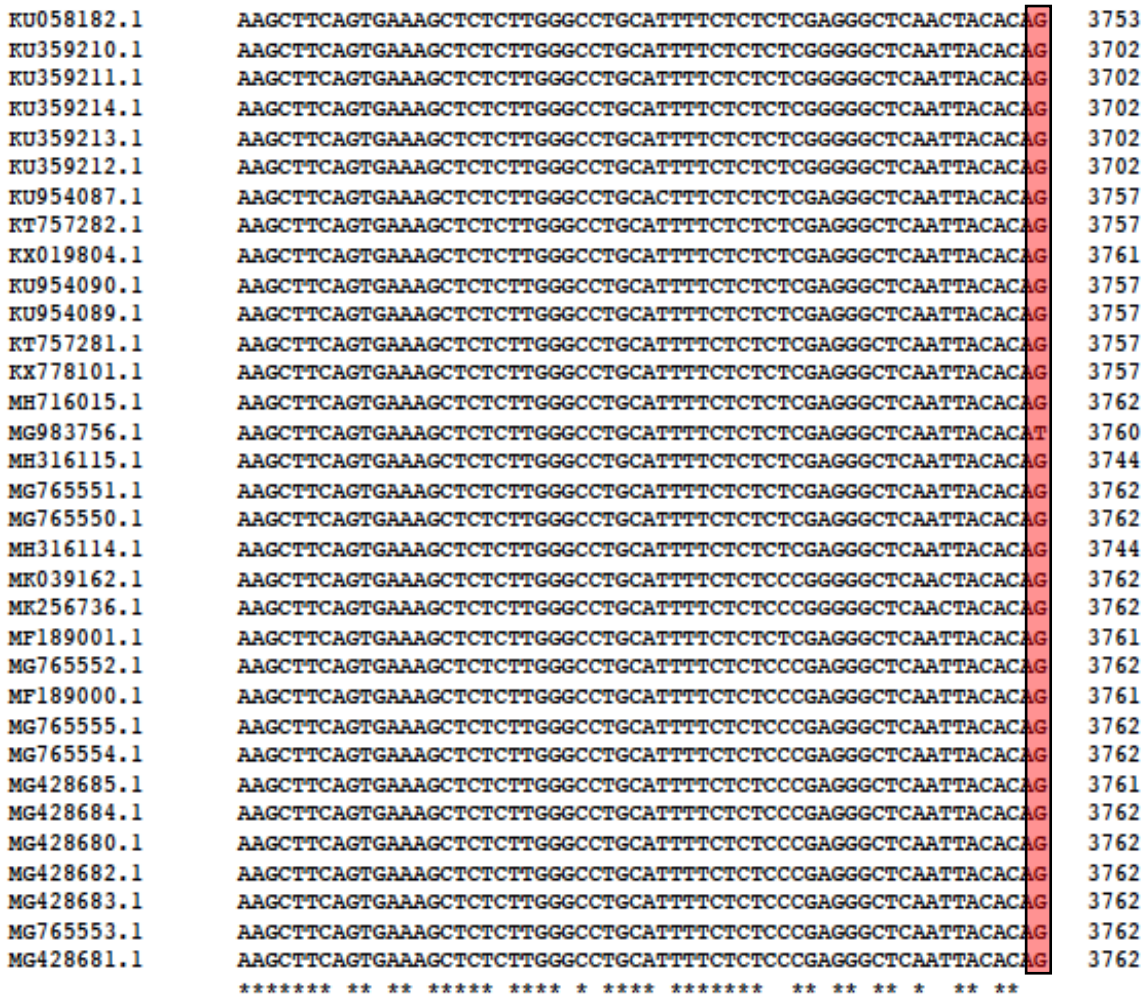


**Figure 29: Clustal omega alignment of the G3777A mutation against analogous sites in 96 Senecavirus A isolates.** Senecavirus isolates that share the mutation are shown in in green, with those that don't shown in red. The G3777A mutation, like the A1776G mutation, does not appear in any other tested Senecavirus isolates.

7.2 ImageJ Fiji analysis of SDS PAGE gels

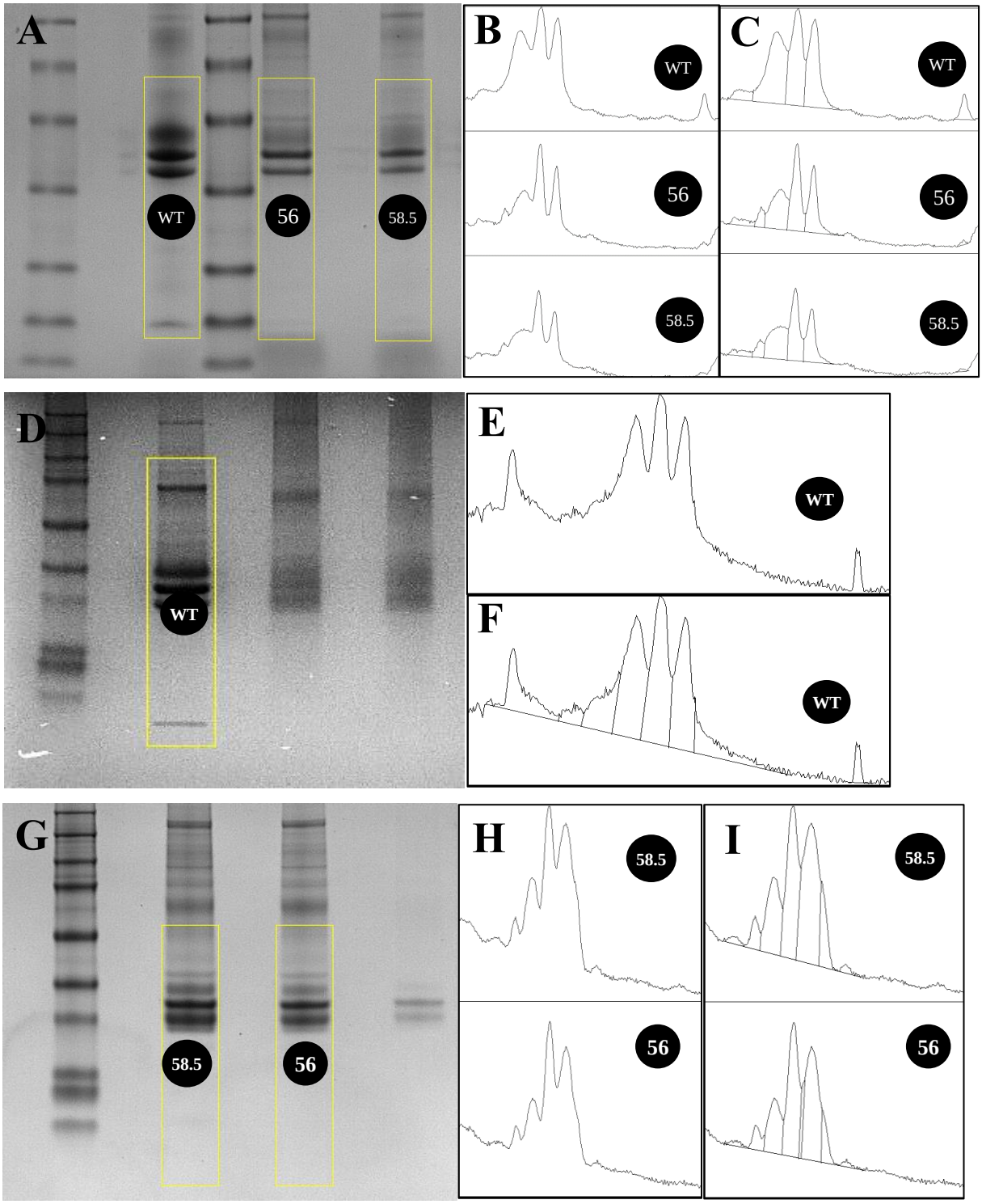


**Figure 30: ImageJ Fiji analysis of SDS PAGE gels. A, D & G** Lanes to be analysed within the SDS PAGE gels were defined using in-built tools **B, E & H** From defined areas, plots were generated as functions of intensity versus position within the defined areas **C, F & I** Area under the curves were calculated for peaks manually divided to better represent discreet bands.